



Birzeit University

Palestine Polytechnic University

Joint Master Degree of Electrical Engineering (JEME)

Faculty of Engineering and Technology

Master Thesis

**Study of DC microgrid transition control between grid-connected and
islanded mode**

Done by:

Wahib Ayman Isayed (1205482)

Supervisor:

Dr. Hakam Shehadeh (Birzeit University)

This thesis was submitted to Birzeit University & Palestine Polytechnic University in fulfillment of the requirements for the joint master's degree of Electrical Engineering (JMEE program).

2024/2025

Master Thesis

Study of DC microgrid transition control between grid-connected and islanded mode

Birzeit University

By

Wahib Ayman Isayed

This thesis was successfully defended on January 4, 2025

Supervisor:

Dr. Hakam Shehadeh

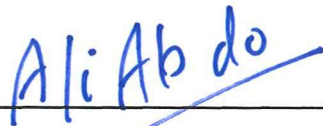


Examiners:

Dr. Mahran Quraan



Dr. Ali Abdo



Declaration of Authorship

I, Wahib Ayman Isayed, declare that this thesis titled, “Study of DC microgrid transition control between grid-connected and islanded mode” and the work presented in it are my own. Also, I confirm that:

- This work was done wholly or mainly while in candidature for a research degree at Birzeit University & Palestine Polytechnic University.
- Where any part of this thesis has previously been submitted for a degree or any other qualification at Birzeit University or any other institution, this has been clearly stated.
- Where I have consulted the publish work of others, this is always clearly attributed.
- Where I have quoted from the work of others, the source is always given. With the exception of such quotations, this thesis is entirely my own work.
- I have acknowledged all main sources of help.
- Where the thesis is based on the work done by myself jointly with others, I have made clear exactly what was done by others and what I have contributed myself.

Signed:

Date:

المستخلص

تقدم الشبكات المصغرة ذات التيار المستمر مزايا مثل الملاءمة لأنظمة التخزين، والمرونة، والكفاءة العالية، والقدرة على العمل بشكل مستقل عن الشبكة الرئيسية أثناء الانقطاعات والأعطال والاضطرابات الأخرى. تركز هذه الدراسة على الشبكات الصغيرة ذات التيار المستمر، مع التركيز على محولات القدرة وطرق التحكم لتطوير نموذج يعمل في حالتين من التشغيل الأول المربوط مع الشبكة والثاني المفصول عن الشبكة والعكس بينهما. حيث تم بناء نموذج المحاكاة باستخدام برنامج MATLAB/Simulink ، مع دمج جميع المكونات الضرورية، بما في ذلك نظام الطاقة الشمسية، والمحولات ذات الاتجاه الواحد والاتجاهين للتيار المستمر، والمحولات ذات الاتجاهين للتيار المتردد. وتركز الدراسة على فهم أثر الانتقال بين حالات التشغيل على الشبكة المصغرة ، والذي يؤدي الى زيادة في الجهد أثناء الانتقال وتكون هذه الزيادة أكثر وضوحًا عند الانتقال من حالة الموصول بالشبكة إلى وضع المعزول عن الشبكة، وتكون أقل تأثيرًا في الانتقال العكسي. حيث تم اختبار طرق تحكم مختلفة لتحقيق انتقالات سلسلة بين حالات التشغيل في الشبكات المصغرة وتشمل الطرق التي تم اختبارها وهي التحكم بالتغذية الراجعة، والتحكم بطريقة الانزلاق، والتعويض، والتحكم بمستوى الجهد.

Abstract

DC microgrids offer several advantages, including suitability for storage systems, resilience, flexibility, high efficiency, and the ability to operate independently from the main grid during outages, faults, or other disruptions. This research examines DC microgrids, with a focus on converters and control methods, to develop a model capable of operating in both grid-connected and islanded modes.

The simulation model was developed using MATLAB/Simulink software, incorporating all essential components, including a PV system, unidirectional and bidirectional DC-DC converters, and a bidirectional AC-DC converter. The study focused on the transition between grid-connected and islanded modes, which is characterized by a voltage overshoot during the transition. This overshoot is more pronounced when transitioning from grid-connected to islanded mode and less significant in the reverse transition.

Various control methods were tested to achieve smooth transitions between islanded and grid-connected modes. These methods include feedback control, sliding mode control, compensation, and voltage level control.

Acknowledgement

All praise is due to Allah, Lord of the worlds, praise from the grateful and the worshipers, for blessing me with this knowledge and making my path easy through it.

I dedicate this work to Allah Almighty, to the Islamic resistance, and to the free people of the world, especially in Gaza and Palestine. I also offer mercy to the righteous martyrs and freedom to the honorable prisoners. All praise is due to Allah, Lord of the worlds, who enabled me to complete this research despite the difficult circumstances and the genocide faced by Muslims everywhere.

I also dedicate this achievement to the three universities that embraced me and contributed to my success in completing this thesis: Birzeit University, Palestine Polytechnic University, and Al-Quds University.

Special thanks to my esteemed supervisor, Dr. Hakam Shehadeh, for his continuous support. I am grateful for his guidance and contributions. Many thanks to the teaching staff at both Birzeit University and Palestine Polytechnic University.

Special thanks to my wife and life partner, Sondos, for her endless support and constant encouragement. To my dear daughters Suwar & Sham. My family, my father, my mother, my brothers, and my sister Bashaer, the supportive and loving family."

Contents

المستخلص.....	I
Abstract.....	II
Chapter 1: Introduction	1
1.1 General Topic and Overview.....	1
1.2 Research Problem.....	2
1.3 Hypotheses	2
1.4 Research Methodology.....	2
1.5 Challenges.....	2
1.6 Contribution.....	2
2 Chapter 2: Literature Review	3
2.1 Microgrid.....	3
2.1.1 Operation modes	4
2.1.2 AC microgrid.....	5
2.1.3 DC microgrid.....	5
2.1.4 Hybrid microgrid	6
2.2 DC Microgrids Structure.....	6
2.2.1 Components	6
2.2.1.3 Loads.....	8
2.2.2 DC bus link, voltage level and polarity	8
2.2.3 Architecture of DC MGs	10
2.2.4 Challenges in DC microgrids.....	11
2.3 Power Electronics Converters in DC Microgrids	12
2.3.1 Bidirectional DC-AC converters.....	12
2.3.2 DC-DC converters	15
2.4 Review of Standards And Regulations Related to DC Microgrid	22
2.5 DC Microgrid Stability (Dynamic Stability).....	23
2.6 DC Microgrid Operation Modes Transition Control.....	24
3 Chapter 3: DC microgrid modeling.....	27
3.1 Introduction	27
3.2 Utility Grid.....	28
3.3 PV System	29
3.4 DC Load	31
3.5 Bidirectional AC/DC Converter	32

3.6	Unidirectional DC/DC Converter.....	37
3.7	Bidirectional DC/DC Converter	42
3.8	DC-DC Converter Control using State Space Matrices.....	45
Chapter 4: Problem analysis and Results.....		46
4.1.	Problem Description and Analysis.....	46
4.2.	Feedback Control.....	48
4.3.	Slide Mode Control.....	49
4.4.	Compensation Control.....	50
4.5.	Voltage Level Control	52
4.6.	Comparison Between Different Control Solutions.....	52
4	Chapter 5: Conclusion	54
5.1.	Summary.....	54
5.2.	Assumptions and Limitations	54
5.3.	Future work	55
5.4.	Conclusion	55
5	References:	57
6	Appendix:	A.I
	Appendix A:.....	A.I
	Appendix B:.....	B.I
	Appendix C:.....	C.I

List of Figures:

Figure 2.1: a) Microgrid structure, b) types of microgrids.....	4
Figure 2.2: AC & DC microgrids structure	5
Figure 2.3: hybrid microgrid structure	6
Figure 2.4: DC Microgrids components	7
Figure 2.5: PV system included in DC microgrid	7
Figure 2.6: converters in dc microgrids.....	8
Figure 2.7: a) Unipolar dc bus. b) Bipolar dc bus.....	10
Figure 2.8: DC microgrid configuration: a) Dual bus, b) ring, c) Radial and d) Meshed.....	11
Figure 2.9: Bidirectional AC-DC converters different types.	12
Figure 2.10: a) VSI circuit diagram. b) AC-DC converter ties between grid and DC bus	13
Figure 2.11: PLL for AC-DC converter.....	14
Figure 2.12: SVPWM vectors diagram.	14
Figure 2. 13: DC-DC converters power flow.....	15
Figure 2.14: DC-DC converter topologies circuit: a) Boost. b) Buck. c) Buck-boost. d) Cuk. e) Zeta. f) SEPIC. g) Forward. h) Flyback. i)Push-pull.....	16
Figure 2.15: Proposed buck-boost converter circuit diagram.	17
Figure 2.16: Bidirectional DC-DC converter types.	18
Figure 2.17: Bidirectional buck-boost converter circuit.	19
Figure 2.18: MPPT techniques.	19
Figure 2. 19: Working principle of P & O algorithm.....	21
Figure 2.20: control strategies of DC microgrid	25
Figure 3.1: DC microgrid modeling main component.....	27
Figure 3. 2 Block diagram representation of the linear state-space equations.....	28
Figure 3. 3: Main grid model.....	29
Figure 3. 4: PV solar system simulation model	30
Figure 3. 5: P-V & I-V curves for the PV solar model.	31
Figure 3.6: Resistive load Simulink model	32
Figure 3.7: Bidirectional AC/DC converter circuit.....	33
Figure 3. 8: a) PLL controller. b) dq controller with SVPWM switching for AC-DC converter.	35
Figure 3. 9: simulation model control of bidirectional AC-DC converter	36
Figure 3.10: Unidirectional buck-boost converter circuit.....	37
Figure 3.11: poles and zeros map for the unidirectional DC-DC converter: a) in islanded mode. b) in grid connected mode.....	41
Figure 3. 12 :Control method and switching sequence of unidirectional buck-boost converter:.....	42
Figure 3.13: Bidirectional DC-DC converter.....	43
Figure 3. 14: Poles and zeros map of bidirectional buck boost converter.	43
Figure 3.15: Control and switching of bidirectional DC-DC converter.....	44
Figure 3. 16: Control method using state space matrices.	45
Figure 4. 1: Transition effect on DC bus voltage. a) using PI controller. b) using state space controller..	47
Figure 4. 2: Feedback control method for unidirectional DC-DC converter.....	48
Figure 4. 3: DC bus voltage waveform with feedback control.....	49

Figure 4. 4: DC bus voltage for slide mode control result between grid connected mode and islanded mode transition & vice versa.	50
Figure 4. 5: compensation control for state space model in islanded mode for unidirectional DC-DC converter.....	51
Figure 4. 6: DC bus voltage waveform for compensation control method	51
Figure 4. 7: voltage level control algorithm for duty cycle modification.....	52
Figure 4. 8: DC bus voltage using voltage level control: a) PI control method. b) state space model method.....	53

List of tables:

Table 2. 1: DC voltage level comparison.....	9
Table 2. 2: Switching scheme of buck-boost converter.....	18
Table 3. 1: characteristics of PV solar system.....	30
Table 3.2: Parameters of bidirectional AC/DC converter	32
Table 3. 3: PI controller coefficient for dq and voltage regulator controllers	37
Table 3.4: Parameters of unidirectional DC-DC converter.	40
Table 3. 5: Parameters of the bidirectional DC/DC converter.	44
Table 3. 6: State space matrices values based on converter type and mode.....	45
Table 4.1: gain values for different load values.....	49
Table 4. 2: Comparison between the different control methods.....	52

List of Abbreviations:

MG	Microgrid
RESs	Renewable Energy Sources
DGs	Distributed Generation
ESSs	Energy Storage Systems
VSC	Voltage Source Converter
BIBO	Bounded Input Bounded Output
SGs	Synchronous Generators
PCC	Point of Common Coupling
CPLs	Constant Power Loads
MPPT	Maximum Power Point Tracking
P&O	Perturb and Observe
IncCond	Incremental Conductance
FOCV	Fractional Open Circuit Voltage
FSCC	Fractional Short Circuit Current
VSC	Voltage Source Converter
PWM	Pulse Width Modulation
SVPWM	Space Vector Pulse Width Modulation
IEEE	Institute of Electrical and Electronics Engineers
IEC	International Electrotechnical Commission

Chapter 1: Introduction

1.1 General Topic and Overview

Stability in power systems and penetration of distributed energy resources on a small and medium scale have developed a new concept in grids and introduced a new type of grid called a "microgrid", which is defined as a subset of an electric power distribution system that consists of dispersed generators, energy storage devices, and regulated loads to create an independent energy system. Microgrids offer a feasible alternative for integrating distributed energy resources into distribution networks, particularly renewable energy sources that are unpredictable and fluctuate, as well as low-voltage and medium-voltage systems [1]. In contrast to conventional power systems with synchronous generators (SGs), microgrids with Distributed Generation (DGs)/Renewable Energy Sources (RESs) have little to no inertia, which is the primary source of stability. The negative impact of low inertia and damping on MG dynamic performance and stability worsens as DG/RES penetration increases [2].

The term microgrid was developed since every component of the traditional grid was used in a much smaller size in these special grids. This shift in size motivated the development of microgrids in remote areas due to the huge cost of connection in such areas. First, the AC microgrid was developed in these remote areas, and after that, DC microgrids were developed due to huge progress in power electronics devices, renewable energy resources and energy storage and the rise of the use of DC loads in many applications that's makes it more reliable, effective, and simple to manage than AC MGs [3].

Microgrids can be categorized as AC MGs, DC MGs, or hybrid MGs. In comparison to AC MG, DC MG has a more natural interaction with a variety of RES and ESSs, and it is more efficient, and compatibility with the consumer electronic product requirements. On the other hand, hybrid microgrids are presented to efficiently include AC and DC power system components. All AC sources and loads are connected to AC buses in an AC sub-grid in these hybrid systems, while DC components are connected to DC buses in DC sub-grids. This takes advantage of both types but increases the complexity of the control and management in the microgrid.

Another advantage of any DC system is the impact of power quality on public utility networks. Because such systems will only connect through a single point of connection, reactive power flow and frequency regulation can be managed efficiently for the main AC grid. This thesis studies the stability of a DC microgrid during the transition between different modes of operation, so to study that effect, there is a need to build a DC microgrid and the bidirectional converters that form the basis for the operations of a DC microgrid that are necessary to study the stability of such a system.

1.2 Research Problem

The operation in microgrid, either grid-connected or islanded mode can be determined by system faults or pricing signals from the grid operator. Consequently, for smooth operation and to preserve power quality and stability, a precise transition between grid-connected mode and island mode and vice-versa is essential. Also, microgrids can be used to supplement the main electrical grid during periods of high demand or as a backup power generation system. So, the research problem is the transient response of this transition between operations mode that must be reduced to maintain stability of the microgrid.

1.3 Hypotheses

Examining different control techniques (like bumpless control method) for transition between different operation modes of DC microgrids and studying its effect on the performance of the microgrid.

1.4 Research Methodology

Research methodology will be based on simulation using in general MATLAB/Simulink to build & test the proposed control system that will be used to study the stability of the transition between different operations mode of DC microgrid.

1.5 Challenges

Many challenges have been overcome during this research and listed as below:

- A need for Study control system including state space representation.
- Huge processing time of the simulation model.
- Identify, understanding and solve the problem using different control methods.

1.6 Contribution

- Made a comparison between the used voltage levels for the DC bus in microgrid.
- Understand the parameters that affect the transition transient response.
- Propose a different control method (feedback, compensation, slide mode and voltage level control) to achieve smooth transition and provide comparison between them.

Chapter 2: Literature Review

2.1 Microgrid

A microgrid is a system that is a local grid that can be controlled locally and serves a specific geographical area. And it can function in both island mode and grid-connected mode. It joins the grid at a single coupling point, adopting the main grid's voltage when operating normally. In times of emergency, it can autonomously or manually cut itself off and function as an island by utilizing its own local energy production units. The idea of a microgrid relies on a collection of distributed energy resource units and a cluster of loads. And modes of operation can depend on the price of the energy to operate in an economical and efficient mode. This term for microgrid comes from the same components of traditional grids but in much smaller size; it has a specialty in terms of control and pricing management. Moreover, its vital feature is the ability to disconnect from the main grid and remain operational [4].

Microgrids have more reliability and resilience compared to traditional systems. They can be sure to supply power to critical loads during grid outages or disruptions, which is especially useful for critical services such as hospitals and data centers. They can also help integrate renewable energy sources, reduce transmission losses, and increase overall energy efficiency.

This special type of grid is commonly used for many reasons, such as to provide backup power and assist the local grid in urban areas, to provide power in areas where expanding the main grid would be expensive, especially in rural communities, to ensure a steady and secure energy supply under critical loads, and to manage energy requirements in off-grid environments in remote areas. Microgrid control systems can range from simple manual operations to sophisticated automated systems that manage energy flow, optimize resource utilization, and respond to changing conditions in real-time.

There are different components that can be used to construct MGs, but they mainly consist of energy sources that are renewable (ex: PV systems) or nonrenewable (ex: diesel generators), energy storage systems (such as batteries), communication and control systems, and power electronics devices. All these components work together harmoniously to supply power to different combinations of loads in specific areas. These constituent parts are the main parts of any type of microgrid as shown in Fig 2.1.a.

Microgrids can be categorized as DC microgrids, AC microgrids, or hybrid microgrids as shown in Fig 2.1.b. hybrid microgrids are presented to efficiently include AC and DC power system components. All AC sources and loads are connected to AC buses in an AC sub-grid in these hybrid systems, while DC components are connected to DC buses in DC sub-grids. This takes advantage of both types but increases the complexity of the control and management in the microgrid [5].

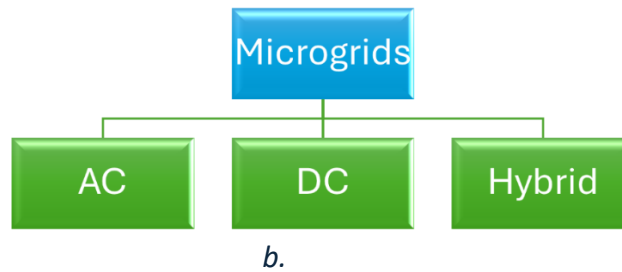
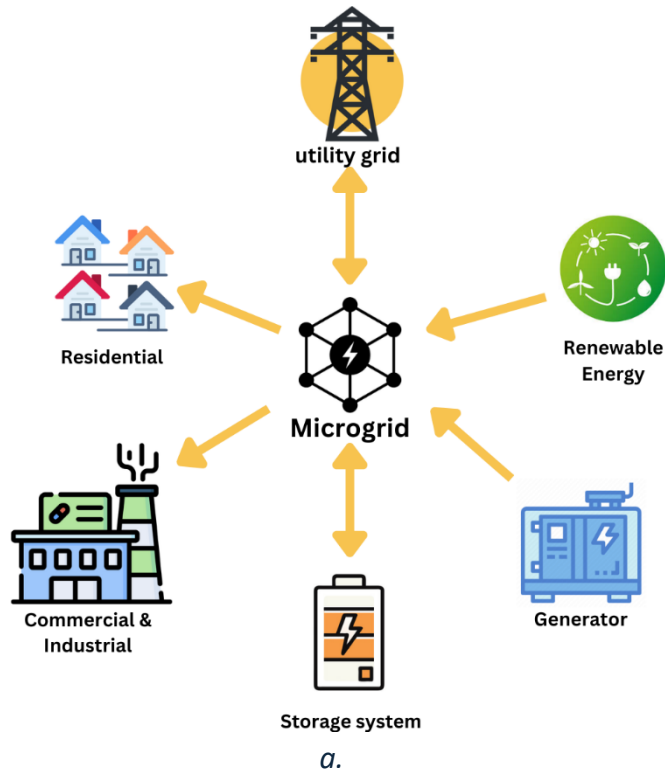


Figure 2.1: a) Microgrid structure, b) types of microgrids

2.1.1 Operation modes

The modes of operation in MGs are mainly divided into two types:

Grid connected mode: In this mode, the microgrid is connected to the grid through a point called the point of common coupling (PCC). The power exchange between the main grid and the microgrid depends on the instantaneous production of distributed generation and the amount of power consumption through the load. In other words, the microgrid can buy power from the main grid when the distributed generation can't generate loads of power [6].

Islanded mode: This mode of operation occurs when a fault occurs, at a main grid blackout, or in any abnormal conditions. In this scenario, the microgrid can be isolated from the main grid and run as an island microgrid [7].

The transition between two modes requires special attention due to the controller and bus voltage will have a volatile and overshoot problem during the transition, Also, transition may cause stability problems due to the low inertia or null inertia of microgrids [8].

There are other sub modes of operation conditions included in grid-connected mode related to the behavior of energy management, like peak shaving conditions, energy export conditions, and emergency backup conditions. These operating conditions describe how to achieve economical and stability benefits for DC microgrids [9]. Also, there are islanded mode conditions like charging conditions, discharging conditions, and load constraints that describe the conditions of off-grid mode.

2.1.2 AC microgrid

This type of microgrid operates mainly using AC current for its electrical distribution, which is compatible with the utility grid. Most electrical infrastructure is designed to work for AC, which makes it simpler, more cost-effective, and suitable for long distances. The AC microgrid can operate AC equipment directly without converters. In terms of protection, it can manage faults at a lower cost and more effectively than the DC microgrid. Fig 2.2 shows the structure of AC and DC microgrids.

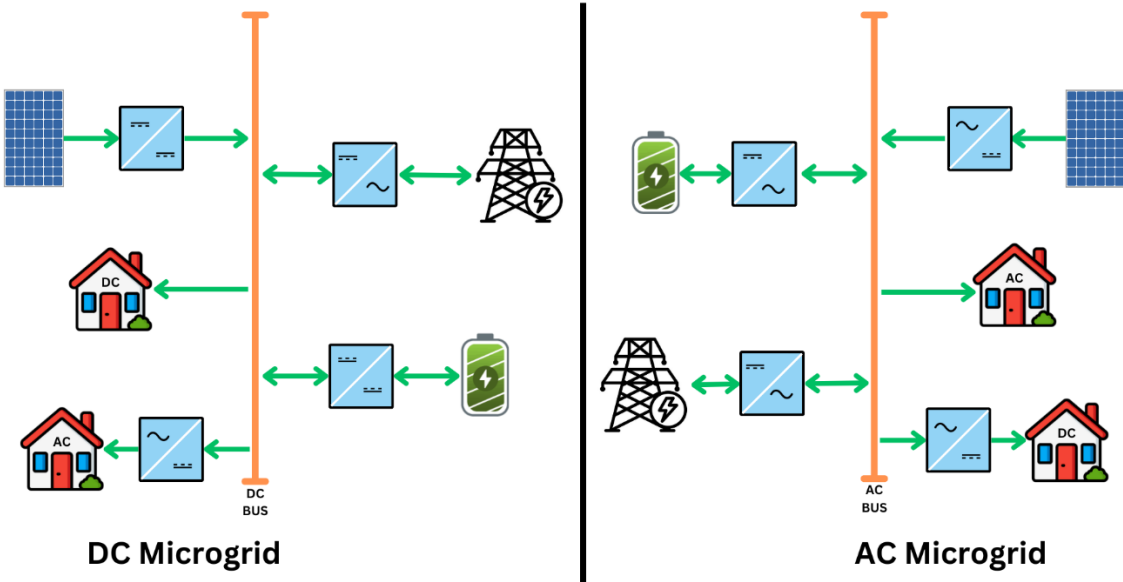


Figure 2.2: AC & DC microgrids structure

2.1.3 DC microgrid

This type of microgrid operates mainly using DC current for its electrical distribution, which requires a conversion stage from AC to DC to interact with the utility grid, AC load, or any AC infrastructure. DC microgrids are more suitable for DC loads, renewable energy sources, electric vehicles, and storage systems as they can operate with only a DC-DC converter avoiding additional

stages of conversion and achieve higher efficiency. This type of microgrid is a suitable solution for remote areas and locations that cannot be connected to the main grid, as it's easier to deal with storage systems in DC MGs. However, handling faults in DC microgrids can be challenging, and advanced control are required to manage power flow and stability.

2.1.4 Hybrid microgrid

To take advantage of the previous two types of microgrids, a combination of AC and DC buses was constructed to cover all types of energy sources and minimize the conversion stages and losses. This combination presents different challenges in terms of protection, technical and operational aspects, and the initial high cost of infrastructure. Also, hybrid microgrids address power quality issues, the requirements of communication systems, and advanced digital control to integrate, synchronize, and operate this unique configuration. Fig. 2.3 shows the structure of a hybrid microgrid that explains how the AC and DC microgrids intergrated to construct a hybrid microgrid.

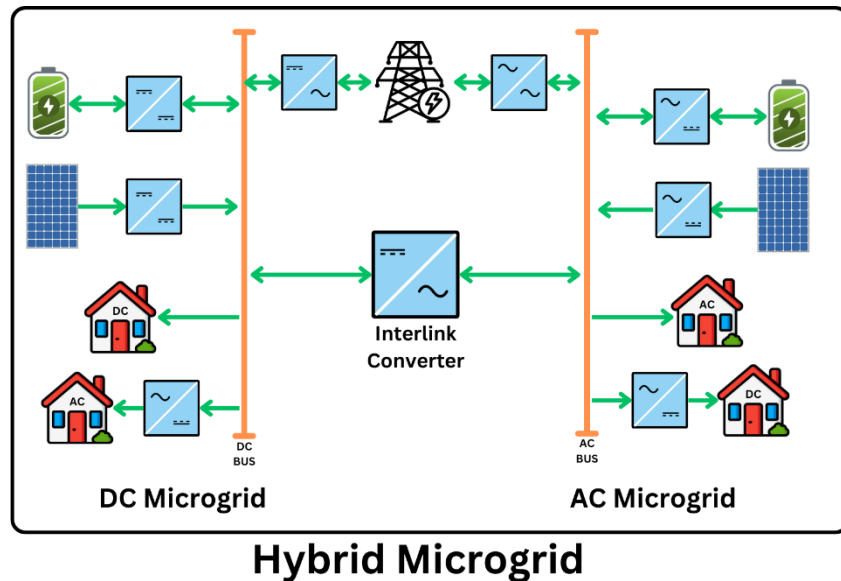


Figure 2.3: hybrid microgrid structure

2.2 DC Microgrids Structure

This section introduces the various components of microgrids, the architecture of DC MGs, the characteristics of the DC bus link, the voltage level and polarity of the DC bus, the operation mode, and finally, the challenges that DC microgrids may face.

2.2.1 Components

In the construction of a DC microgrid, various components collaborate to form a complete system. These components are interconnected with the DC bus, which in turn is linked to the main grid. These components can be categorized into three main groups: power resources, converters, and loads. Fig. 2.4 shows the general components of DC microgrid.

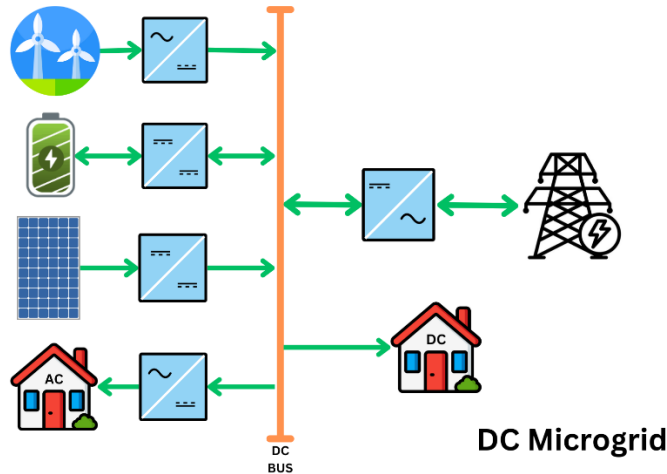


Figure 2.4: DC Microgrids components

2.2.1.1 Power resources

Resources are divided into conventional and renewable power resources based on source type and into AC output and DC outputs.

The most common conventional power source is the utility grid, which operates as a constant AC voltage and frequency source. AC power can also be generated by fossil fuel generators and wind turbines. These alternating current sources are linked by AC-DC converters.

Energy storage systems and other renewable energy sources, such as photovoltaic systems and fuel cells, are connected to the DC bus throughout the DC-DC converters. Energy storage serves as a backup energy source and is also used as a tool for energy cost management based on matching demand with supply at the lowest possible cost [10].

One of the most popular renewable energy systems is the photovoltaic solar system, which converts sunlight into electrical power. The main components of such systems as shown in the figure 2.5 that consist of PV panels and DC-DC converters that adjust the PV output voltage to a suitable voltage for the DC bus to supply loads, and AC-DC converters that supply AC power to AC loads or the utility grid.

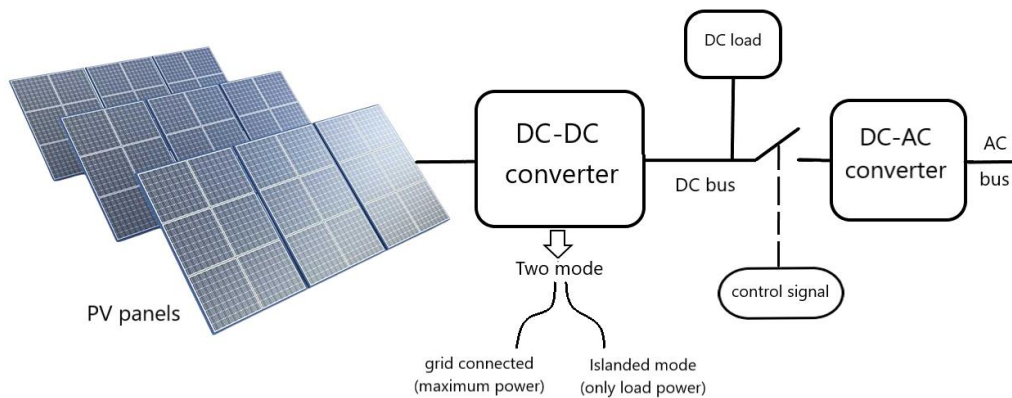


Figure 2.5: PV system included in DC microgrid

2.2.1.2 Converters

The key structure in microgrids in general and DC microgrids here are two main categories of converters used in DC microgrid, DC-DC converters to link between different DC voltage levels and AC-DC converters used to connect AC bus to DC bus. The converters that are used in DC microgrid can be unidirectional or bidirectional based power interacting between dc bus and different components. Fig. 2.6 shows the different converters in DC microgrids.

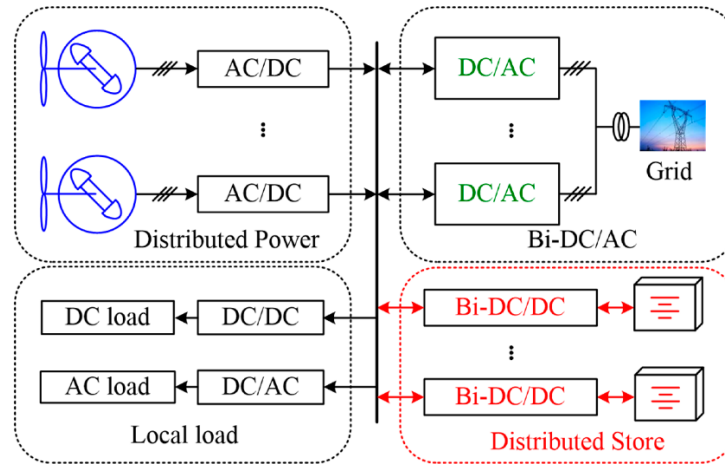


Figure 2.6: converters in dc microgrids. [11]

2.2.1.3 Loads

DC buses supply power to different kinds of loads, such as resistive load and Constant Power Loads (CPLs), which has negative impedance characteristics and may be induce limit cycle oscillations in microgrid voltage and current [12]; electric vehicles, which have two characteristics: first, as loads that may increase peak loads; and second, as energy storage; but in general, electric vehicles in effective cost management work without serious issues [13], and many more DC home appliances. On the other hand, AC loads are connected to DC buses through DC-AC converters. In terms of Electric vehicles are considered as load when charging and as power source when feeding backward the power to DC bus [14].

2.2.2 DC bus link, voltage level and polarity

The DC bus connects different loads and supply. Reliability, safety, energy efficiency, and cost savings should all be considered while choosing a voltage level. Line thermal restrictions, voltage drop, and power losses in the cables that connect local loads to the DC bus are hence some of the difficulties that must be considered [15].

Due to the absence of inductance and capacitance, which enhances voltage regulation, a DC microgrid often has a lower voltage drop than an AC microgrid. Reactive power and utility grid synchronization are also unnecessary [16]. In both residential and commercial applications, DC microgrids have different DC bus voltage levels ranging from 12V to 400V, which presents a

standardization and regulation difficulty. To choose a suitable voltage level, the voltage level comparison is displayed in the following table.

Table 2. 1: DC voltage level comparison.

Reference	DC Voltage level	Justifications
[17]	12 V	This voltage level is considered safe to work with, and DC appliances compatible with it are widely available on the market.
[18]	48 V for residential 400 V for commercial	Various voltage levels and a suitable power electronic interface for a dc system are examined in terms of efficiency, cost, and safety. Given the reduced power requirement, greater safety and efficiency. So, 48 V for best performance and 400 V for increased efficiency.
[19]	110 -120 V	In comparison to 48 V and 24 V, 110 V has a higher DC-DC converter efficiency. Suitable for home appliances and minimum optimal voltage level in line losses.
[20]	230 V	Related to the common 230 V AC voltage, most of appliance can work on this voltage level because of use of switched mode power supply, suitable to commercial loads and finally suitable voltage level for hybrid and electric vehicles chargers.
[21]	380-400 V	Aligned with the standards of the Emerge Alliance of buildings and can be easily compatible with the main grid. DC microgrid residential applications are a better fit. However, additional converters are required, and protection is required.

2.2.2.1 DC voltage bus polarity

Referring to the polarity of the DC microgrid, there are two configurations: the unipolar, which uses two wires, and the bipolar, which uses three wires. Fig 2.7 illustrates the unipolar and bipolar configuration of DC bus.

Unipolar configurations use two wires: one positive and the other negative, to construct the DC bus with a single voltage level, connecting all the components of the DC microgrid. In contrast, the bipolar configuration employs three wires, constructing a DC bus with three voltage levels (+V_{dc}, -V_{dc}, and 2 V_{dc}) using positive, negative, and neutral wires [22]. The bipolar configuration offers several advantages over the unipolar configuration, including improved stability, reliability, and flexibility. However, it also comes with increased costs and may require a voltage balancer in cases of unbalanced loads. Fig 2.7 illustrates the unipolar and bipolar configurations of DC microgrids [15].

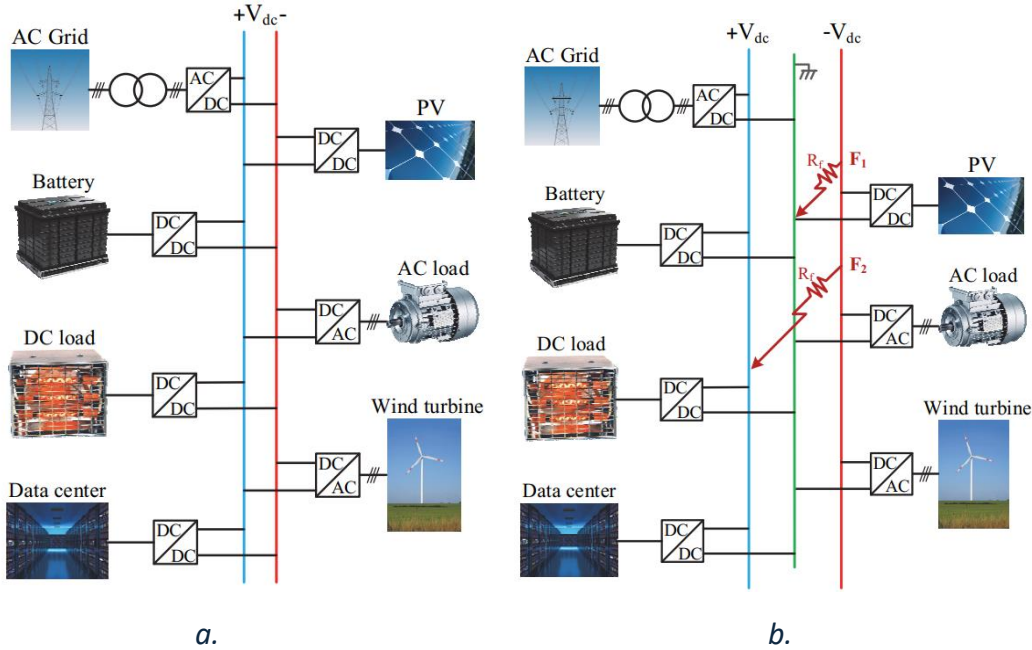


Figure 2.7: a) Unipolar dc bus. b) Bipolar dc bus. [23]

2.2.3 Architecture of DC MGs

DC microgrids have a distinct architecture that is determined by topology, polarity, and configurations. These DC bus properties were chosen based on their individual characteristics, which were influenced by the energy source and its capacity, load type and load profile, flexibility and reliability, cost constraints, energy management, and, finally, technological solutions [24].

The configuration of DC bus may take different types, as shown in Fig. 2.8:

- **Dual bus configuration:** this type is built based on using two buses connected to the DC/AC converter to increase the MPP (Maximum Power Point) and reduce the level of step-up of the voltage. Wang and others suggested a dual bus with two voltage levels, low voltage, and medium voltage, with a DC/DC converter to connect between two buses [25].
- **Radial bus:** most used in AC grids and most famous configuration in DC microgrid, that begin with source and end with user/load. This configuration is simple and robust [26].
- **Ring DC bus:** the ring connection that ties every microgrid component together is more reliable, flexible and fault management more than the previous configuration [27].
- **Meshed DC bus:** a framework made up of interconnected nearby sources and loads, Meshed networks may benefit power losses, voltage regulation, and network reliability [28].

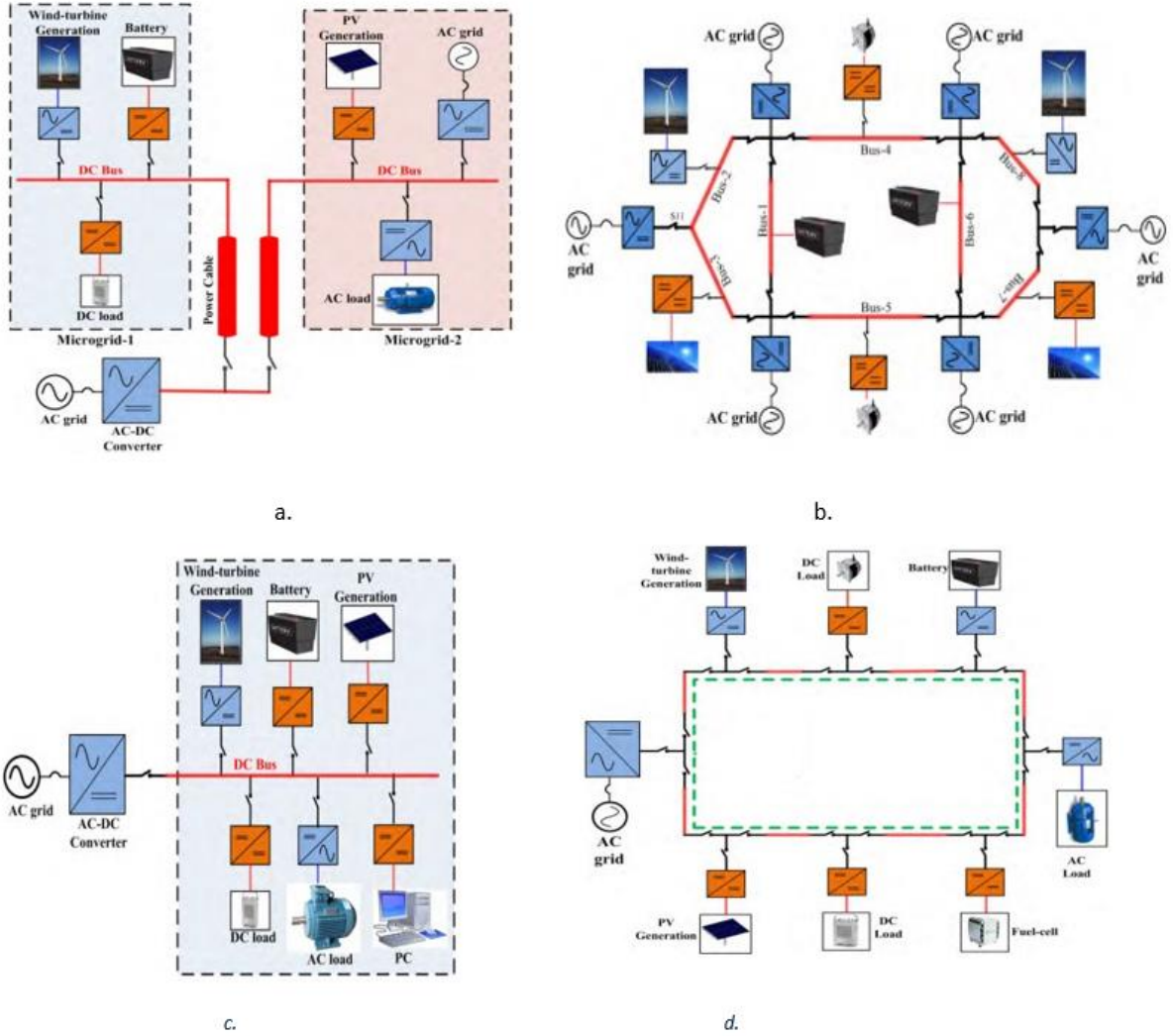


Figure 2.8: DC microgrid configuration: a) Dual bus, b) ring, c) Radial and d) Meshed. [29]

2.2.4 Challenges in DC microgrids

Like any new technology or idea there are numerous challenges that could impede the widespread adoption of DC microgrids. These challenges are summarized as following:

- Handling different operation modes can lead to voltage oscillations due to poor damping of DC microgrids. So, the design needed to be robust to handle different operational modes, faults, and dynamic loads to ensure resilience, reliability, and economic operability [30,31].
- The control and stability of DC microgrids are essential issues that need to be carefully studied to handle dynamic loads and faults [32].
- lack of standards, policies, and regulations related to DC microgrids [33]. A review of international standards will be summarized in section 2.4 of this thesis.

2.3 Power Electronics Converters in DC Microgrids

The main backbone of DC microgrids are power electronics devices that adjust and convert the power from a source (voltage or current source) to a desired value, type, and operating mode to serve different applications (loads or other sources). There are different types of converters that can be used in DC MGs, such as:

- Bidirectional AC-DC converters.
- Unidirectional and bidirectional DC-DC converters.

2.3.1 Bidirectional DC-AC converters

These converters are responsible for AC-to-DC conversion and vice versa to ensure bidirectional power flow between the utility grid and the DC bus. This converter is called an interlink converter and has different converter topologies that produce varying levels of quality and complexity. Choosing a suitable topology is mostly determined by the application's requirements. Fig. 2.9 shows the different topologies of these converters.

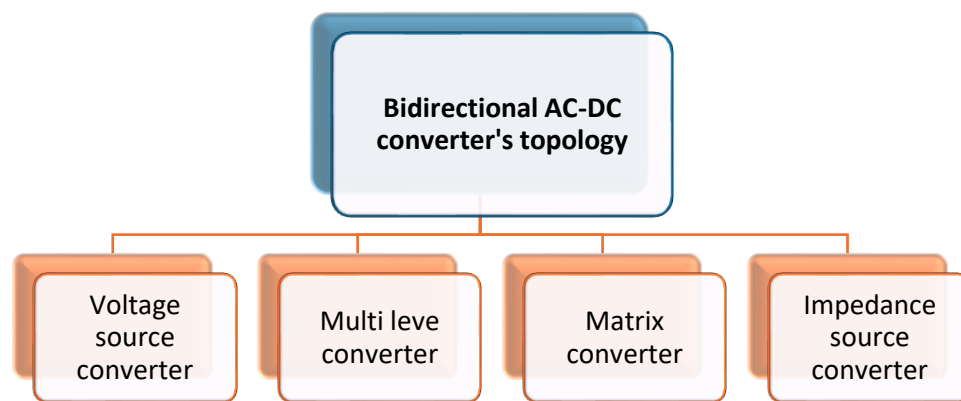


Figure 2.9: Bidirectional AC-DC converters different types.

The most famous topology is the voltage source converter (VSC) the circuit diagram shown in Fig 2.10.a and interaction between the PV system and utility grid using AC-DC converter shown in Fig. 2.10.b, which has been used in this thesis. In DC microgrids with low voltage (< 500 V), the VSC converts AC to DC electricity in rectifiers using boost mode (step-up) and DC to AC in inverters using buck mode (step-down). To accomplish the desired AC output with the grid, as well as the DC output for inverters and rectifier modes, an additional structure for voltage regulation is required.

One of the most essential parts of renewable grid connectivity is the adoption of conversion control systems. Inverters in general and voltage source inverters in specific must meet grid criteria and international standards for interconnection, including voltage and power regulation.

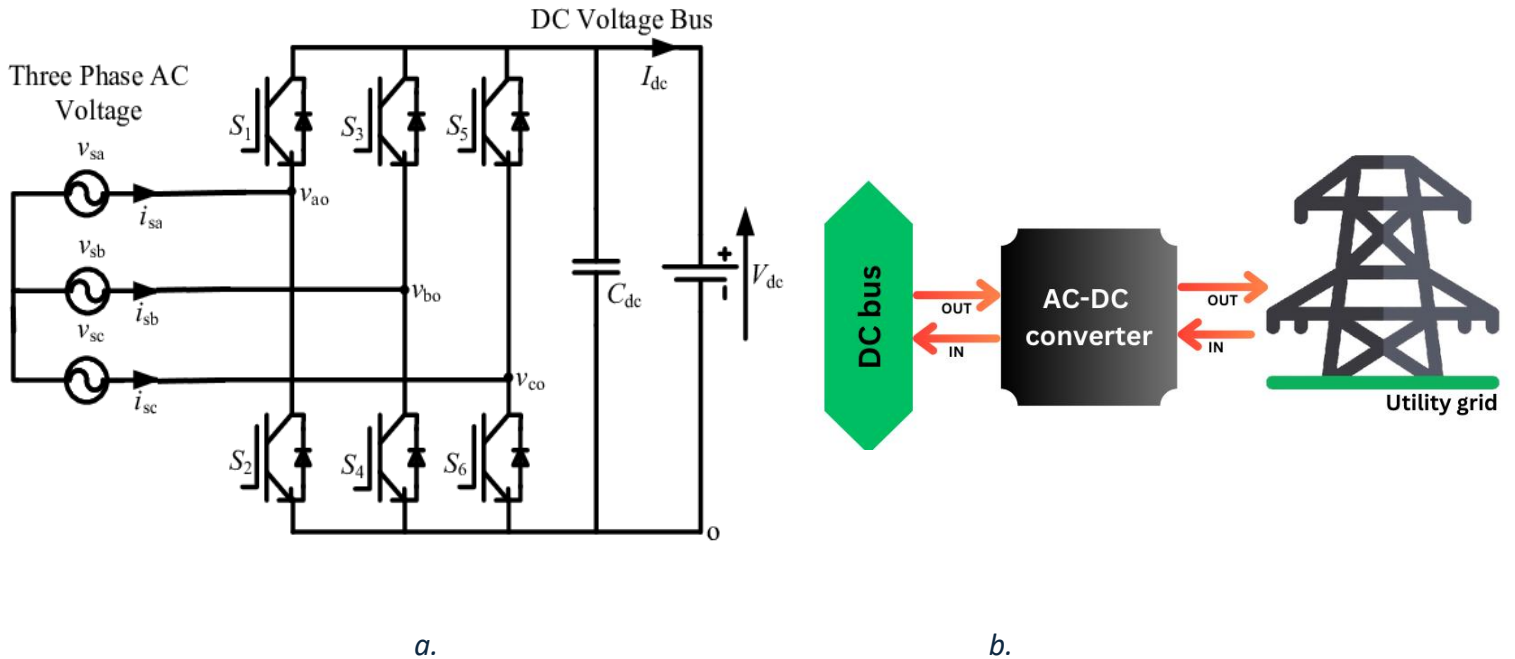


Figure 2.10: a) VSI circuit diagram. b) AC-DC converter ties between grid and DC bus

Various control techniques and controllers are used for the optimal operation of AC-DC converters, manipulating different aspects of their operation. These aspects can be summarized as follows:

- Synchronization with the main grid (including frequency matching) [34].
- Output current control [35].
- Output voltage control [36].
- Real reactive power control [37].

Also, there are new modern control approaches such as Artificial Neural Networks [38] and Fuzzy Logic Controllers [39].

In this thesis, the focus is exclusively on the controller of a bidirectional AC-DC converter. The thesis controller is based on a direct-quadrature (dq) controller with a phase-locked loop (PLL) as the synchronization controller and space vector pulse width modulation (SVPWM) as the modulation technique.

dq control is used to manage the output voltage and current by regulating both the amplitude and phase of the AC output. The d and q axes help control the real and reactive voltage and current components independently, decoupling the real and reactive power control. The basics of dq control depend on the transformation to a dq frame, which converts the sinewave AC three-phase signal into DC signal with a rotating reference frame, which is easier to control. This process uses Clarke and Park transformations. The Clarke transformation converts three-phase AC quantities

into two-phase quantities ($\alpha\beta$), and the Park transformation then converts these into a rotating reference frame (dq) [40].

The PLL, which is a feedback control system that synchronizes the phase and frequency of the converter's outputs with a grid, consists of three main components as shown in Fig2.11, a phase detector that compares the phase of the converter output with the grid and calculates the phase error signal. Second, a loop filter that removes high-frequency noise, and finally, a voltage-controlled oscillator that adjusts the frequency and phase of the converter based on the filtered error signal [41].

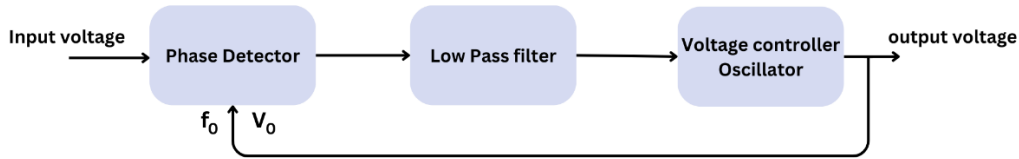


Figure 2.11: PLL for AC-DC converter.

SVPWM is a control method used to control the voltage of the converter by representing the three-phase voltages as vectors in a two-phase voltage using Clarke's transformation, which results in vector representation in the α - β plane. This plan is divided into six sectors, each of them defined by two adjacent active vectors and two null vectors. And the position of the space vector determines which sector it is in, and then the sector identification is determined by adjacent active and null vectors. SVPWM approximates the desired output voltage using adjacent vectors. Time calculation is done by solving linear equations to determine pulse widths. PWM signals are generated to produce the desired output voltage [42]. The space vector diagram is shown in Fig. 2.12.

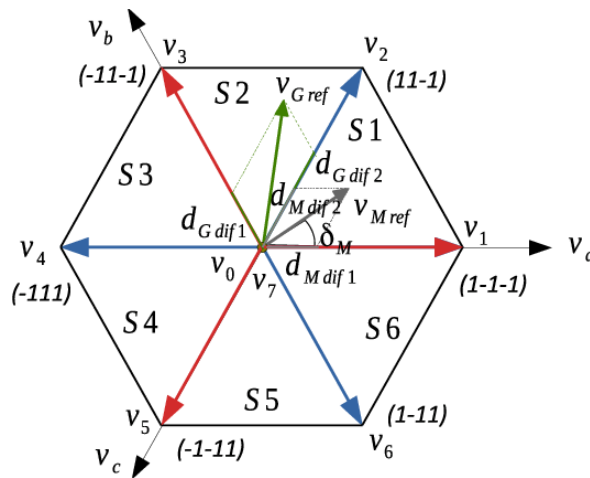


Figure 2.12: SVPWM vectors diagram [43].

2.3.2 DC-DC converters

This kind of converter is used in many applications to convert the DC voltage from one level to another as shown in Fig. 2.13. There are three categories of classification of DC-DC converters: first, the power flow direction; second, the topology of the converter; and finally, based on the use isolated or non-isolated circuit either by use transformer or not.

There are two types of converters based on the direction of power flow: unidirectional and bidirectional converters. The unidirectional system supplies power from one source to the load or another source in one direction, while the bidirectional system transfers power between the two sources in both directions. The figure below illustrates the power flow in both types of converters.

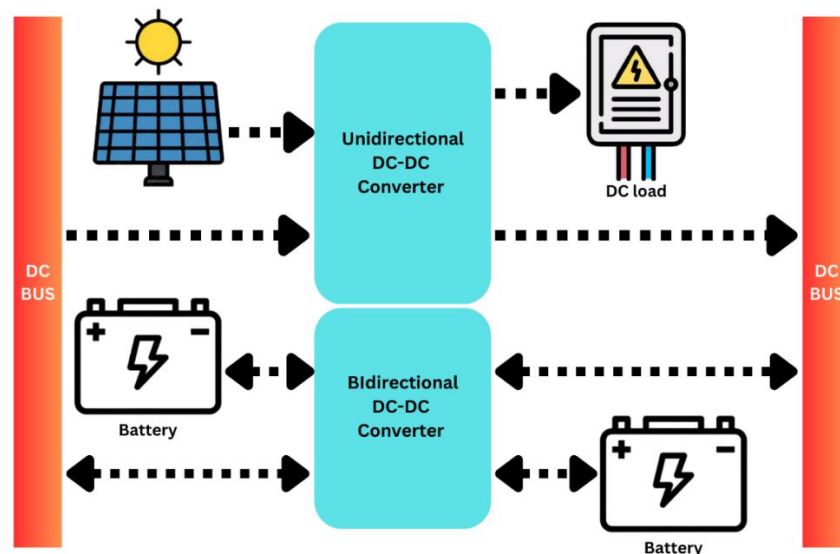


Figure 2. 13: DC-DC converters power flow.

On the other side, there are many configurations of DC-DC converter circuits that vary based on specific requirements of the application, such as voltage and power level, flow direction, efficiency, isolation level, and control complexity. Mainly, the topologies that will be discussed here are the unidirectional and bidirectional converters.

2.3.2.1 Unidirectional converters

The most famous and commonly used topologies belong to this type of converters some of these topologies are shown in Fig. 2.14. The main topologies are:

- Buck Converter
- Boost Converter
- Buck Boost Converter
- Cuk Converter
- SEPIC Converter
- Zeta Converter
- Flyback Converter
- Forward Converter
- Push-Pull Converter
- Other Topologies

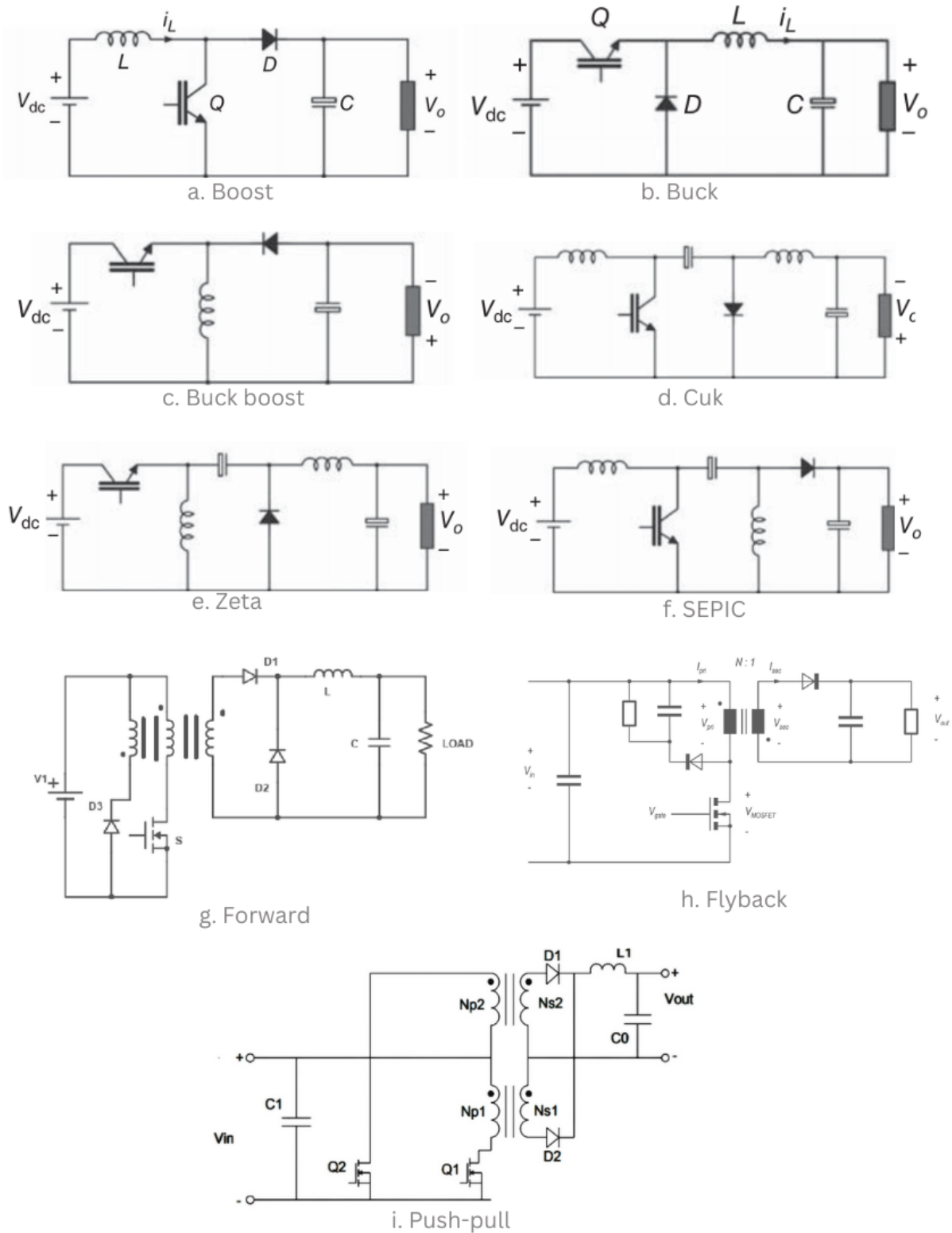


Figure 2.14: DC-DC converter topologies circuit: a) Boost. b) Buck. c) Buck-boost. d) Cuk. e) Zeta. f) SEPIC. g) Forward. h) Flyback. i) Push-pull.

The unidirectional DC-DC converter used is a buck-boost converter with a modified circuit suitable for two modes of operation. Fig. 2.15 shows the circuit for the proposed buck-boost converter.

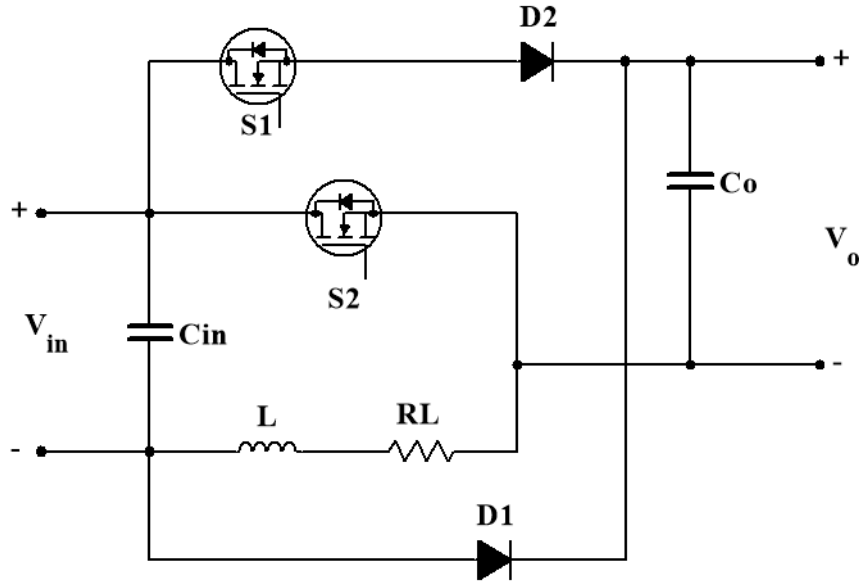


Figure 2.15: Proposed buck-boost converter circuit diagram.

This circuit uses two switches, two diodes, and a single inductor. It is more efficient than traditional buck-boost due to fewer conduction and switching losses, and it can work in buck, boost, and buck-boost modes. The special advantage of this topology is that each switch can work with the same or different duty cycles, which makes the converter work like two stages of converters. This feature gives the converter an advantage in handling different modes of operation [42]. So, the voltage conversion ratio for the buck-boost converter is:

$$V_o = \frac{D_1}{1 - D_2} V_{in}$$

Where $D_1 = D_2$ in buck boost mode, $D_1 = 1$ in boost mode and $D_1 = 0$ in buck mode.

Table 2.2 shows the switching scheme of the buck-boost converter with which semiconductor devices are conducting at which subinterval.

2.3.2.2 Bidirectional converters

Bidirectional DC-DC converters are suitable for battery management systems and widely used in electric vehicles and charging equipment. Compared with the traditional DC-DC converter, the bidirectional converter works flexibly, has a fast response, and high efficiency. The bidirectional converters have different topologies with various properties [44], Fig. 2.16 shows some of these circuits.

Table 2. 2: Switching scheme of buck-boost converter.

Mode	Subinterval	Switching mode		Conducting semiconductor
		S1	S2	
Buck	Subinterval 1	ON	OFF	S ₁ , D ₂
	Subinterval 2	OFF	OFF	D ₁
Boost	Subinterval 3	ON	ON	S ₂
	Subinterval 4	ON	OFF	S ₁ , D ₂
Buck-boost	Subinterval 5	OFF	ON	S ₁
	Subinterval 6	OFF	OFF	D ₁

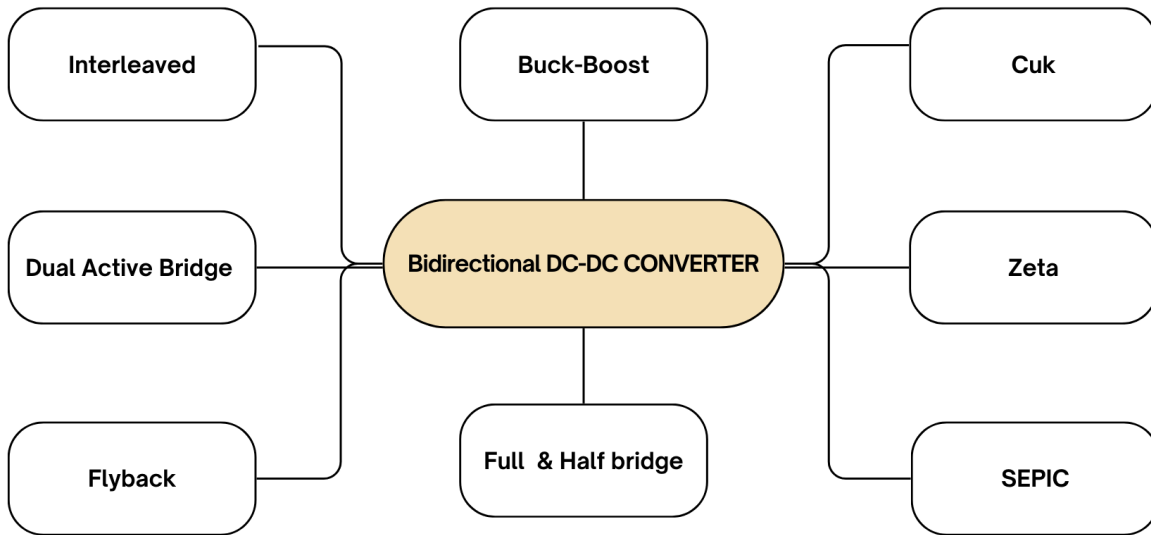


Figure 2.16: Bidirectional DC-DC converter types.

The most used topology for bidirectional DC-DC converters is the bidirectional buck-boost converter because of its simplicity and high efficiency. It has two modes of operation: step-up and step-down. During the step-up operation, switch S₂ is conducted according to the duty cycle, whereas S₁ will not be conducted in this mode. In step-down mode, S₁ will conduct according to the duty cycle, and S₂ will not conduct in this mode. The circuit diagram for this converter is shown in Fig. 2.17.

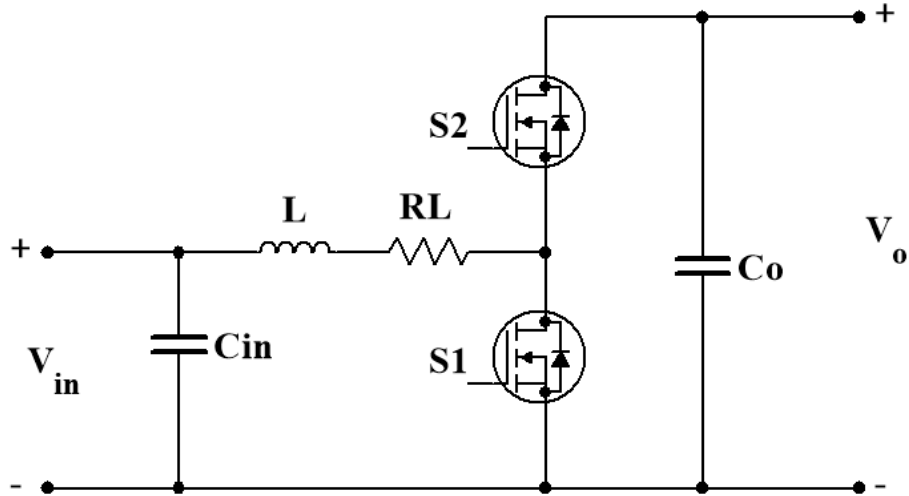


Figure 2.17: Bidirectional buck-boost converter circuit.

2.3.2.3 Maximum power point tracking (MPPT) techniques for DC-DC converters

Due to the widespread adoption of PV solar systems due to the relatively higher PV panel efficiency, a technique called MPPT was introduced to extract the highest possible amount of power from the PV panels. There are many types of MPPT implemented in DC-DC converter controllers, as shown in Fig. 2.18.

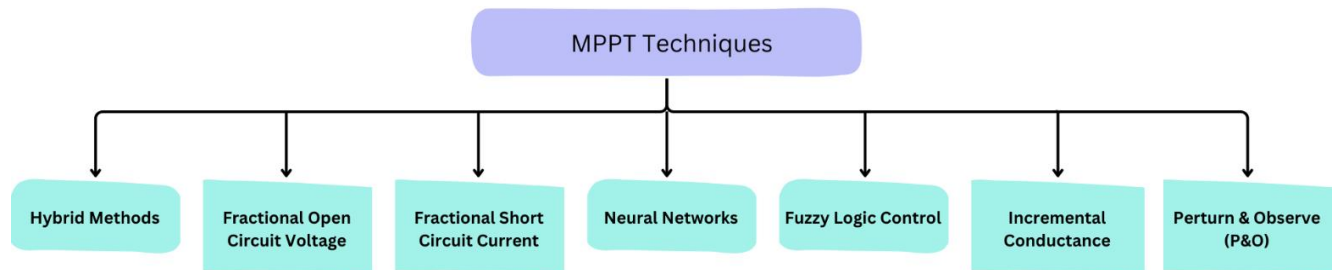


Figure 2.18: MPPT techniques.

- Perturb and Observe (P&O): Also known as the hill-climbing approach, this technique perturbs the operating voltage and measures the resulting power. If the power increases, the perturbation remains in the same direction; otherwise, it reverses.
- Incremental Conductance (IncCond): This approach computes the incremental changes in current and voltage to identify which direction the maximum power point (MPP) sits. It is more precise than P&O in quickly changing situations.
- Fractional Open Circuit Voltage (FOCV): This method calculates the MPP voltage as a fixed proportion of the open-circuit voltage. It's straightforward, but less accurate than other ways.

- Fractional Short Circuit Current (FSCC): Like FOCV, this approach calculates the MPP current as a fixed proportion of the short-circuit current.
- Neural Networks: These employ artificial intelligence to forecast the MPP based on past data and current inputs. They are capable of handling complex and nonlinear interactions, but they require substantial training.
- Fuzzy Logic Control: This method uses fuzzy logic to deal with the PV system's uncertainties and nonlinearities. It is durable and can adapt to changing environments.
- Hybrid Methods: These integrate two or more strategies to maximize their respective strengths. For example, merging P&O with neural networks can boost accuracy and response time.

The Perturb and Observe (P&O) method employs a straightforward feedback system with minimal observable parameters. It works by periodically adjusting the duty cycle that controls the array current, either increasing or decreasing it, and comparing the resulting PV output power to that of the previous cycle. If the perturbation leads to an increase (or decrease) in array power, the next perturbation will follow the same direction. This peak power tracking technique continuously searches for the maximum power point [45]. Fig. 2.19 illustrates the algorithm and operational concept of the P&O technique.

The MPPT algorithm explained in the following steps that shown in Fig. 2.19 [45]:

1. The suggested MPPT algorithm uses the PV module's current VPV and IPV as input signals. The variables "Flag_start" and "Flag_reset" are both set to 1 for rapid tracking speed at the beginning point of $VPV = VOC$ and to set the PMPP and VMPP to the current PPV and VPV, where $PPV = VPV \cdot IPV$, respectively.
2. The operational point is identified as being at the beginning of $VPV = VOC$ if Flag_start is 1. Consequently, the operating point soon approaches the MPP, and the reference variable (V_{ref}) is originally set to $1/VPV (=1/VOC)$. Flag_start is then set to zero.
3. This procedure computes PPV as $VPV \cdot IPV$, computes ΔPPV and ΔVPV using current (PPV and VPV) and past (PPV_b and VPV_b) values, then computes the slope coefficient (S) as $|\Delta PPV / \Delta VPV|$.
4. PMPP and VMPP are set to the current PPV and VPV if Flag_reset is set to 1, and Flag_reset is set to 0 otherwise.
5. It is concluded that the MPP has not yet been discovered if the current PPV is greater than PMPP. Consequently, PMPP and VMPP are reset to the current PPV and VPV, and the operating point is compelled to continue moving in the direction of the MPP. The variable step size ($=k1 \cdot S \cdot V_{step}$) is employed in this procedure to rapidly determine the MPP.

6. The small fixed step size ($=k_2 \cdot V_{step}$) is utilized to precisely track the MPP if the operational point is situated within the MPP region.
7. The operating point is identified as being in the non-MPP zone if the PPV is less than the border value ($\beta \cdot P_{MPP}$) between the MPP and non-MPP regions. Because the MPP varies in dynamic weather, this procedure is typically carried out in such circumstances. For a quick dynamic response, the variable step size ($=k_1 \cdot S \cdot V_{step}$) is automatically modified based on the slope of $\Delta P_{PV} / \Delta V_{PV}$, and $Flag_reset$ is set to 1 to locate a new MPP.
8. To avoid DC-DC converter malfunction, V_{ref} is restricted by its maximum and minimum values ($V_{ref,max}$ and $V_{ref,min}$).
9. A fresh V_{ref} is acquired through the procedures. To regulate the DC-DC converter, a new duty ratio (D) is created by comparing V_{ref} with the carrier signal ($V_{carrier}$).

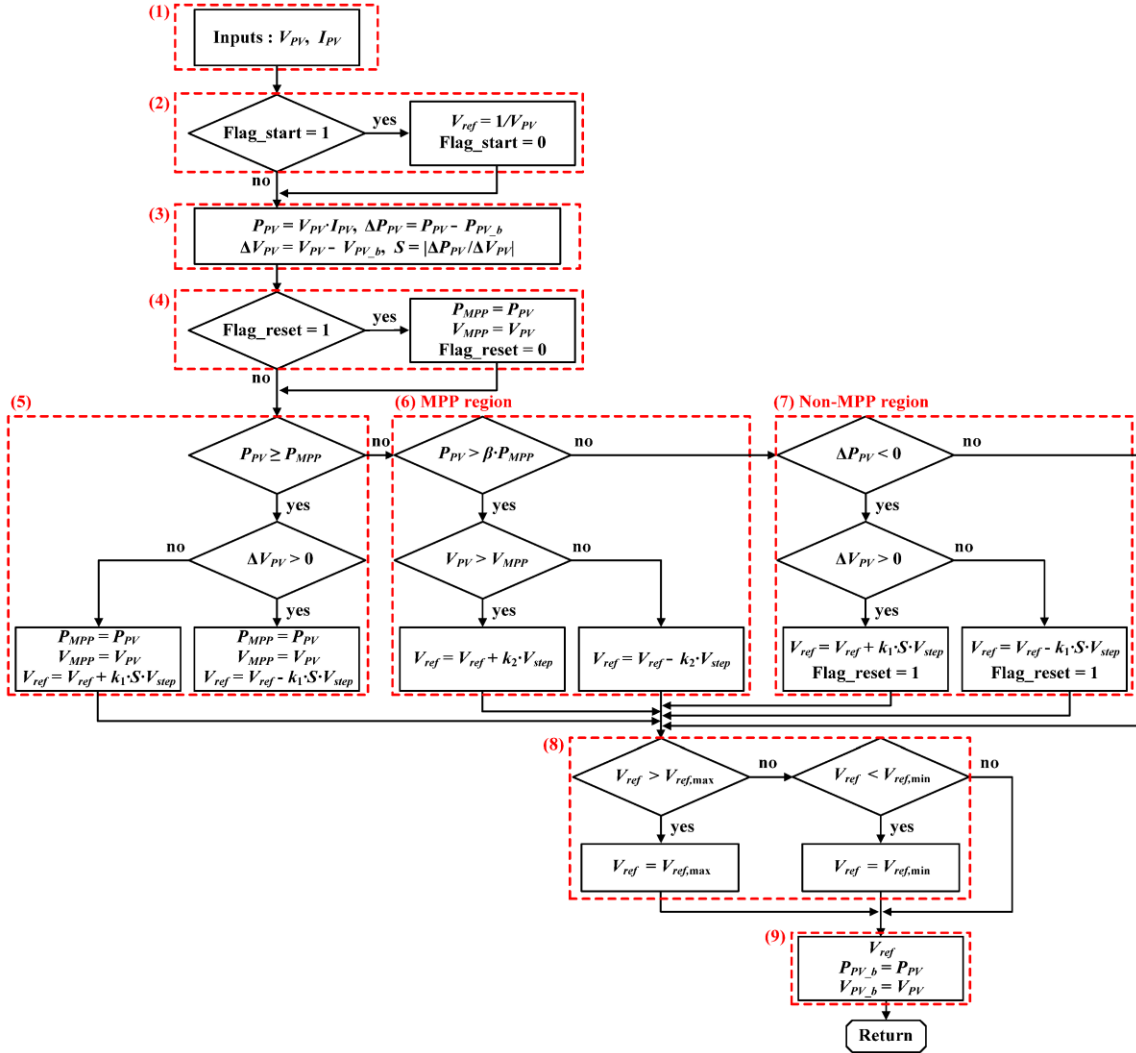


Figure 2. 19: Working principle of P & O algorithm [45].

2.4 Review of Standards and Regulations Related to DC Microgrid

The dominance of AC voltage on electrical networks and their high dependency on AC have greatly impacted and delayed the development of standards and regulations that provide a general framework for DC networks and DC voltage. But after developing DC transmission lines and huge progress in the technology of inverters and storage batteries, as well as the high penetration of renewable energy resources and electric vehicles, there is an urgent need for standards that regulate the networks, devices, and systems that use DC voltage, including DC microgrids.

The leading institution in electrical standards, the Institute of Electrical and Electronics Engineers (IEEE), developed standards that provide guidance for the technical specifications and testing of the interconnection and interoperability between utility electric power systems (EPSs) and distributed energy resources (DERs) and were published as IEEE 1547-2018 (under the name IEEE Standard for Interconnection and Interoperability of Distributed Energy Resources with Associated Electric Power Systems Interfaces) [46].

Also, there is another standard, IEC/IEEE 80005, that describes “low-voltage DC shore connection systems up to and including 1500 V DC. It applies onboard the ship and on shore to supply the ship with electrical power from shore”, focusing on the design, installation, and testing of DC shore distribution systems and shore-to-ship connection and interface equipment [47].

In pursuit of its 2030 vision, the IEEE published the IEEE 2030™ family of standards, which provide a road map for integrating power, communications, and information technologies in the present and future. The standards lay out the integration protocols for DER operations and smart-grid interoperability, with a focus on sustainability. Specifically, in 2021, the IEEE published the IEEE 2030.10 standard (Distribution Resources Integration Working Group/Remote DC Microgrid), which addresses the design, operation, and maintenance of a DC microgrid for rural or remote applications. It also specifies the standards for providing low-voltage DC and AC power to off-grid loads. Moreover, IEEE 2030.10 proposes a bottom-up, scalable DC power system, eliminating the need for centralized power production and distribution. The standards focus on safety in DC voltage and specify 48 VDC as the maximum utilization voltage for efficiency and safety; consider a higher voltage level in negotiations between providers of power and loads; and suggest a voltage of 380 V with an underground distribution system [48].

Also, many related standards in IEEE 2030 series discuss different issues related to new power trends including control, automation and protection of microgrids such as:

- [IEEE P2030™](#) – Guide for Interoperability of Energy Technology with the Electric Power System (Revision of IEEE 2030™-2011).
- [IEEE 2030.7™-2017](#) – Standard for the Specification of Microgrid Controllers.
- [IEEE 2030.8™-2018](#) – Standard for the Testing of Microgrid Controllers.
- [IEEE 2030.11™-2021](#) – Guide for Distributed Energy Resources Management Systems (DERMS) Functional Specification.

- [IEEE 2030.4™-2023](#) – Guide for Control and Automation Installations Applied to the Electric Power Infrastructure.
- [IEEE P2030.12™](#) – Draft guide for the Design of Microgrid Protection Systems.
- [IEEE P2030.13™](#) – Draft guide Functional Specification for an Electric Transportation Fast Charging Station Management System.
- [IEEE P2030.14™](#) – Draft Guide for Functional Specifications for Alternate and Multi-Source Generation in Virtual Power Plants.

The European standard ETSI EN 300 132-3-1 covers low-voltage DC systems. It is mostly used for data and telecom equipment that requires power levels up to 400 V. IEEE Standard 946 outlines suggested practices for direct current auxiliary power systems. It was initially intended for battery-based DC auxiliary power systems in generation stations, but it can also be utilized in DC microgrids. Other standards, such as IEC SG4, are being developed to offer specifications for LVDC distribution systems with voltages up to 1500 V [49].

The IEEE 1547.4-2011 categorized the operating conditions of distributed resource island systems as follows [50]:

- Grid-connected (normal parallel operation).
- Islanded (operating without grid).
- Transition to island (grid-connected to islanded).
- Reconnection mode (islanded to grid-connected mode).

2.5 DC Microgrid Stability (Dynamic Stability)

Any power system's stability can be defined as its ability to return to equilibrium after some form of disturbance. There are two types of disturbances: large disturbances that cause huge changes in the system, such as faults, and small disturbances that cause minor changes in the system and are more likely to happen, such as small load variations and switching operations, and the system must habituate them easily. In terms of stability, there are three types: steady state, transient stability, and dynamic stability [51].

Steady state stability: It refers to the system's ability to recover to equilibrium after slight slow changes in load or generation.

Transient stability: refers to the response of the system to large disturbances, which may cause huge changes in the behavior of the system.

Dynamic stability: the stability response to deal with minor fluctuations or pauses that occur more frequently but have fewer serious consequences such as interconnection between control systems.

Stability as mentioned before refers to the robustness of a system to remain functional or recover

to a desirable state following disturbances. In the context of power electronics and microgrids, dynamic stability is a major issue and especially critical as the adoption of power electronic-interfaced technologies grows, resulting in increasingly complicated and fast-response dynamics [52].

One of the important characteristics of a DC microgrid is maintaining a voltage level within an acceptable range and close enough to the nominal value. The capacity to maintain or restore supply and demand balance is known as voltage stability. Voltage instability results in a reduction or increase in voltage at the DC bus, which can cause outages and load losses. [52].

The stability and robustness of DC MG depend on the performance of the power electronics converters. There are different kinds of control strategies to improve their stability and performance in both grid-connected and islanded operation modes. By keeping the microgrid's voltage levels appropriate during the islanding process to enable a safe transition, the used controllers are meant to increase microgrid resilience. In any case, instability issues may arise from this very strong disturbance, particularly for microgrids with little to no inertia. Indeed, significant transients can result from an unplanned interruption of the main grid supply, putting the system in the stability area's insecure operating point in less than a second. [53].

2.6 DC Microgrid Operation Modes Transition Control

There are two types of control that can be considered to reduce transients during a transition process [54]:

- One level of control is used to operate and plans for both modes of operation using a single control scheme that remains in service during the two modes.
- Two control levels: one before and one after the transition to grid-connected mode. Additional mechanisms are used during the transition.

Most one-level controllers are based on nonlinear control theory, such as the Lyapunov control method and model predictive control. These methods primarily require a precise model of the system and the dynamic behavior of distributed energy resources. These controllers have complex structures with highly computational behavior, challenging real-life implementation. In contrast, two-level control schemes use different control strategies, with each mode activated based on the operation mode. These techniques are often specific to each microgrid and cannot be easily generalized [55].

The transition between operation modes has special requirements, such as synchronization, interconnection switch closing, power flow control, and stabilization in both the microgrid and main grid before, during, and after the transition process. This is known as seamless transfer [56].

While the DC microgrid achieves faster stability than the AC microgrid when the fault is cleared, especially when connected to a weak grid, the essential concepts behind the stability of conventional energy supply and the microgrid are identical. Due to the high degree of penetration

of DG sources and the accompanying converters, the dynamics and control of the converters are the origin of or have a substantial impact on microgrid stability problems. Various methodologies are utilized to evaluate and forecast microgrid stability and provide systematic tools for building microgrid controllers. A small-signal and time-domain simulation is commonly employed for inclusive stability analysis [57].

Some researchers investigate the impact of microgrids on the main grid during the transition between grid-tied and islanded modes. By classifying control schemes into inverter control and microgrid control, the study highlights that seamless transitions can be achieved through either approach. Which focuses on primary control loops for inverter control, demonstrating that smooth transitions are possible when all inverters maintain acceptable deviations in voltage magnitude and phase, frequency, and power angle, which collectively determines power sharing on the grid. In contrast, microgrid control explores decentralized, centralized, and distributed control strategies and concludes that distributed control offers the most effective means for achieving seamless transitions. And finally, it presented some future methods that may be used to achieve resilient microgrids [58].

A review of different control methods for DC microgrid summarized in Fig.2.20.

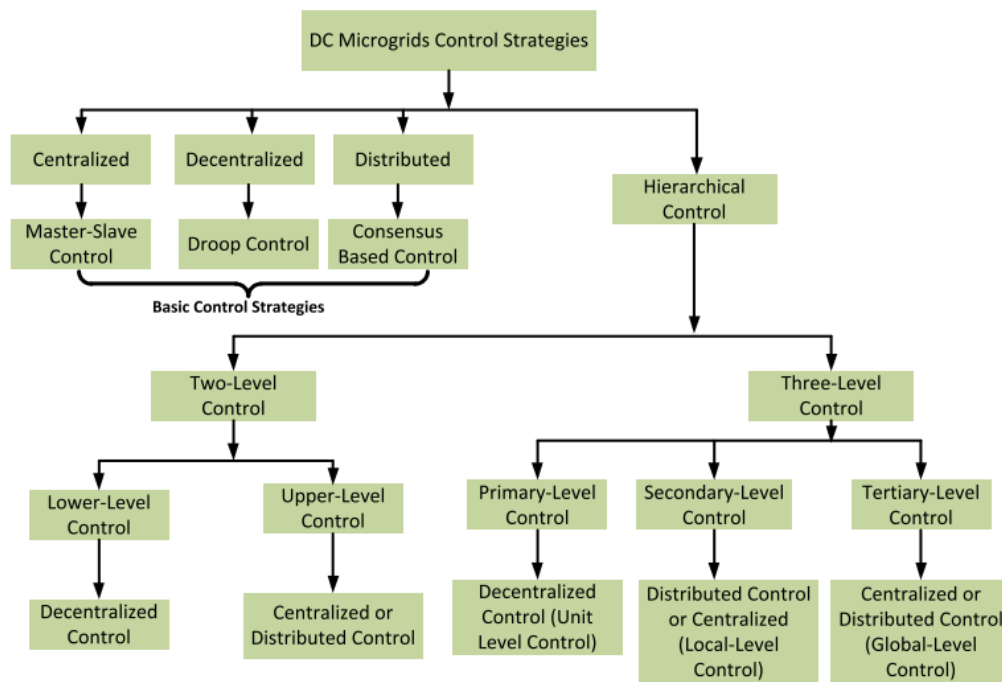


Figure 2.20: control strategies of DC microgrid [59].

For a seamless transition between the voltage controller (islanded) and current controller (grid-connected), mode switching is essential. Current control uses the grid as a reference for voltage and frequency. The current controller creates current references according to the desired power set point (P_{ref} and Q_{ref}). In contrast, the voltage controller must balance local generation and load

requirements while internally generating references in the event of island operation. The voltage controller oversees the synchronization process that enables the microgrid to be linked to the grid and black start, which is the initial start-up without the grid [60].

A bumpless control was proposed to achieve stability & smooth transition from island mode to grid mode & vice versa [54]. While others proposed an adaptive droop control method to accomplish accurate control, the virtual impedance value is altered adaptively [8].

Master-slave strategy control method proposed for smooth transition which has master controller that work as voltage source to control the DC bus voltage and the rest of converters works as slave converter as current source converters, the paper contribution based on use peer to peer control that represent in I- Δ V droop control [61].

Chapter 3: DC microgrid modeling

3.1 Introduction

Designing a new solution for any real-world problem requires modeling to test, predict, and improve the solution. Various modeling methods, such as mathematical modeling, can effectively represent the DC microgrid. For optimal control problems, the state space modeling technique is used, while transient responses are studied using the transfer function approach, which is recommended over all other modeling methods. Once a mathematical model has been developed for the given system, numerous computational methods can be employed for synthesis and analysis.

Fig. 3.1 displays the major parts of a DC microgrid. It is made up of a DC load, a PV system, and a utility grid connection. Through their power converters, each component is linked to the microgrid's shared DC bus. The efficiency of the converters is disregarded in order to simplify the DC microgrid system. Modeling converters often involves state space averaging. It is common to choose the energy storage elements as the state of the system, which includes current for inductors and voltage for capacitors [62].

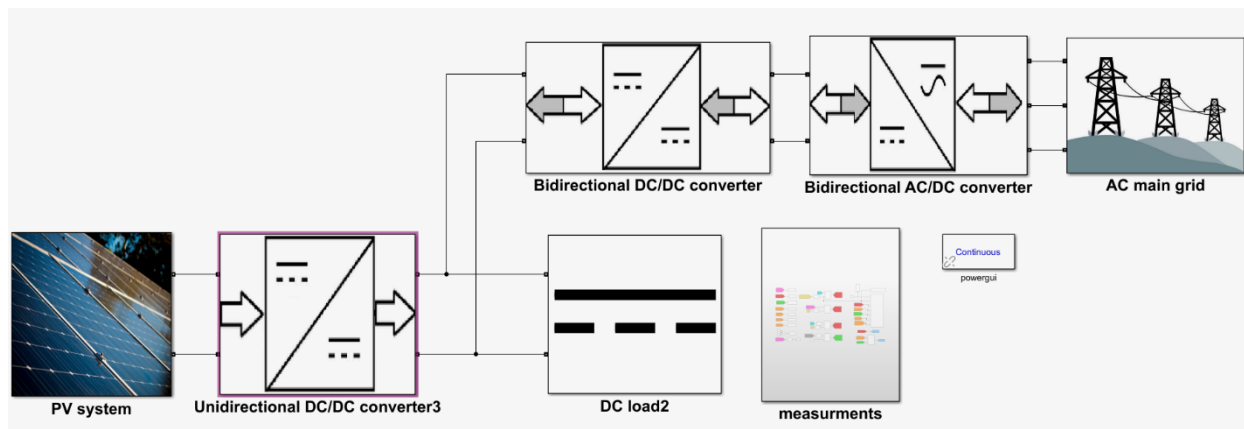


Figure 3.1: DC microgrid modeling main component

State space model is a mathematical representation of a physical system that is expressed as a collection of variables, inputs, and outputs linked by different equations or first-order differential equations. The state-space average model is frequently used for modeling PWM converters. However, this modeling method requires operating under conditions of low frequency, small ripple, and the small-signal hypothesis [63]. Fig. 3.2 shows the block diagram for linear space equations, while Eq. 3.1 shows state space equations.

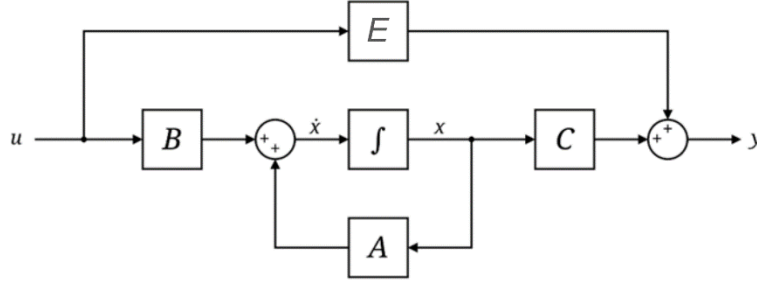


Figure 3. 2 Block diagram representation of the linear state-space equations

$$\begin{aligned} \dot{x} &= Ax + Bu \\ y &= Cx + Eu \end{aligned} \quad (3.1)$$

Where:

\dot{x} : is called the state vector.

y : is called the output vector.

u : is called the input (or control) vector.

A : is the state (or system) matrix.

B : is the input matrix.

C : is the output matrix.

E : is the feedthrough (or feedforward) matrix (is null matrix in most of the systems).

The following equation represents the state space with two modes of operations. (where D : represents the present state and $(1-D)$ represents the next state)

$$\begin{aligned} \dot{x} &= \{A_1D + A_2(1 - D)\}x + \{B_1D + B_2(1 - D)\}u \\ y &= \{C_1D + C_2(1 - D)\}x + \{E_1D + E_2(1 - D)\}u \end{aligned} \quad (3.2)$$

Where A_1, B_1, C_1 & E_1 are state space matrices for present state and A_2, B_2, C_2 & E_2 for the next state. The transfer function using state space matrices shown in Eq. (3.3) below:

$$\frac{y(s)}{u(s)} = \frac{Vo(s)}{Vin(s)} = C[SI - A]^{-1}B + E \quad (3.3)$$

3.2 Utility Grid

The utility grid can be represented by a steady-state, constant voltage source with infinite power capacity that can supply or absorb power in both directions to and from the microgrid. The microgrid is connected to the main grid during the grid-connected mode of operation and can work as a power supply source in case the distributed generation in the microgrid can't supply enough power to cover the load. On the other hand, the grid works as an AC bus to absorb extra power in the microgrid, but in the islanded mode, the utility grid is disconnected and has no effect on the

microgrid. Fig. 3.3 below shows the main grid model that consists of three single voltage sources that are connected to generate an AC bus with constant voltage and frequency values (380 V and 50 Hz).

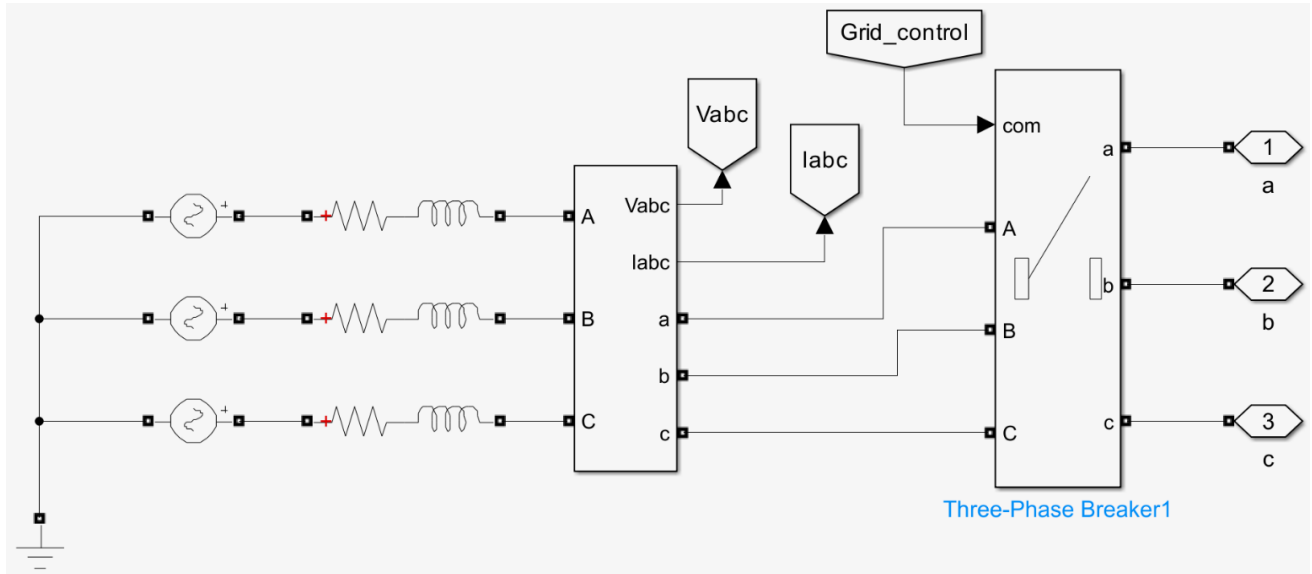


Figure 3. 3: Main grid model.

The grid voltage is given by the following equations:

$$V_a = V_m \cos \theta \quad (3.4)$$

$$V_b = V_m \cos(\theta - 2\pi/3) \quad (3.5)$$

$$V_c = V_m \cos(\theta + 2\pi/3) \quad (3.6)$$

$$\theta = \omega t + \varphi_v \quad (3.7)$$

Where: V_a , V_b & V_c : the three phase voltages. θ : is the phase angle

The grid voltage V_α and V_β are represented after Clarke transformation:

$$V_{\alpha\beta} = V_\alpha + j V_\beta = \frac{2}{3} (V_a + V_b e^{j\frac{2\pi}{3}} + V_c e^{-j\frac{2\pi}{3}}) = V_m e^{j\theta} \quad (3.8)$$

3.3 PV System

The most common type of renewable energy source is the PV solar system, so a PV solar system model was constructed as shown in Fig.3.4 with total power of 41.175 kW_{peak} of PV panels with unidirectional DC/DC converter. Table 3.1 shows the specifications of the PV solar system that is connected to DC bus.

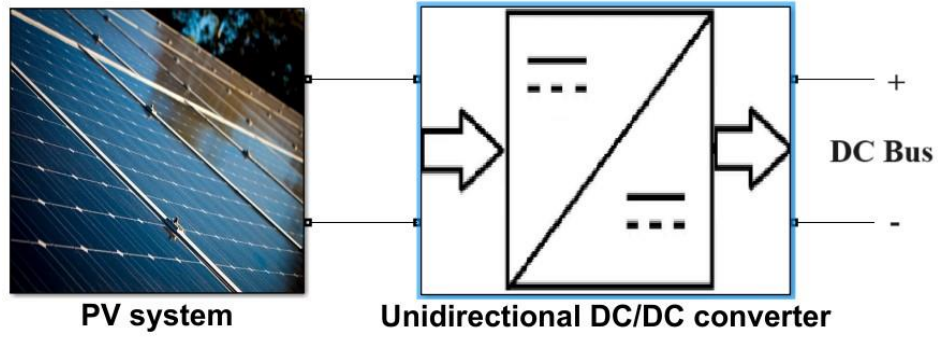


Figure 3. 4: PV solar system simulation model

Table 3. 1: characteristics of PV solar system.

Solar irradiance	1000 W/m ²
Cell temperature	25 °C
Rating voltage of each panel	36.1 V
Rating current of each panel	8.45 A
Power rating of each panel	305 watts
PV series connected panels in each string	5 panels
Parallel PV strings	27 strings
Total power of PV system	41.175 kWpeak

The characteristics curves of the solar system (P-V & I-V curves) are shown in Fig. 3.5.

The mathematical model of PV module based on the following equations:

$$I_{Module} = I_{cell} = I_{SC} - I_o(e^{(38.9V_d)} - 1) - \frac{V_d}{R_P} \quad (3.9)$$

$$V_{module} = n(V_d - I_{cell}R_s) \quad (3.10)$$

Where:

I_{SC} : short-circuit current (A).

V_{module} : output voltage (V)

I_o : reverse saturation current (A)

R_s : series resistance (Ω)

R_P : shunt resistance (Ω)

n : number of cells in the module.

V_d : diode voltage (V).

V_d : Diode voltage.

I_{cell} : current output of PV cell (A)

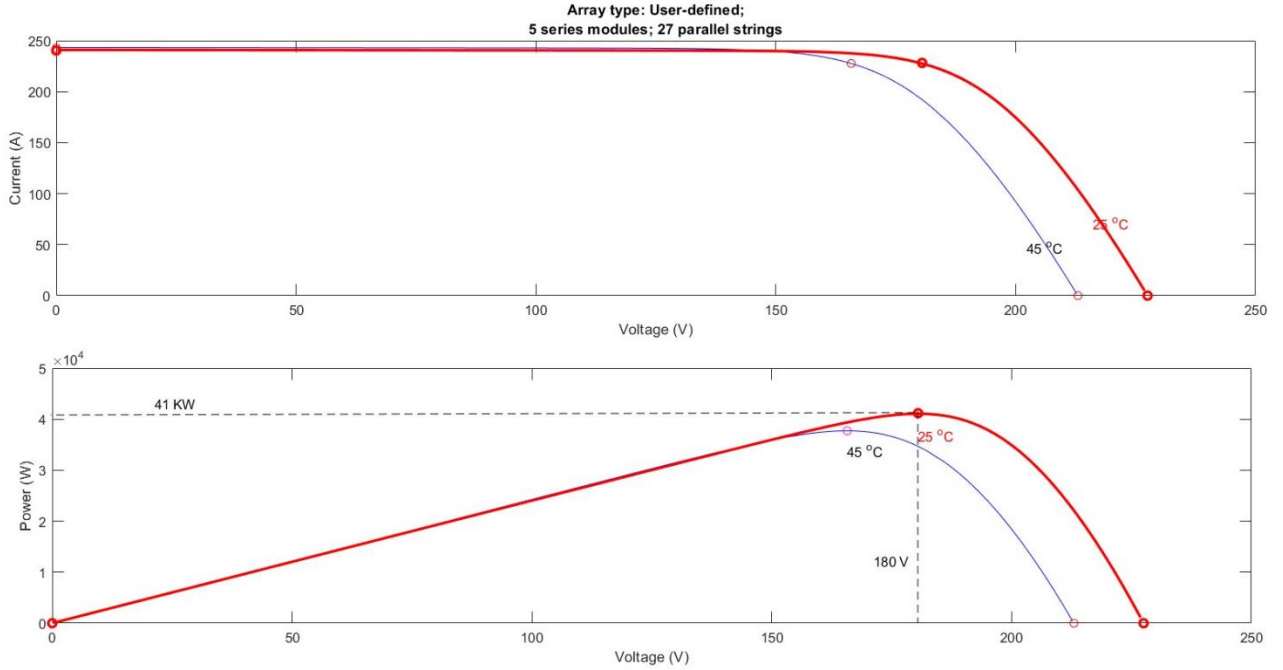


Figure 3. 5: P-V & I-V curves for the PV solar model.

The equation for PV array system of N_s series-connected cells (in a module) and N_p parallel strings (multiple modules):

$$V_{array} = N_s * V_{panel} \quad (3.11)$$

$$I_{array} = N_p * I_{panel} \quad (3.12)$$

3.4 DC Load

The simulation model tests the DC microgrid three steps of DC power loads. Each step of the load equals 10 kW except step 4 equals 5 kW and each step connected at specific time to simulate an increase of load. Fig. 3.6 shows the Simulink model of load the connection and disconnecting timing of these loads. Eq. 3.13 that represents the resistive load:

$$I_R = \frac{V_o}{R} \quad (3.13)$$

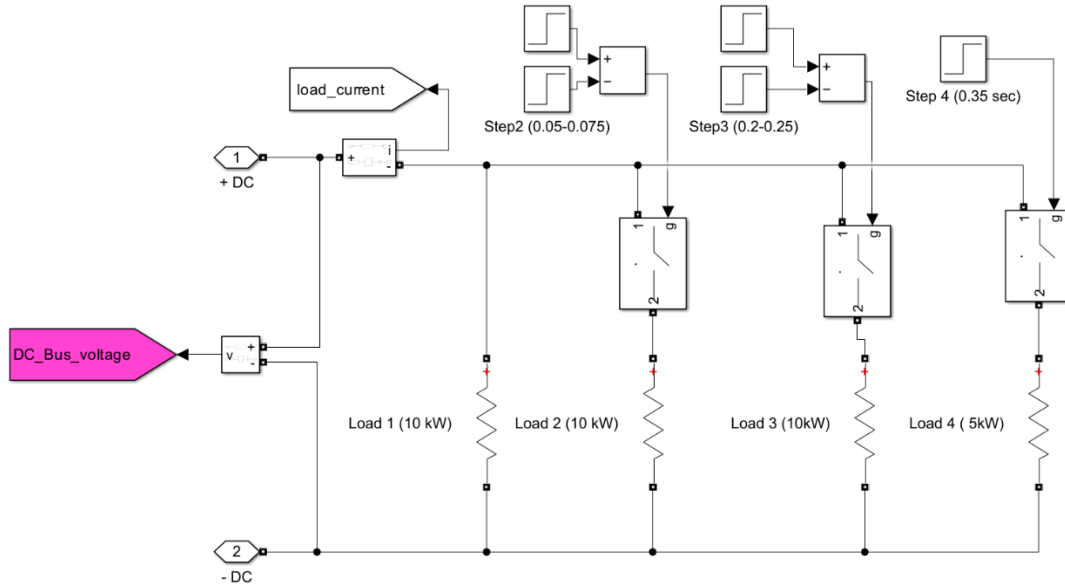


Figure 3.6: Resistive load Simulink model

3.5 Bidirectional AC/DC Converter

The non-isolated DC microgrid is linked through a bidirectional AC/DC converter to exchange power between the microgrid and the AC grid. The control of this kind of converter uses a phase lock loop with a dq control loop and SVPWM technique. Fig. 3.7 shows the topology circuit for bidirectional AC/DC converter, Fig. 3.8. a show the control of bidirectional AC/DC converter and Fig. 3.8.b shows the PLL control. Table 3.2 shows the parameters of the bidirectional AC/DC converter.

Table 3.2: Parameters of bidirectional AC/DC converter

Parameter	Value
Input voltage (L-N)	220 V AC
Output voltage	450 V DC
Frequency at input	50 Hz
Nominal power	25 kW
Control method	dq controller with PLL

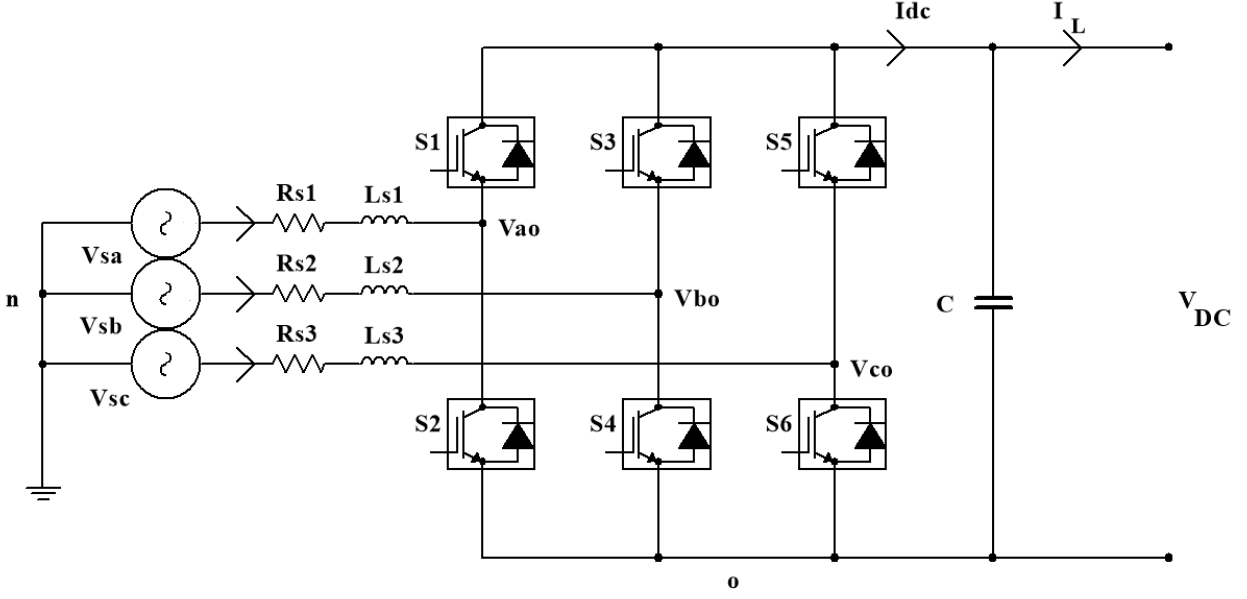


Figure 3.7: Bidirectional AC/DC converter circuit.

Because there are two modes of operation, the first mode to work as an inverter (DC to AC converter) and the second mode to work as a rectifier (AC to DC converter), the equations below derived in inverter mode can also represent rectifier mode by inverse the power direction. These equations are built using Kirchhoff's current and voltage law.

$$V_{sa} = L \frac{di_a}{dt} + Ri_a + u_{ao} + u_{no} \quad (3.14)$$

$$V_{sb} = L \frac{di_b}{dt} + Ri_b + u_{bo} + u_{no} \quad (3.15)$$

$$V_{sc} = L \frac{di_c}{dt} + Ri_c + u_{co} + u_{no} \quad (3.16)$$

$$C \frac{du_{dc}}{dt} = i_{dc} - i_L \quad (3.17)$$

The following equations with switching state of the transistor (S_a for S_1 & S_2 segment, S_b for S_3 & S_4 segment and finally S_c for S_5 & S_6 segment).

$$V_{sa} = L \frac{di_a}{dt} + Ri_a + u_{dc} \left[s_a - \frac{1}{3}(s_a + s_b + s_c) \right] \quad (3.18)$$

$$V_{sb} = L \frac{di_b}{dt} + Ri_b + u_{dc} \left[s_b - \frac{1}{3}(s_a + s_b + s_c) \right] \quad (3.19)$$

$$V_{sc} = L \frac{di_c}{dt} + Ri_c + u_{dc} \left[s_c - \frac{1}{3}(s_a + s_b + s_c) \right] \quad (3.20)$$

$$C \frac{du_{dc}}{dt} = i_a s_a + i_b s_b + i_c s_c - i_L \quad (3.21)$$

After doing Clarke transformation (α - β) to the previous equations:

$$V_\alpha = L \frac{di_\alpha}{dt} + R i_\alpha + s_\alpha u_{dc} \quad (3.22)$$

$$V_\beta = L \frac{di_\beta}{dt} + R i_\beta + s_\beta u_{dc} \quad (3.23)$$

$$C \frac{du_{dc}}{dt} = \frac{3}{2} (i_\alpha s_\alpha + i_\beta s_\beta) - i_L \quad (3.24)$$

After doing park transformation (dq) to the previous equations:

$$V_d = L \frac{di_d}{dt} + R i_d - \omega_0 L i_q + s_d u_{dc} \quad (3.25)$$

$$V_q = L \frac{di_q}{dt} + R i_q - \omega_0 L i_d + s_q u_{dc} \quad (3.26)$$

$$C \frac{du_{dc}}{dt} = \frac{3}{2} (i_d s_d + i_q s_q) - i_L \quad (3.27)$$

Inverter control dq controller (inner control loop), The closed loop transfer function given by:

$$\frac{Y(s)}{X(s)} = \frac{K_1/L\tau_d}{s^2 + (1/\tau_d)s + (K_1/L\tau_d)} \quad (3.28)$$

τ_d : Time constant

Outer control loop: Estimation of i_d^* and i_q^* :

$$i_d^* = K_{1,dc}(v_{dc}^* - v_{dc}) + K_{2,dc} \int (v_{dc}^* - v_{dc}) dt \quad (3.29)$$

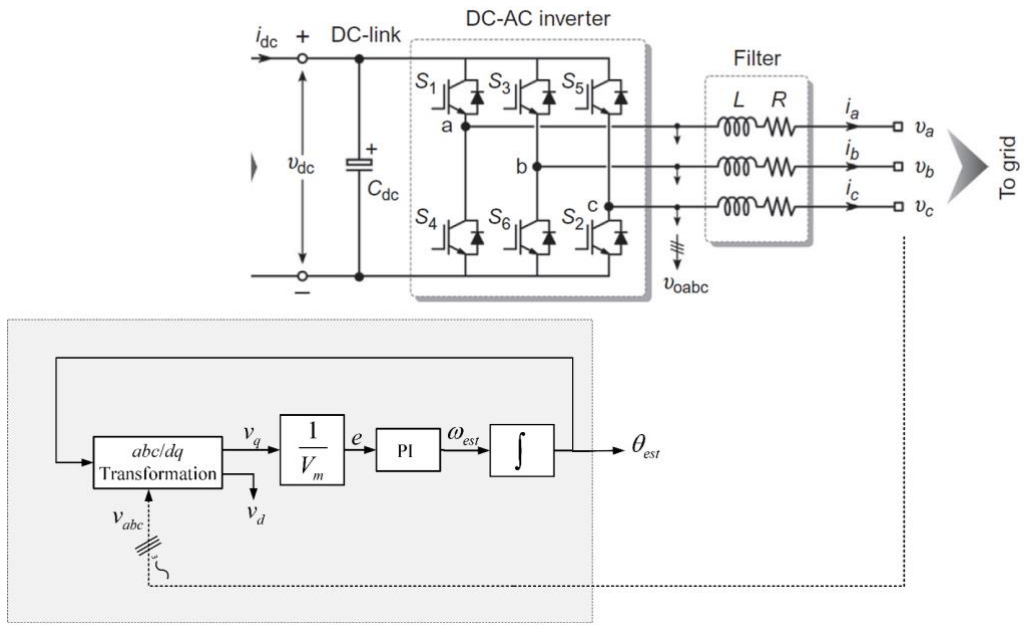
$$i_q^* = -\frac{2Q^*}{3v_d} \quad (3.30)$$

The open loop transfer function:

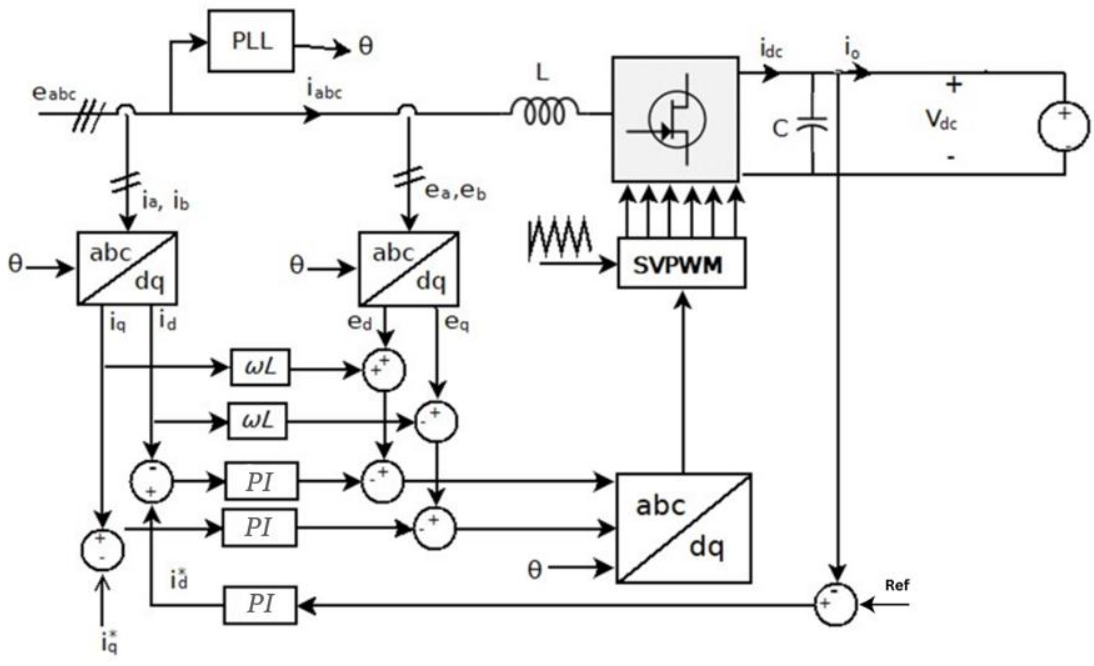
$$\frac{Y(s)}{X(s)} = \frac{3V_m K_{1,dc} (1 + \tau_{i,dc} s)}{2V_{dc} C_{dc} \tau_i (1 + \tau s) s^2} \quad (3.31)$$

Closed loop Transfer function of phase lock loop function:

$$T_{PLL} = \frac{(1 + \frac{K_{1,PLL}}{K_{2,PLL}} s) K_{2,PLL}}{s^2 + K_{1,PLL} s + K_{2,PLL}} \approx \frac{K_{2,PLL}}{s^2 + K_{1,PLL} s + K_{2,PLL}} \quad (3.32)$$



a.



b.

Figure 3. 8: a) PLL controller. b) dq controller with SVPWM switching for AC-DC converter.

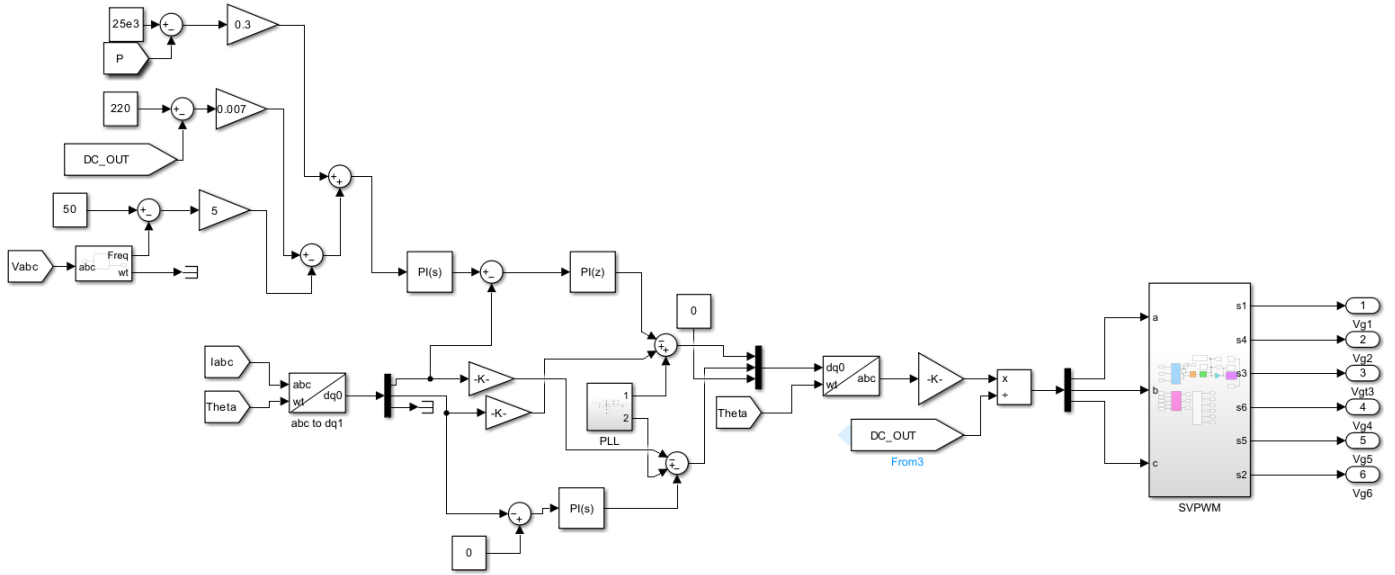


Figure 3. 9: simulation model control of bidirectional AC-DC converter

The design of PI controller for the DQ current controller and the DC voltage regulator of the inverter will be based on the symmetrical optimum method that usually used for second-order systems, which used depending on the desired closed-loop dynamics to achieve critically damped or lightly underdamped behavior by placing the poles of the closed-loop transfer function symmetrically with respect to the real axis in the left-half plane [64].

The coefficient of PI controller for dq current controller can be determined for the desired damping ratio ($\zeta = 0.707$) and overshoot (5%) determined by:

$$K_p = \frac{L}{2\tau} \quad (3.33)$$

$$K_I = \frac{R}{2\tau} \quad (3.34)$$

Where $\tau = \frac{L}{R}$ is the time constant of the inverter. ($R=0.1 \Omega$, $L= 1\mu\text{H}$)

The coefficient of PI controller for voltage regulator controller can be determined for the desired damping ratio ($\zeta = 0.707$) and overshoot (5%) determined by:

$$K_p = -0.12 \frac{C_{dc}}{\tau} \quad (3.35)$$

$$K_I = -0.0213 \frac{RC_{dc}}{\tau^2} \quad (3.36)$$

Where $\tau = RC$ is the time constant of the inverter. ($R=0.1 \Omega$, $C_{dc}= 1\text{mF}$)

The initial value of PI controller for both controllers were calculated based on Eq.3.33-3.36 and tuned by PID Tuner in the Simulink tool. The table 3.3 shows the values of the PI controller for both controllers.

Table 3. 3: PI controller coefficient for dq and voltage regulator controllers

coefficient	Value
Proportional (DQ)	10
Integral (DQ)	10
Proportional (regulator)	1
Integral (regulator)	100

3.6 Unidirectional DC/DC Converter

The unidirectional DC/DC converter (Buck-Boost converter) used in the PV solar system converts the generated power from the PV panels of voltage of 180 V to the appropriate voltage level for the DC bus (220 voltage DC). The buck boost converter that is shown on Fig.3.9, works in two modes of operations and each mode has a transfer function. The two modes of operations:

- Mode 1: buck -boost converter in grid connected operation mode.
- Mode 2: boost converter in islanded operation mode.

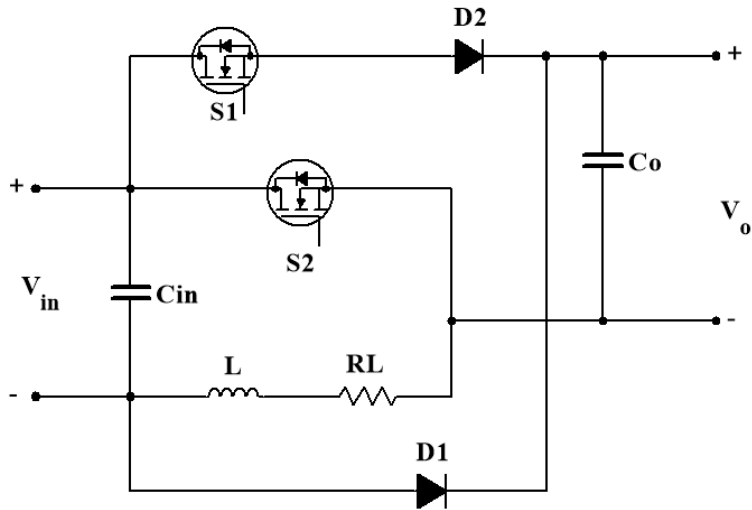


Figure 3.10: Unidirectional buck-boost converter circuit.

The energy storage components (capacitor voltage and inductor current) are selected as the states which are internal system variables representing energy storage and dynamics. The inputs are the input voltage and the output load which are external factors influencing the system. The controllable variables are defined as the input current, output voltage, and inductor current., which are key quantities regulated to ensure proper system functionality and performance. The equation 3.37 of state space are derived based on the non-linear elements of the converters (the inductor and capacitor)

$$x = \begin{bmatrix} i_L \\ v_{Co} \\ v_{Cin} \end{bmatrix} \quad u = \begin{bmatrix} i_o \\ v_{in} \end{bmatrix} \quad y = \begin{bmatrix} i_{in} \\ i_L \\ v_o \end{bmatrix} \quad (3.37)$$

Where:

- | | |
|--|--------------------------------------|
| i_L : inductor current. | v_o : output voltage of converter. |
| i_o : output current of converter. | v_{Co} : output capacitor voltage. |
| i_{in} : input current of converter. | v_{Cin} : input capacitor voltage. |
| v_{in} : input voltage of converter. | |

The transfer function for grid connected mode is: (more details in Appendix A)

$$\frac{Vo(s)}{Vin(s)} = \frac{\frac{s(D_1 - D_2)}{LC_{in}} - \frac{D_1 D_2}{L^2 C_{in}}}{s^2 + \frac{(R_L + R_{on2})D_1 + R_L D_2}{L} s + \frac{D_2^2}{LC_o} + \frac{D_1^2}{LC_{in}}} \quad (3.38)$$

The transfer function for islanded mode is: (more details in Appendix A)

$$\frac{Vo(s)}{Vin(s)} = \frac{\frac{s(D_1^2 - D_2^2)}{LC_{in}} + \frac{(D_1^2 - D_2^2)D_2}{L^2 C_{in}}}{s^2 + \frac{R_L(D_1 + D_2) + D_2 R_{on1} + D_1 R_{on2}}{L} s - \frac{D_2^2}{LC_o} + \frac{(D_1^2 + D_2^2)}{LC_{in}}} \quad (3.39)$$

The equations used to determine the values of inductor, input and output capacitor are:

$$L_{min_boost} = \frac{(V_o - V_{in})V_{in}^2}{2P f_{sw} V_o} \quad (3.40)$$

$$L_{min_buck} = \frac{(1 - D)V_o}{2f_{sw} I_o} \quad (3.41)$$

$$C_{in_min} = \frac{D(1 - D)I_o}{f_{sw} \Delta V_{in}} \quad (3.42)$$

$$C_{o_min} = \frac{V_o D}{\frac{P}{I_o^2} \times f_{sw} \times \Delta V_o} \quad (3.43)$$

- | | |
|---|--|
| V_o : output voltage of converter. | ΔI_L : inductor current ripple. |
| V_{in} : the input voltage of the converter. | f_{sw} : switching frequency of the converter. |
| I_o : output current. | P : maximum power rating. |
| $\Delta V_o, \Delta V_{in}$: ripple voltage. (based on the maximum allowed voltage ripple 2%). | |

The converter parameters and input and output capacitor values and inductor values calculated and used shown in Table 3.3.

Poles and zeros are basic concepts in control systems that describe the system's input-output relationship; it is important to study the stability and frequency response of the converter. Table 3.3 displays the values of the poles and zeros. Fig. 3.10.a visualizes the poles and zeros for boost mode (islanded mode) of operation. Also, Fig. 3.10.b shows the poles and zeros for buck-boost operation mode. Which indicates that this converter is asymptotically stable, and it is always Bounded Input Bounded Output Stable (BIBO stability).

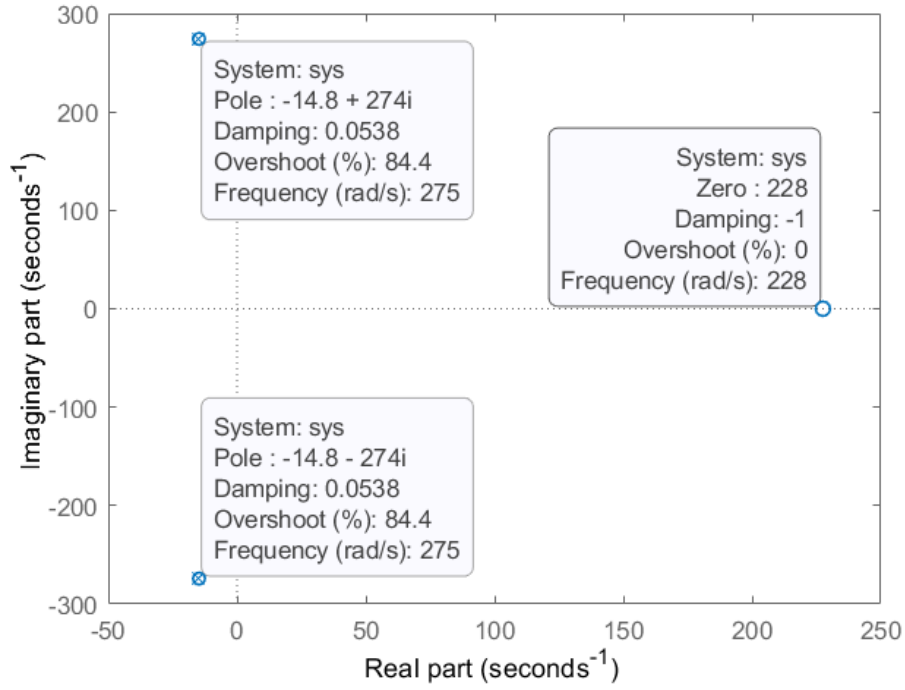
The analysis of poles and zeros found that the converter has low damping ratio due to the capacitance, inductance that cause low damping because the energy dissipation in the components is minimal, leading to oscillatory behavior in the circuit's response. Moreover, converter's switching operation causes ripple and dynamic behavior, which might lead to oscillatory tendencies. The effectiveness of the system to dampen these oscillations is determined by the control loop's architecture and frequency responsiveness. Without proper damping, these oscillations last longer, resulting in a low damping ratio. These effects can be mitigated by properly setting the switching frequency, filters, and control loops [65].

The control of a unidirectional buck-boost converter based on two controllers depends on the operating mode. In a grid-connected system, the MPPT controls the switching of the S2 MOSFET (the P & O method ensures maximum power is injected into the DC bus as a current source by following the DC bus voltage), as shown in Fig. 3.11.a, which illustrates the control method and switching sequence of the converter in grid-connected mode, in which the MOSFET S1 is always off in both states and S2 is on in state 1, while D1 is on in state 2. In islanded mode, the MOSFET S2 and the diode D2 are on in state 2, while the MOSFET S1 is on in state 1. Fig. 3.11.b shows the control method and switching sequence in islanded mode, highlighting that the PI controller is used to generate the switching signal for the circuit.

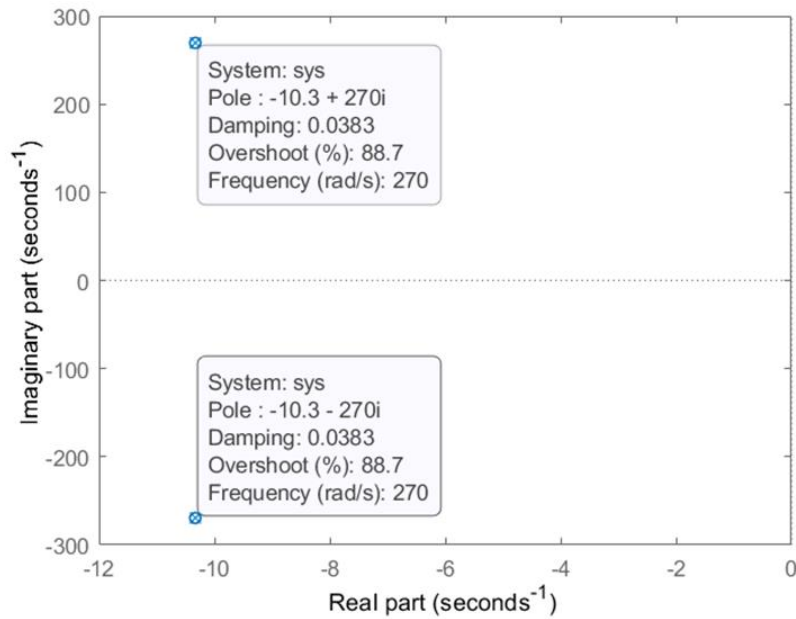
The code of P & O algorithm for MPPT technique using in MATLAB is shown in appendix.

Table 3.4: Parameters of unidirectional DC-DC converter.

converter parameters	Mode/ minimum Value	Used value
Rated power	-	41 kW
Input voltage	-	180 V
Output voltage	-	220 V
Switching frequency	-	100 kHz
Duty cycle	-	$D_1=D_2 =0.551$ (grid connected mode)
		$D_1 =1$ & $D_2 =0.182$ (islanded mode)
Inductor (buck-boost)	2.65 μ H	8 mH $R_L= 0.1\Omega$
inductor (boost)	7.18 mH	
Input capacitor	127.8 μ F (buck boost) 76.9 μ F (boost)	1500 μ F
Output capacitor	232 μ F (buck-boost) 76 μ F (boost)	800 μ F
Transfer function	Buck-boost (Grid connected)	$\frac{Vo(s)}{Vin(s)} = \frac{17425432.39}{s^2 + 20.66s + 72737.73}$
	Boost (Islanded mode)	$\frac{Vo(s)}{Vin(s)} = \frac{80573s - 18330357.5}{s^2 + 29.55s + 75397.37}$
Poles and zeros of transfer function	Buck-boost (Grid connected)	Poles (- 10.33 \pm 269.5i), Zeros: none
	Boost (Islanded mode)	Poles (-14.77 \pm 274i), Zeros: 227.5

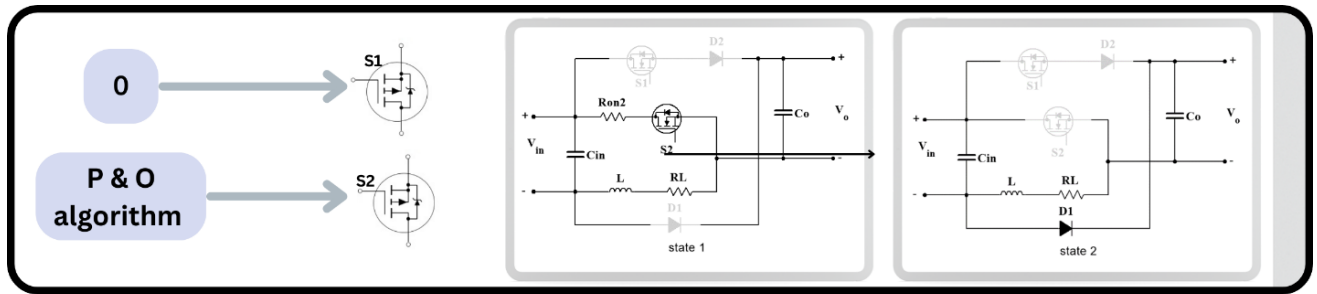


a.



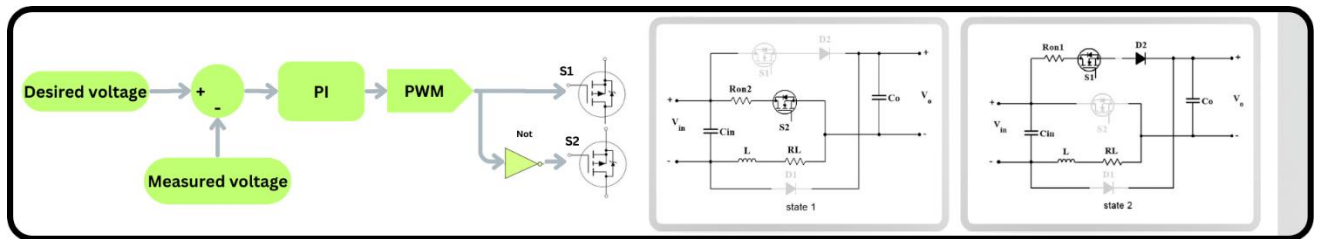
b.

Figure 3.11: poles and zeros map for the unidirectional DC-DC converter: a) in islanded mode. b) in grid connected mode.



Grid-connected control

a.



Islanded control

b.

Figure 3. 12 :Control method and switching sequence of unidirectional buck-boost converter:

a) grid connected mode. b) islanded mode

3.7 Bidirectional DC/DC Converter

The simulation model of the bidirectional DC/DC converter is used after the bidirectional AC/DC converter interconnects the DC bus and the AC/DC converter, achieving the desired voltage level. This is necessary because the AC/DC converter alone cannot reach the suitable voltage level of 220 V DC. Figure 3.12 shows the bidirectional DC/DC converter that converts the output DC voltage of the AC/DC converter into 220 V DC. This converter has two modes of operation based on the direction of the power, either buck or boost mode. If the grid supplies the DC bus, the converter works in buck mode, and if the DC bus has excess power exported to the grid, the converter works in boost mode.

The transfer function for bidirectional DC-DC converter that represents the converter in two modes is: (more details in Appendix B)

$$\frac{V_o(s)}{V_{in}(s)} = \frac{\frac{s(1-2D)^2}{LC_{in}} + \frac{(2D-1)(1-2D)D}{L^2C_{in}}}{s^2 + \frac{R_L + DR_{on1} + (1-D)R_{on2}}{L}s + \frac{D^2}{LC_o} - \frac{4D - 4D^2 - 1}{LC_{in}}} \quad (3.44)$$

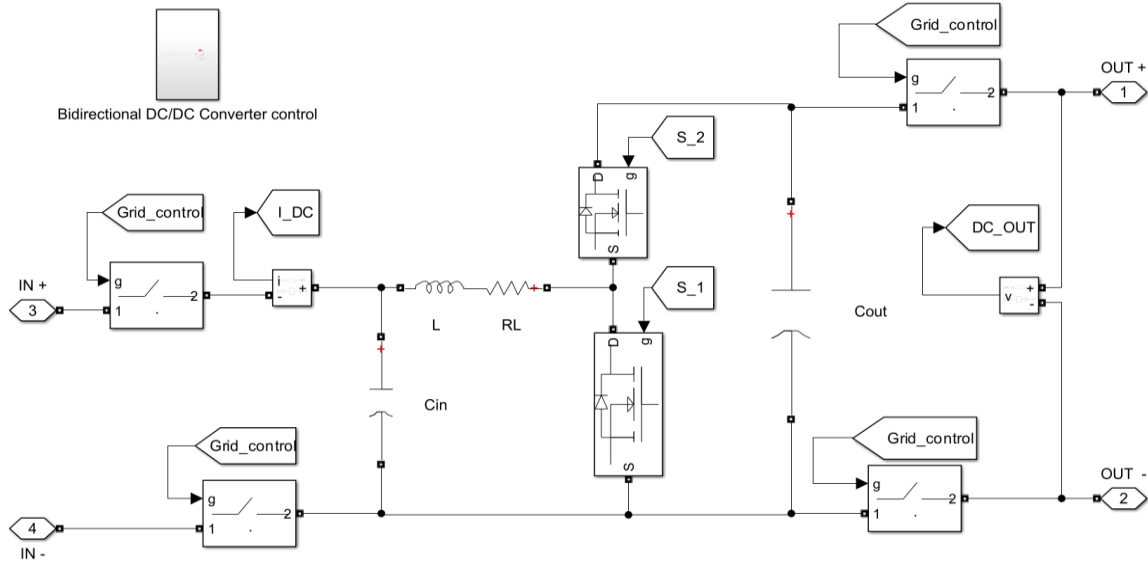


Figure 3.13: Bidirectional DC-DC converter.

The parameters and characteristics of bidirectional DC-DC converter are shown in table 3.4, also, Fig.3.13 shows the poles and zeros of converter transfer function. Which indicates that this converter is asymptotically stable, and it is always BIBO stable (The equations (3.36 -3.39) were used to calculate the values of inductor, input capacitor and output capacitor).

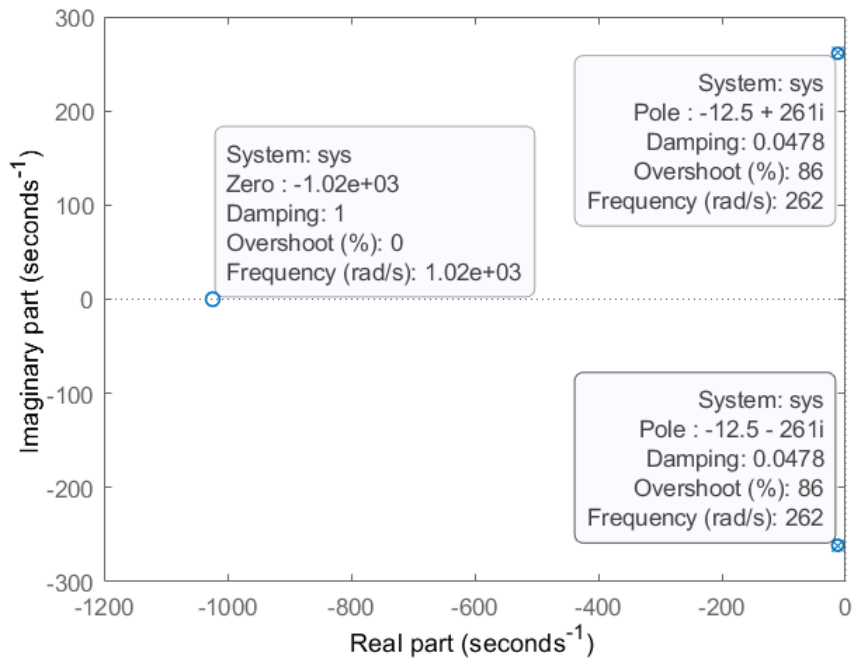


Figure 3. 14: Poles and zeros map of bidirectional buck boost converter.

The control of the bidirectional buck-boost converter is managed by a PI controller. Fig. 3.14 illustrates the control method and switching sequence of the converter, which operates only in grid-connected mode. In islanded mode, this converter is not needed and will be disconnected.

Table 3. 5: Parameters of the bidirectional DC/DC converter.

Converter parameters	Mode/ minimum Value	Used value
Rated power	-	41 kW
Input voltage	-	220 V
Output voltage	-	450 V
Switching frequency	-	100 kHz
Duty cycle	-	D =0.512 (at boost mode) D =0.488 (at buck mode)
Inductor	12.6 μ H (buck), 3 μ H (boost)	8 mH , $R_L= 0.1\Omega$
Input capacitor	51.6 μ F	206 μ F
Output capacitor	51.7 μ F (buck), 49.2 μ F (boost)	500 μ F
Transfer function	Buck boost (the converter works only in grid connected mode)	$\frac{V_o(s)}{V_{in}(s)} = \frac{-14563s - 14912621}{s^2 + 25s + 68448}$
Poles and zeros		Poles ($-12.5 \pm 261i$), Zeros: -1024

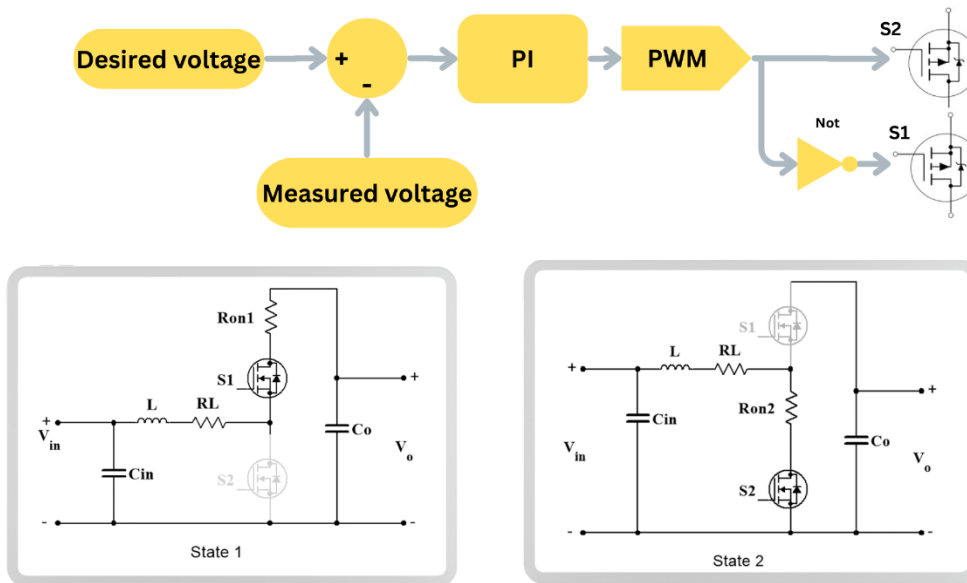


Figure 3.15: Control and switching of bidirectional DC-DC converter.

3.8 DC-DC Converter Control using State Space Matrices

There is another control method using state space matrices to control the unidirectional and bidirectional DC/DC converter as shown in Fig.3.16 and table 3.5 shows the matrices values. These values are calculated by the state space equations using MATLAB script that is shown in Appendix C.

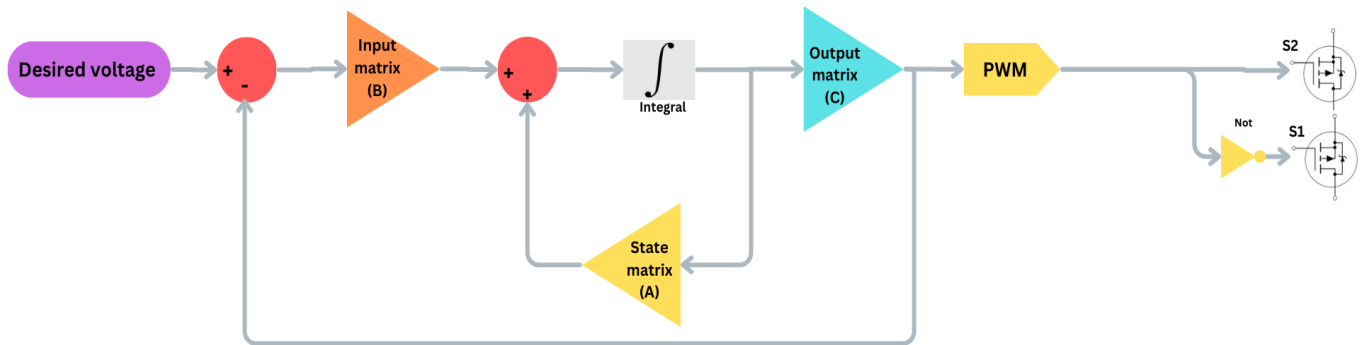


Figure 3. 16: Control method using state space matrices.

Table 3. 6: State space matrices values based on converter type and mode.

Converter	Unidirectional (Boost mode)	Unidirectional (Buck-Boost mode)	Bidirectional
State matrix (A)	$\begin{bmatrix} -29.55 & -75397.37 \\ 1 & 0 \end{bmatrix}$	$\begin{bmatrix} -20.66 & -72737.73 \\ 1 & 0 \end{bmatrix}$	$\begin{bmatrix} -25 & -68448.62 \\ 1 & 0 \end{bmatrix}$
Input matrix (B)	$\begin{bmatrix} 1 \\ 0 \end{bmatrix}$	$\begin{bmatrix} 1 \\ 0 \end{bmatrix}$	$\begin{bmatrix} 1 \\ 0 \end{bmatrix}$
Output matrix (C)	$[80573.0 \quad -18330357.5]$	$[0 \quad 17425432.39]$	$[14563.10 \quad -14912621.35]$
Feedforward matrix (E)	0	0	0

Chapter 4: Problem analysis and Results

4.1. Problem Description and Analysis

The thesis problem is the unsmooth transitions between grid-connected and islanded modes in DC microgrids, which cause a voltage impulse during the transition. Figure 4.1.a shows the DC bus voltage under PI control, while Figure 4.1.b shows the DC bus voltage under state-space control.

The microgrid operates in grid-connected mode from 0 to 0.1 seconds and 0.3 to 0.4 seconds, while it operates in islanded mode from 0.1 to 0.3 seconds. The effect of this transition is explained in Fig. 4.1.a. It shows that the transition causes a small overshoot of up to 235 V in both grid-connected and islanded modes, and vice versa. Fig. 4.1.b shows that the transition from grid-connected to islanded mode causes a large overshoot of up to 540 V, while the impulse value during the transition from islanded to grid-connected mode is around 230 V.

From observing the transition effect, it is evident that the load value affects the transition impact. For both light and heavy loads, the impulse value increases, but light loads have a higher impact. Medium loads have a lower impulse value than both light and heavy loads.

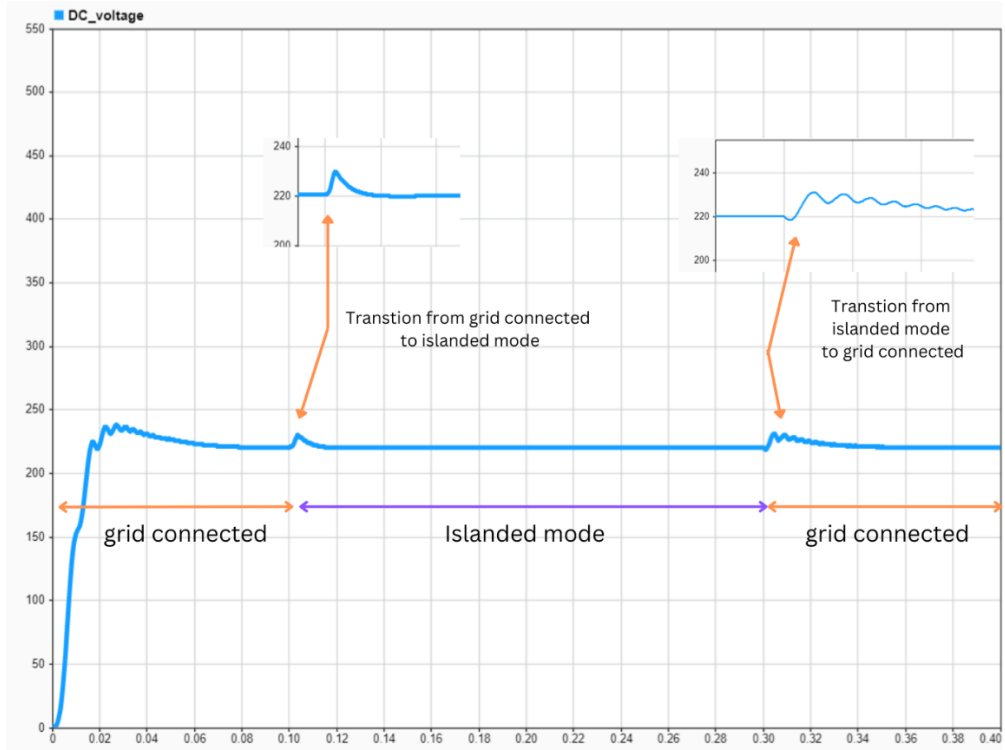
Additionally, parasitic resistance and the internal resistance of MOSFETs, diodes, and inductors affect the transition impact on the DC bus voltage. If these resistance values increase, the transition impact decreases, making the microgrid easier to control and losses increasing. Conversely, exceedingly small resistance values increase the transition impact, making the microgrid more difficult to control and lower losses.

Thus, from the analysis of the transition problem between different modes, it can be concluded that the controller for islanded mode is the key solution. Since the only converter that operates in islanded mode is the unidirectional buck-boost converter, the control method in this mode needs to be improved to mitigate the transition impact and achieve a smooth transition.

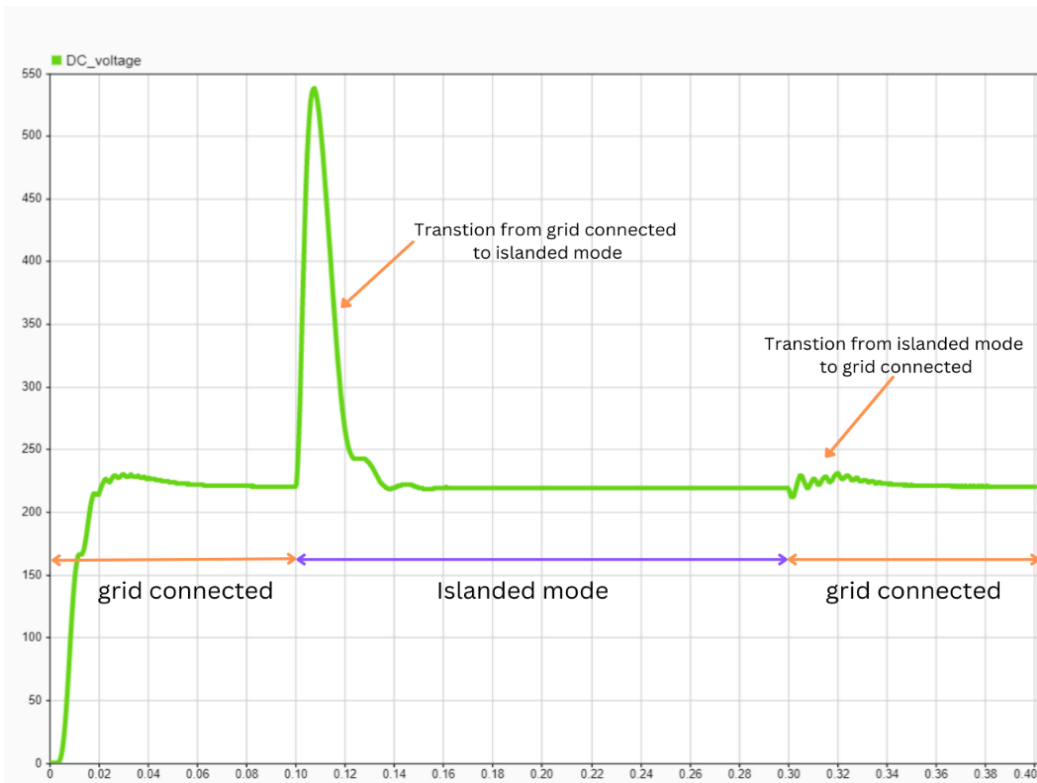
This thesis proposes four different control methods applied to the islanded mode of a unidirectional buck-boost converter, as follows:

- feedback control.
- Sliding mode control.
- Use of a compensator.
- Voltage level control.

The mentioned control methods will explain in detail in the next sections.



a.



b.

Figure 4. 1: Transition effect on DC bus voltage. a) using PI controller. b) using state space controller

4.2. Feedback Control

Feedback control is an essential concept in control systems. The system's output is continuously monitored and compared to a preset setpoint. This feedback mechanism takes the system's output (y) and applies it to its state vector (\dot{x}) with a specific gain. By doing so, feedback helps reduce transients that occur during transitions, thereby stabilizing the system [66].

The feedback control for state space model of unidirectional DC-DC converter in islanded mode is shown in Fig.4.2.

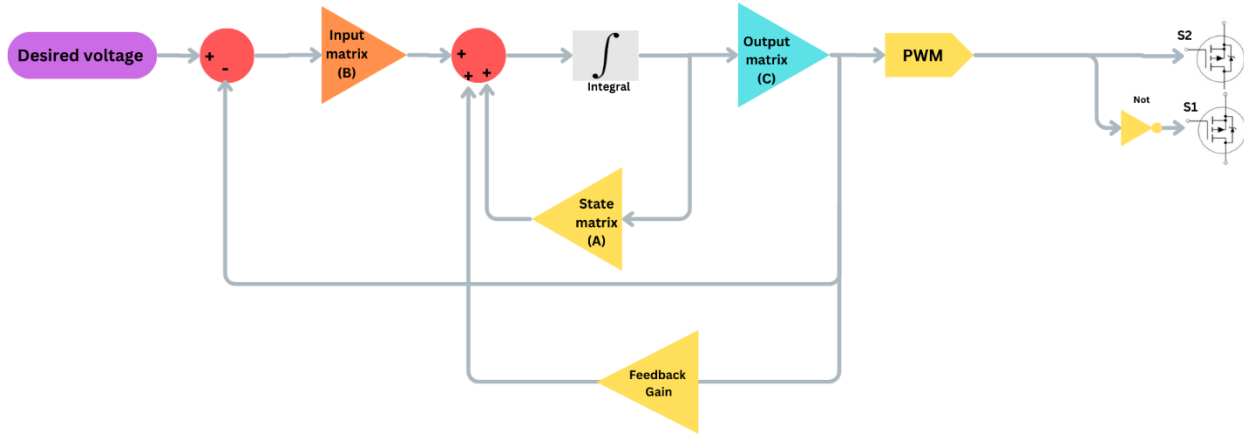


Figure 4. 2: Feedback control method for unidirectional DC-DC converter.

The state equations for the system that gives the response as shown in Fig.4.1a ruled by the following equation:

$$\begin{aligned} \dot{x} &= Ax + B(-y + r) \\ y &= Cx \end{aligned} \quad (4.1)$$

Where r : is the desired voltage value.

After adding feedback, the equation of the system become:

$$\begin{aligned} \dot{x} &= Ax + B(-y + r) + Ky \\ y &= Cx \end{aligned} \quad (4.2)$$

Where K is the gain value.

solving the output equation for y and substituting in the state equation results in:

$$\begin{aligned} \dot{x} &= (A - BC + KC)x + Br \\ y &= Cx \end{aligned} \quad (4.3)$$

This control method only works for constant load value and table 4.1 shows the suitable gain values for different load values. These values chosen based trial and error method.

Figure 4.3 shows the DC bus voltage at load with 10 kW in state space, and the waveform analysis proves that this method reduces the overshoot and maintains the voltage at 220 V. Compared to Figure 4.1.b the overshoot decreases from 540 V to 238 V.

Table 4.1: gain values for different load values.

Load value	Gain value
5 kW	7.7
10 kW	3.49
15 kW	2.3
20 kW	1

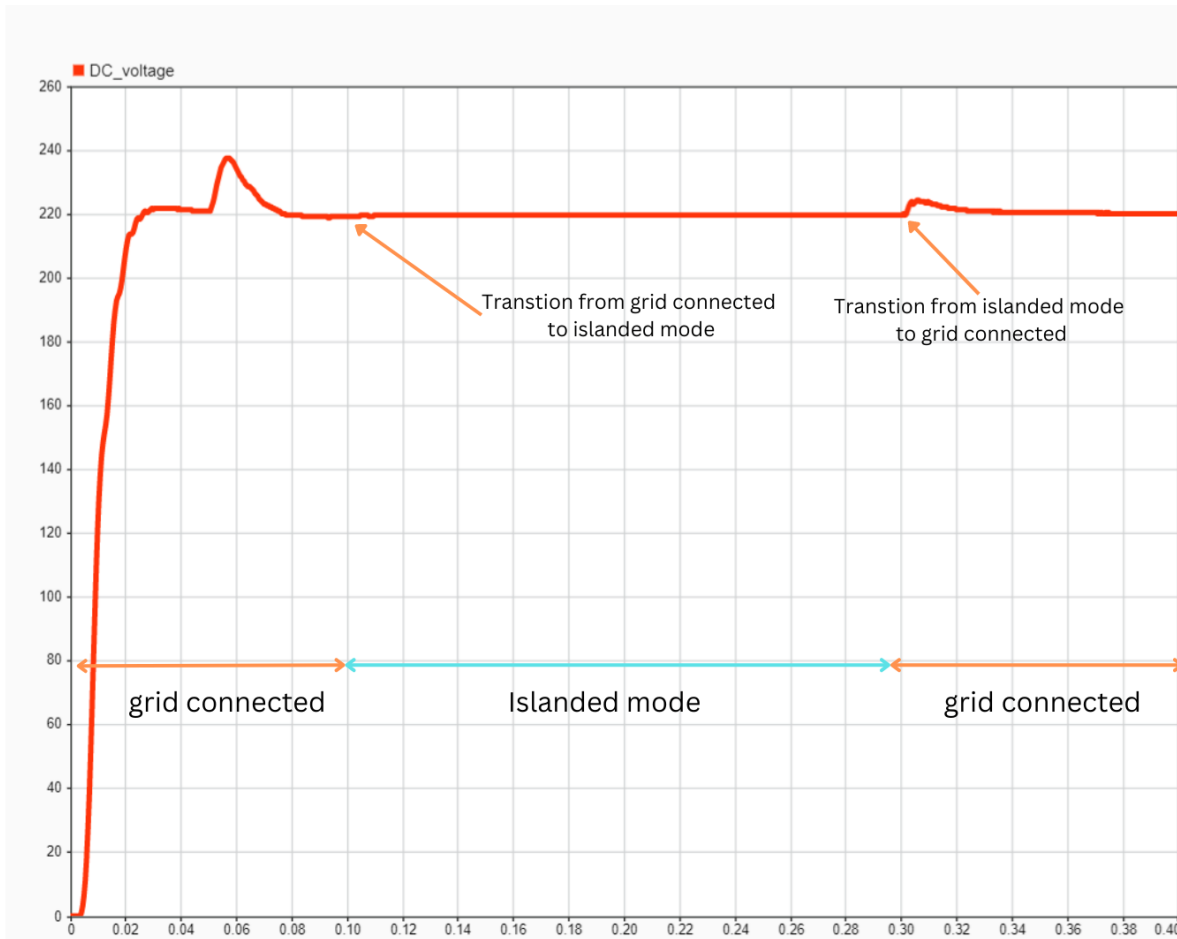


Figure 4. 3: DC bus voltage waveform with feedback control

4.3. Slide Mode Control

A nonlinear control technique that applies a discontinuous control signal to modify the system's dynamics, forcing the system to slide along a preset surface called a sliding surface [67].

The following equation shows the slide mode approach:

$$u = 5(e + 2e \operatorname{sign}(s)) \quad (4.4)$$

Where: u is the output of the slide mode, e : is the error value.

After adding the slide mode equation with PI control, the following equation represents the slide mode with PI controller. Where K_p is proportional coefficient and K_i is integral coefficient.

$$y = (5(e + 2e \operatorname{sign}(s))) * [K_p + K_i \frac{1}{s}] \quad (4.5)$$

Where $K_p = 0.8$ & $K_i = 80$ and these values obtained by PID tuner in Simulink/MATLAB tool.

The simulation result for slide mode control for the DC bus voltage are shown in Fig.4.4. that show that the overshoot reduced slightly with slowly change to reach steady state.

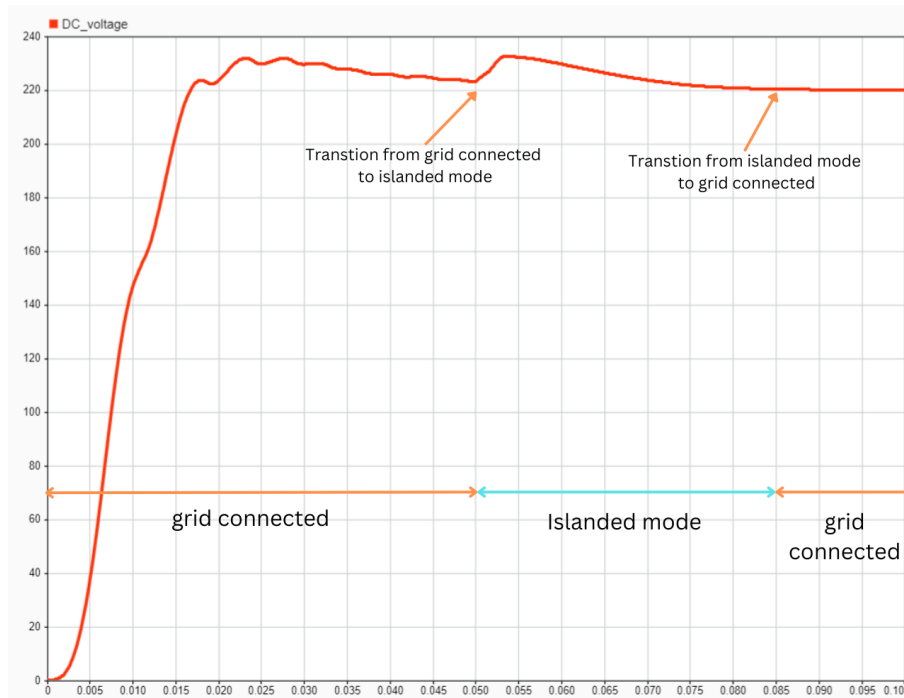


Figure 4. 4: DC bus voltage for slide mode control result between grid connected mode and islanded mode transition & vice versa.

4.4. Compensation Control

In control systems, compensation refers to the process of modifying a system to improve its performance, stability, and accuracy. This is typically achieved by adding the error value with output value to space vector, Compensators are crucial in ensuring that control systems meet desired specifications and perform optimally under various conditions [68].

The compensation for state space is shown in Fig.4.5, which has feedback from the output state added to error value with gain and the result added to state vector to modify the control system response to achieve the desired DC voltage bus and reduce transient response.

For this method, the compensation equation with state space becomes:

$$\begin{aligned} \dot{x} &= Ax + B(-y + r) + y + G * error \\ y &= Cx \end{aligned} \quad (4.6)$$

Where G is the gain of compensation and has a value of 0.35.

After simplify the previous equation:

$$\begin{aligned} \dot{x} &= (A - BC + Br + C)x + G * error \\ y &= Cx \end{aligned} \quad (4.7)$$

The output waveform after adding the compensation is shown in Fig. 4.6. Moreover, this result demonstrates the applicability of the compensation in regulating the voltage with load changes over time in different modes of operation.

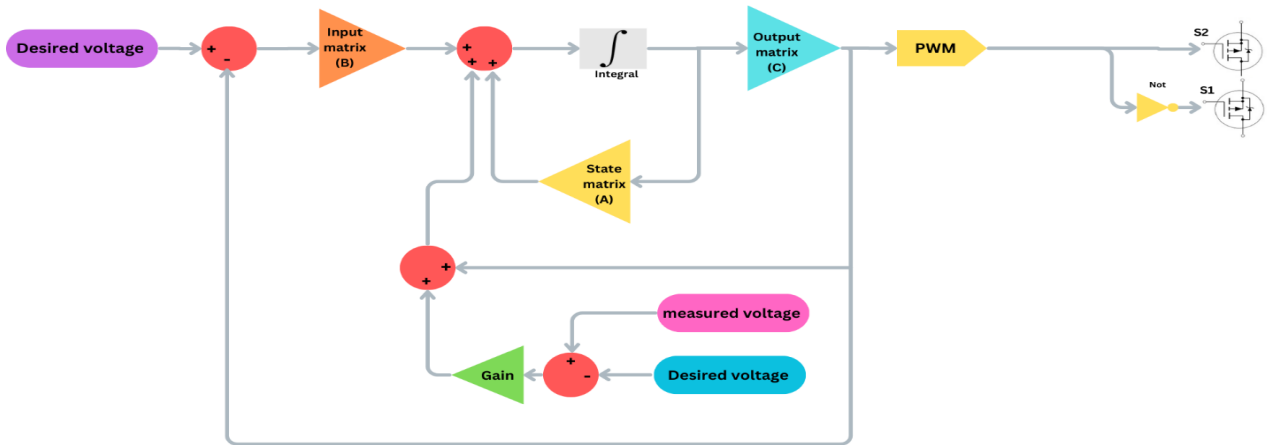


Figure 4. 5: compensation control for state space model in islanded mode for unidirectional DC-DC converter.

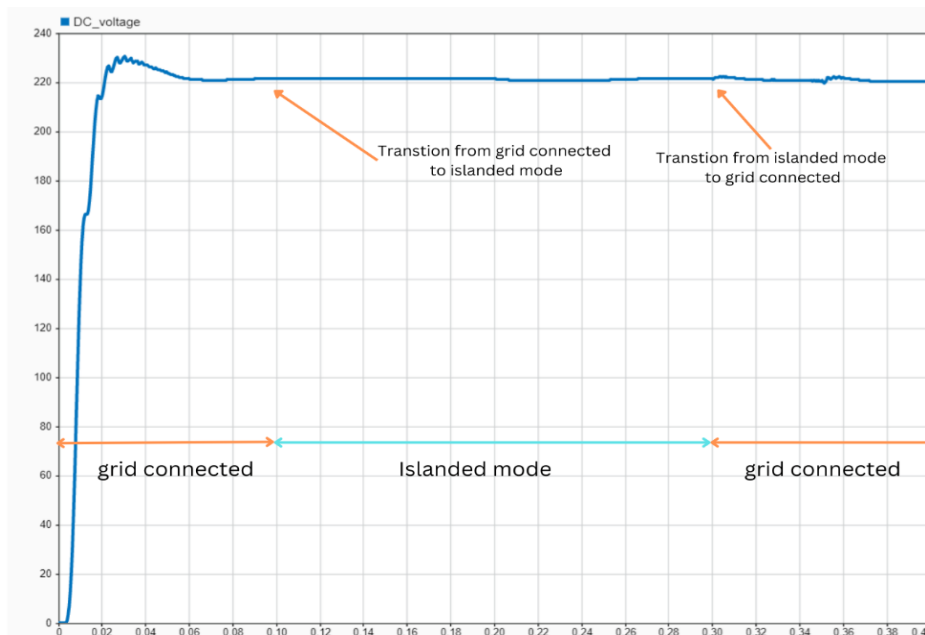


Figure 4. 6: DC bus voltage waveform for compensation control method

4.5. Voltage Level Control

This method controls the duty cycle of the switching MOSFET. Using this approach, the output voltage can be regulated and stabilized to the nominal voltage value of the DC bus. The controller generates the switching signal for the transistors, and an additional control stage adjusts the signal based on the voltage level, either increasing or decreasing the duty cycle according to the measured voltage, as outlined in Fig.4.7.

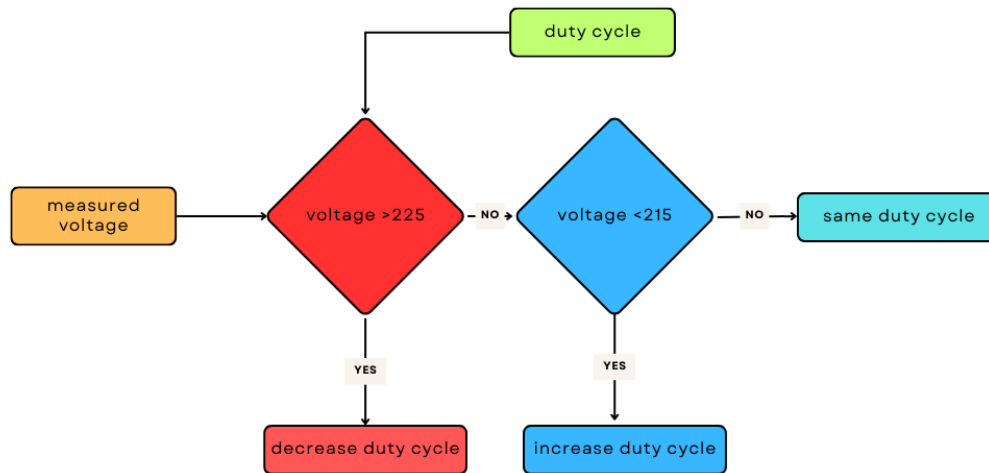


Figure 4. 7: voltage level control algorithm for duty cycle modification.

This approach can manage the transition between different modes of operation and load change in any mode of operation to ensure dynamic stability of the DC microgrid. This method tested two different primary controls, PI controller and state space control and the result for PI control with voltage level control shown in Fig.4.8. a, while Fig.4.8. b shows the result with state space control. which reduced effectively the overshoot with acceptable response to reach steady state.

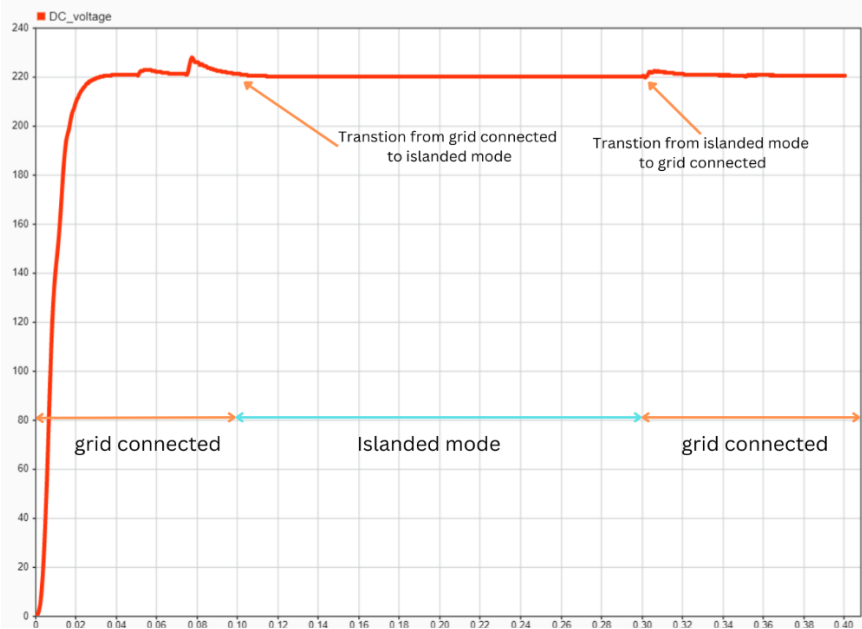
4.1. Comparison Between Different Control Solutions

Based on the results presented in the previous sections for different control solutions during the transition between modes of operation, the following table provides a brief comparison of the tested control methods.

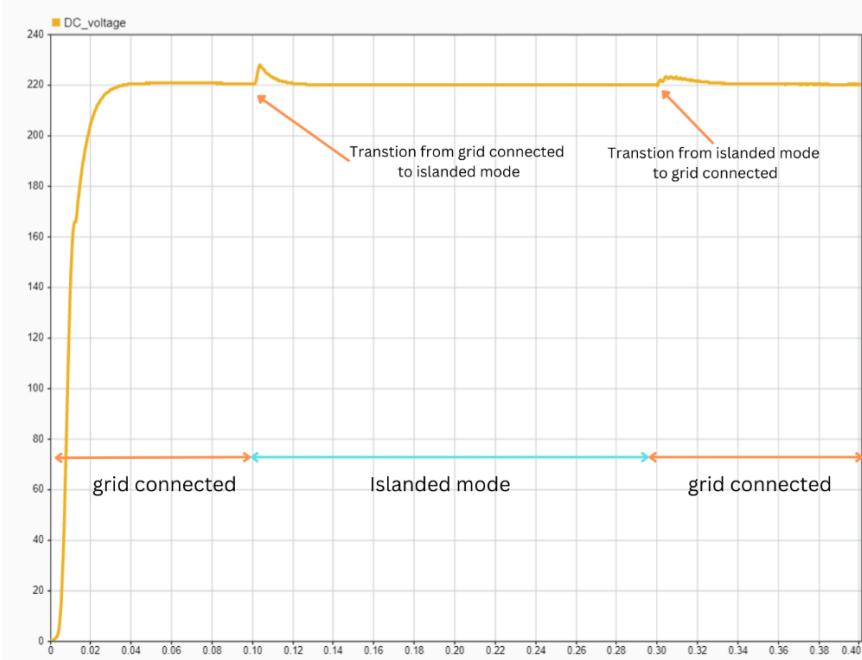
Table 4. 2: Comparison between the different control methods.

Method	The overshoot during the transition (V)	Time (sec)	Load change handle
Slide mode	236	0.02	No
Compensation	222	Very small	Yes
Feedback	238	0.35	Yes
Voltage level control	228	0.02	Yes

From table, 4.2 it can conclude that the compensation control method has reduced the transient effect of the transition and load change during the two modes of operations.



a.



b.

Figure 4. 8: DC bus voltage using voltage level control: a) PI control method. b) state space model method.

Chapter 5: Conclusion

5.1. Summary

This thesis examines the DC microgrid by developing a simulation model and focusing on the transition between two modes of operation. It proposes and tests four different control methods for two models to address the transient response during the transition.

The simulation model was developed using the Simulink/MATLAB tool. The system consists of a PV array with a peak capacity of 41 kW and a buck-boost converter to connect the system to the DC bus. Additionally, the setup includes a utility grid and a three-phase inverter with a bidirectional buck-boost converter to facilitate interaction between the grid and the DC bus. Lastly, a time-varying load is included to simulate changes in load on the DC bus.

The control used for the three-phase inverter is dq controller with PLL and SVPWM, this inverter has a bidirectional power flow to import the shortage power or export the excess power from the DC bus to the grid. The inverter needed to interlink DC-DC converter to step up/down the voltage based on the power flow direction and the two controllers used for both grid connected and island modes, these controllers built with two different structures, PI control and state space control in both modes.

The unidirectional buck boost converter used for the PV system has two controllers for both modes of operation, and the topology of this converter was selected carefully to work with two different duty cycles of the transistors (MOSFET's) because the converter has to work in MPPT under grid-connected mode and also regulate the output voltage within 220 V (current source), while working in islanded mode to supply the needed power with 220 V for the DC bus (voltage source).

The thesis presents four different solutions for managing transients during the transition between modes and tests. These solutions using either state-space methods, PI control, or both to ensure a smooth transition for the DC microgrid. Some of these solutions also help mitigate the effects of dynamic load changes.

5.2. Assumptions and Limitations

This thesis has a few assumptions and limitations:

- The load tested in this model is a DC load and a resistive power load.
- The DC microgrid model is a bipolar and radial bus configuration.
- The inertia of this microgrid is relatively low, which makes the control of this DC microgrid more difficult to handle.
- There is no storage system in the model that can help to regulate the voltage at the DC bus.

5.3. Future work

There are many suggestions that could be implemented in the future to provide valuable additions to this research, such as:

- Adding a storage system, wind turbine, and electric vehicle to the DC microgrid test model.
- Testing other control methods, such as bumbles control.
- Using a single controller for both modes of operation instead of having one controller for each mode.
- Focusing on automatic transitions between modes based on protection scenarios and cost management strategies.

5.4. Conclusion

Stability is crucial for any system, and it must operate effectively under different conditions, including normal and transient events. In this study, this principle applies to the DC microgrid, with a focus on ensuring a smooth transition between different operating modes. The simulation model, which includes power electronics converters, loads, a PV system, and primary control for each converter in both grid-connected and islanded modes, it built to study the effects of this transition.

The transition primarily reflected in the overshoot of the DC bus voltage, which depends on the inertia of the microgrid, itself influenced by the resistance values of the microgrid components and how they change between different modes. Additionally, the presence of storage systems can increase inertia, further minimizing the impact of transitions.

The contribution in this thesis focuses on achieving a smooth transition by selecting an appropriate converter topology that operates in both modes and then modifying the control strategy for the islanded mode in these converters to ensure a seamless transition. Four different solutions were proposed, assessed, and designed for this purpose after deriving the mathematical equations governing the operation of each converter in each mode. The proposed solutions are feedback control, compensation, sliding mode control, and voltage-level control. The thesis also compares these control methods to identify the best one for ensuring a smooth transition.

In State Space Control, the methods evaluated include feedback, compensation, and voltage-level control. All these methods reduce overshoots by 95% to 99% while also keeping the impact of load changes within acceptable limits.

In PI control, the methods evaluated were sliding mode control and voltage-level control, which reduced overshoot by 9% to 20%, a smaller reduction compared to state-space control. Only voltage-level control evaluated under load changes, and the results showed a reduction in the impact of load variations. Sliding mode control not evaluated due to the extensive simulation time required to obtain results.

At the end, it can conclude that the characteristics and components of the DC microgrid affect the transition impact on the DC bus, and it can reduce by understanding each DC microgrid and designing a control system to operate the microgrid effectively under the different operating conditions. This research recommends to use voltage level control because is suitable for state space control and PI control and reduce the transition effect and load change within the acceptable values.

References:

- [1] A. Cagnano, E. De Tuglie, and P. Mancarella, "Microgrids: Overview and guidelines for practical implementations and operation," *Applied Energy*, vol. 258, p. 114039, Nov. 2019, doi: 10.1016/j.apenergy.2019.114039.
- [2] H. Bevrani, B. Francois, and T. Ise, "Microgrids: Concept, Structure, and Operation Modes," pp. 119–163, Jul. 2017, doi: <https://doi.org/10.1002/9781119263739.ch3>.
- [3] L. F. N. Delboni, D. Marujo, P. P. Balestrassi, and D. Q. Oliveira, "Electrical Power Systems: Evolution from Traditional Configuration to Distributed Generation and Microgrids," *Microgrids Design and Implementation*, pp. 1–25, Nov. 2018, doi: https://doi.org/10.1007/978-3-319-98687-6_1.
- [4] D. Ioris, P. T. De Godoy, K. D. R. Felisberto, P. Poloni, A. B. De Almeida, and D. Marujo, "Microgrid operation and control: From Grid-Connected to Islanded Mode," in *Lecture notes in electrical engineering*, 2022, pp. 233–256. doi: 10.1007/978-3-030-90812-6_9.
- [5] D. R. Aryani, F. S. Adi, J.-S. Kim, and H. Song, "An improved model-based interlink converter control design in hybrid AC/DC microgrids," *Energy Reports*, vol. 8, pp. 520-531, 2022, doi: 10.1016/j.egy.2022.10.146.
- [6] D.-K. Jeong, H.-S. Kim, J.-W. Baek, H.-J. Kim, and J.-H. Jung, "Autonomous Control Strategy of DC Microgrid for Islanding Mode Using Power Line Communication," *Energies*, vol. 11, no. 4, 2018, doi: 10.3390/en11040924.
- [7] H. Lee et al., "Energy Management System of DC Microgrid in Grid-Connected and Stand-Alone Modes: Control, Operation and Experimental Validation," *Energies*, vol. 14, no. 3, 2021, doi: 10.3390/en14030581.
- [8] H. Wang, M. Wang, Q. Cheng, S. Lv, and X. Ji, "Modeling simulation and inverter control strategy research of microgrid in grid-connected and island mode," *Energy Reports*, vol. 8, pp. 206–218, Nov. 2022, doi: 10.1016/j.egy.2022.09.117.
- [9] M. M. Rana, M. Atef, M. R. Sarkar, M. Uddin, and G. M. Shafiullah, "A Review on Peak Load Shaving in Microgrid—Potential Benefits, Challenges, and Future Trend," *Energies*, vol. 15, no. 6, 2022, doi: 10.3390/en15062278.
- [10] R. Kandari, N. Neeraj, and A. Micallef, "Review on Recent Strategies for Integrating Energy Storage Systems in Microgrids," *Energies*, vol. 16, no. 1, 2022, doi: 10.3390/en16010317.
- [11] C. Zhang, P. Li, and Y. Guo, "Bidirectional DC/DC and SOC drooping control for DC microgrid application," *Electronics*, vol. 9, no. 2, p. 225, Jan. 2020, doi: 10.3390/electronics9020225.

- [12] M. Srinivasan and A. Kwasinski, "Control analysis of parallel DC-DC converters in a DC microgrid with constant power loads," *International Journal of Electrical Power & Energy Systems*, vol. 122, 2020, doi: 10.1016/j.ijepes.2020.106207.
- [13] H. M. Mohan and S. K. Dash, "Renewable Energy-Based DC Microgrid with Hybrid Energy Management System Supporting Electric Vehicle Charging System," *Systems*, vol. 11, no. 6, 2023, doi: 10.3390/systems11060273.
- [14] B. Aluisio, S. Bruno, L. De Bellis, M. Dicorato, G. Forte, and M. Trovato, "DC-Microgrid Operation Planning for an Electric Vehicle Supply Infrastructure," *Applied Sciences*, vol. 9, no. 13, 2019, doi: 10.3390/app9132687.
- [15] S. Moussa, M. J. -B. Ghorbal and I. Slama-Belkhdja, "DC voltage level choice in residential remote area," *2018 9th International Renewable Energy Congress (IREC)*, Hammamet, Tunisia, 2018, pp. 1-6, doi: 10.1109/IREC.2018.8362444.
- [16] K. K. Nandini, N. S. Jayalakshmi, and V. K. Jadoun, "An overview of DC Microgrid with DC distribution system for DC loads," *Materials Today: Proceedings*, vol. 51, pp. 635-639, 2022, doi: 10.1016/j.matpr.2021.06.093.
- [17] H. Sabry, A. H. Shallal, H. S. Hameed, and P. J. Ker, "Compatibility of household appliances with DC microgrid for PV systems," *Heliyon*, vol. 6, no. 12, p. e05699, Dec 2020, doi: 10.1016/j.heliyon.2020.e05699.
- [18] S. Moussa, M. J.-B. Ghorbal, and I. Slama-Belkhdja, "Bus voltage level choice for standalone residential DC nanogrid," *Sustainable Cities and Society*, vol. 46, 2019, doi: 10.1016/j.scs.2019.101431.
- [19] M. Alam, K. Kumar, J. Srivastava and V. Dutta, "A Study on DC Microgrids Voltages based on Photovoltaic and Fuel Cell Power Generators," *2018 7th International Conference on Renewable Energy Research and Applications (ICRERA)*, Paris, France, 2018, pp. 643-648, doi: 10.1109/ICRERA.2018.8566854.
- [20] Bogno et al., "230 VDC elementary block in off-grid PV systems," *Sustainable Energy Technologies and Assessments*, vol. 29, pp. 1-11, 2018, doi: 10.1016/j.seta.2018.06.013.
- [21] S. Ali, Z. Zheng, M. Aillerie, J.-P. Sawicki, M.-C. Péra, and D. Hissel, "A Review of DC Microgrid Energy Management Systems Dedicated to Residential Applications," *Energies*, vol. 14, no. 14, 2021, doi: 10.3390/en14144308.
- [22] T. Ahmadi, E. Rokrok, and M. Hamzeh, "Mitigation of voltage unbalances in bipolar DC microgrids using Three-Port multidirectional DC-DC converters," *Journal of Power Electronics*, vol. 18, no. 4, pp. 1223-1234, Jul. 2018, doi: 10.6113/jpe.2018.18.4.1223.

- [23] S. Pourjafar, H. Afshari, P. Mohseni, O. Husev, O. Matiushkin, and N. Shabbir, "Comprehensive comparison of isolated high step-up DC-DC converters for low power application," *IEEE Open Journal of Power Electronics*, vol. 5, pp. 1149–1161, Jan. 2024, doi: 10.1109/ojpel.2024.3433554.
- [24] Q. Qu, D. Xu, Z. Zhai, Q. Li, and W. Zhang, "Research on development technology of AC / DC hybrid distribution network construction in smart Grid," *IOP Conference Series Earth and Environmental Science*, vol. 558, no. 5, p. 052062, Aug. 2020, doi: 10.1088/1755-1315/558/5/052062.
- [25] X. Wang, Y. Peng, J. Chai, Y. Xia, W. Wei, and M. Yu, "An Ideal DC Transformer for Active DC Distribution Networks Based on Constant-Transformation-Ratio DABC," *IEEE Transactions on Power Electronics*, vol. 35, no. 2, pp. 2170-2183, 2020, doi: 10.1109/tpel.2019.2922402.
- [26] Modu, M. P. Abdullah, M. A. Sanusi, and M. F. Hamza, "DC-based microgrid: Topologies, control schemes, and implementations," *Alexandria Engineering Journal*, vol. 70, pp. 61-92, 2023, doi: 10.1016/j.aej.2023.02.021.
- [27] C. Lv, X. Zheng, N. Tai, and S. Chen, "Single-Ended protection scheme for VSC-Based DC microgrid lines," *Energies*, vol. 11, no. 6, p. 1440, Jun. 2018, doi: 10.3390/en11061440.
- [28] M. Parada Contzen, "Power sharing in actuated DC grids in mesh topology," *Sustainable Energy, Grids and Networks*, vol. 28, 2021, doi: 10.1016/j.segan.2021.100523.
- [29] D. Kumar, F. Zare and A. Ghosh, "DC Microgrid Technology: System Architectures, AC Grid Interfaces, Grounding Schemes, Power Quality, Communication Networks, Applications, and Standardizations Aspects," in *IEEE Access*, vol. 5, pp. 12230-12256, 2017, doi: 10.1109/ACCESS.2017.2705914.
- [30] V. F. Pires, A. Pires, and A. Cordeiro, "DC Microgrids: Benefits, Architectures, Perspectives and Challenges," *Energies*, vol. 16, no. 3, 2023, doi: 10.3390/en16031217.
- [31] M. Ahmed, L. Meegahapola, A. Vahidnia, and M. Datta, "Stability and Control Aspects of Microgrid Architectures—A Comprehensive Review," *IEEE Access*, vol. 8, pp. 144730-144766, 2020, doi: 10.1109/access.2020.3014977.
- [32] K. K. Nandini, N. S. Jayalakshmi, and V. K. Jadoun, "An overview of DC Microgrid with DC distribution system for DC loads," *Materials Today: Proceedings*, vol. 51, pp. 635-639, 2022, doi: 10.1016/j.matpr.2021.06.093.
- [33] Hirsch, Y. Parag, and J. Guerrero, "Microgrids: A review of technologies, key drivers, and outstanding issues," *Renewable and Sustainable Energy Reviews*, vol. 90, pp. 402-411, 2018, doi: 10.1016/j.rser.2018.03.040

- [34] H. S. Kamil, D. M. Said, M. W. Mustafa, M. R. Miveh, and N. Ahmad, "Recent advances in phase-locked loop based synchronization methods for inverter-based renewable energy sources," *Indonesian Journal of Electrical Engineering and Computer Science*, vol. 18, no. 1, p. 1, Apr. 2020, doi: 10.11591/ijeecs.v18.i1.pp1-8.
- [35] A. F. Jabbar and M. Mansor, "Current control loop of 3-phase grid-connected inverter," *IOP Conference Series Earth and Environmental Science*, vol. 16, p. 012069, Jun. 2013, doi: 10.1088/1755-1315/16/1/012069.
- [36] S. Nowak, M. S. Metcalfe, W. Eberle and L. Wang, "Comparison of voltage control methods in distribution systems using Q-V based PI and droop controls of solar inverters," *2017 IEEE Power & Energy Society General Meeting*, Chicago, IL, USA, 2017, pp. 1-5, doi: 10.1109/PESGM.2017.8273969.
- [37] B. Rathnayake *et al.*, "Grid Forming Inverter Modeling, Control, and Applications," in *IEEE Access*, vol. 9, pp. 114781-114807, 2021, doi: 10.1109/ACCESS.2021.3104617.
- [38] M. Alzayed, M. Lemaire, H. Chaoui and D. Massicotte, "A Novel Bi-directional Grid Inverter Control Based on Virtual Impedance Using Neural Network for Dynamics Improvement in Microgrids," in *IEEE Transactions on Power Systems*, doi: 10.1109/TPWRS.2024.3400039.
- [39] K. B. Adam and M. Ashari, "Design of bidirectional converter using fuzzy logic controller to optimize battery performance in Electric Vehicle," *2015 International Seminar on Intelligent Technology and Its Applications (ISITIA)*, Surabaya, Indonesia, 2015, pp. 201-206, doi: 10.1109/ISITIA.2015.7219979.
- [40] M. Mnider, D. J. Atkinson, M. Dahidah and M. Armstrong, "A simplified DQ controller for single-phase grid-connected PV inverters," *2016 7th International Renewable Energy Congress (IREC)*, Hammamet, Tunisia, 2016, pp. 1-6, doi: 10.1109/IREC.2016.7478941.
- [41] M. Surprenant, I. Hiskens and G. Venkataramanan, "Phase locked loop control of inverters in a microgrid," *2011 IEEE Energy Conversion Congress and Exposition*, Phoenix, AZ, USA, 2011, pp. 667-672, doi: 10.1109/ECCE.2011.6063833.
- [42] H. Y. Jung, S. H. Kim, B. Moon and S. -H. Lee, "A New Circuit Design of Two-Switch Buck-Boost Converter," in *IEEE Access*, vol. 6, pp. 47415-47423, 2018, doi: 10.1109/ACCESS.2018.2866886.
- [43] J. Samanes, E. Gubía, Xabier Juancorena, and C. Girones, "Common-Mode and Phase-to-Ground Voltage Reduction in Back-to-Back Power Converters With Discontinuous PWM," *IEEE Transactions on Industrial Electronics*, vol. 67, no. 9, pp. 7499–7508, Sep. 2019, doi: <https://doi.org/10.1109/TIE.2019.2942553>.

- [44] J. Wang, B. Wang, L. Zhang, J. Wang, N. I. Shchurov, and B. V. Malozyomov, "Review of bidirectional DC–DC converter topologies for hybrid energy storage system of new energy vehicles," *Green Energy and Intelligent Transportation*, vol. 1, no. 2, p. 100010, Sep. 2022, doi: 10.1016/j.geits.2022.100010.
- [45] H.-S. Lee and J.-J. Yun, "Advanced MPPT algorithm for distributed photovoltaic systems," *Energies*, vol. 12, no. 18, p. 3576, Sep. 2019, doi: 10.3390/en12183576.
- [46] "IEEE Standard for Interconnection and Interoperability of Distributed Energy Resources with Associated Electric Power Systems Interfaces," in *IEEE Std 1547-2018 (Revision of IEEE Std 1547-2003)*, vol., no., pp.1-138, 6 April 2018, doi: 10.1109/IEEESTD.2018.8332112.
- [47] "IEC/IEEE Draft International Standard - Utility Connections in Port - Part 3: Low Voltage Shore Connection (LVSC) Systems - General Requirements," in *IEC/IEEE P80005-3 ED1, February 2024*, vol., no., pp.1-47, 6 March 2024.
- [48] "IEEE Standard for DC Microgrids for Rural and Remote Electricity Access Applications," in *IEEE Std 2030.10-2021*, vol., no., pp.1-47, 15 Dec. 2021, doi: 10.1109/IEEESTD.2021.9646866.
- [49] T. Dragičević, X. Lu, J. C. Vasquez and J. M. Guerrero, "DC Microgrids—Part II: A Review of Power Architectures, Applications, and Standardization Issues," in *IEEE Transactions on Power Electronics*, vol. 31, no. 5, pp. 3528-3549, May 2016, doi: 10.1109/TPEL.2015.2464277.
- [50] "IEEE Guide for Design, Operation, and Integration of Distributed Resource Island Systems with Electric Power Systems," in *IEEE Std 1547.4-2011*, vol., no., pp.1-54, 20 July 2011, doi: 10.1109/IEEESTD.2011.5960751.
- [51] F. Chang, X. Cui, M. Wang, W. Su and A. Q. Huang, "Large-Signal Stability Criteria in DC Power Grids With Distributed-Controlled Converters and Constant Power Loads," in *IEEE Transactions on Smart Grid*, vol. 11, no. 6, pp. 5273-5287, Nov. 2020, doi: 10.1109/TSG.2020.2998041
- [52] M. Giannuzzi, V. Mostova, C. Pisani, S. Tessitore, and A. Vaccaro, "Enabling technologies for enhancing power system stability in the presence of Converter-Interfaced generators," *Energies*, vol. 15, no. 21, p. 8064, Oct. 2022, doi: 10.3390/en15218064.
- [53] A. Cagnano *et al.*, "Transitions from grid-connected to island operation of Smart Microgrids," *2019 IEEE International Conference on Environment and Electrical Engineering and 2019 IEEE Industrial and Commercial Power Systems Europe (EEEIC / I&CPS Europe)*, Genova, Italy, 2019, pp. 1-6, doi: 10.1109/EEEIC.2019.8783746.
- [54] A. H. Etemadi and R. Iravani, "Supplementary mechanisms for smooth transition between control modes in a microgrid," *Electric Power Systems Research*, vol. 142, pp. 249–257, Jan. 2017, doi: 10.1016/j.epsr.2016.09.033.

- [55] M. Ganjian-Aboukheili, M. Shahabi, Q. Shafiee and J. M. Guerrero, "Seamless Transition of Microgrids Operation From Grid-Connected to Islanded Mode," in *IEEE Transactions on Smart Grid*, vol. 11, no. 3, pp. 2106-2114, May 2020, doi: 10.1109/TSG.2019.2947651.
- [56] M. E. T. Souza and L. C. G. Freitas, "Grid-Connected and Seamless Transition Modes for Microgrids: An Overview of Control Methods, Operation Elements, and General Requirements," in *IEEE Access*, vol. 10, pp. 97802-97834, 2022, doi: 10.1109/ACCESS.2022.3206362.
- [57] A. El-Shahat and S. Sumaiya, "DC-MicroGrid system design, control, and analysis," *Electronics*, vol. 8, no. 2, p. 124, Jan. 2019, doi: 10.3390/electronics8020124.
- [58] S. D'silva, M. Shadmand, S. Bayhan and H. Abu-Rub, "Towards Grid of Microgrids: Seamless Transition between Grid-Connected and Islanded Modes of Operation," in *IEEE Open Journal of the Industrial Electronics Society*, vol. 1, pp. 66-81, 2020, doi: 10.1109/OJIES.2020.2988618.
- [59] F. S. Al-Ismael, "DC Microgrid Planning, Operation, and Control: A Comprehensive Review," in *IEEE Access*, vol. 9, pp. 36154-36172, 2021, doi: 10.1109/ACCESS.2021.3062840.
- [60] T. M. a. J. Jiang, "Design and implementation of a microgrid controller for bumpless transitions between grid-connected and island operation," in *IECON 2014 - 40th Annual Conference of the IEEE Industrial Electronics Society*, Dallas, TX, USA, 2014.
- [61] W. Zhao, X. Zhang, Y. Li and N. Qian, "Improved master-slave control for Smooth Transition Between Grid-connected and Islanded Operation of DC Microgrid Based on I- ΔV Droop," *2020 IEEE 9th International Power Electronics and Motion Control Conference (IPEMC2020-ECCE Asia)*, Nanjing, China, 2020, pp. 1194-1198, doi: 10.1109/IPEMC-ECCEAsia48364.2020.9367870.
- [62] M. U. Khan, A. F. Murtaza, A. M. Noman, H. A. Sher, and M. Zafar, "State-Space Modeling, Design, and Analysis of the DC-DC Converters for PV Application: A review," *Sustainability*, vol. 16, no. 1, p. 202, Dec. 2023, doi: 10.3390/su16010202.
- [63] D. Yan et al., "Review of general modeling approaches of power converters," in *Chinese Journal of Electrical Engineering*, vol. 7, no. 1, pp. 27-36, March 2021, doi: 10.23919/CJEE.2021.000002.
- [64] G. F. Franklin, J. D. Powell, and A. Emami-Naeini, in *Feedback control of Dynamic Systems*, 8th edition., New York: Pearson, 2019.
- [65] A. Ullah, S. S. Rizvi, A. Khatoon and S. Jin Kwon, "The Empirical Analysis, Mathematical Modeling, and Advanced Control Strategies for Buck Converter," in *IEEE Access*, vol. 12, pp. 19924-19941, 2024, doi: 10.1109/ACCESS.2024.3357537.

- [66] F. Ji, J. Xiang, W. Li, and Q. Yue, "A feedback passivation design for DC Microgrid and its DC/DC converters," *Energies*, vol. 10, no. 1, p. 14, Dec. 2016, doi: 10.3390/en10010014.
- [67] Q. Xu, N. Vafamand, L. Chen, T. Dragičević, L. Xie and F. Blaabjerg, "Review on Advanced Control Technologies for Bidirectional DC/DC Converters in DC Microgrids," in *IEEE Journal of Emerging and Selected Topics in Power Electronics*, vol. 9, no. 2, pp. 1205-1221, April 2021, doi: 10.1109/JESTPE.2020.2978064.
- [68] Ghosh and S. Banerjee, "Design and implementation of Type-II compensator in DC-DC switch-mode step-up power supply," *Proceedings of the 2015 Third International Conference on Computer, Communication, Control and Information Technology (C3IT)*, Hooghly, India, 2015, pp. 1-5, doi: 10.1109/C3IT.2015.7060164

Appendix:

Appendix A:

- State space representation for unidirectional buck boost converter:

$$\dot{x} = \{A_1D + A_2(1 - D)\}x + \{B_1D + B_2(1 - E)\}u \quad (A8)$$

$$y = \{C_1D + C_2(1 - D)\}x + \{E_1D + E_2(1 - E)\}u \quad (A9)$$

$$\text{Transfer function} = \frac{y(s)}{u(s)} = \frac{V_o(s)}{V_{in}(s)} = C[SI - A]^{-1}B + E \quad (A10)$$

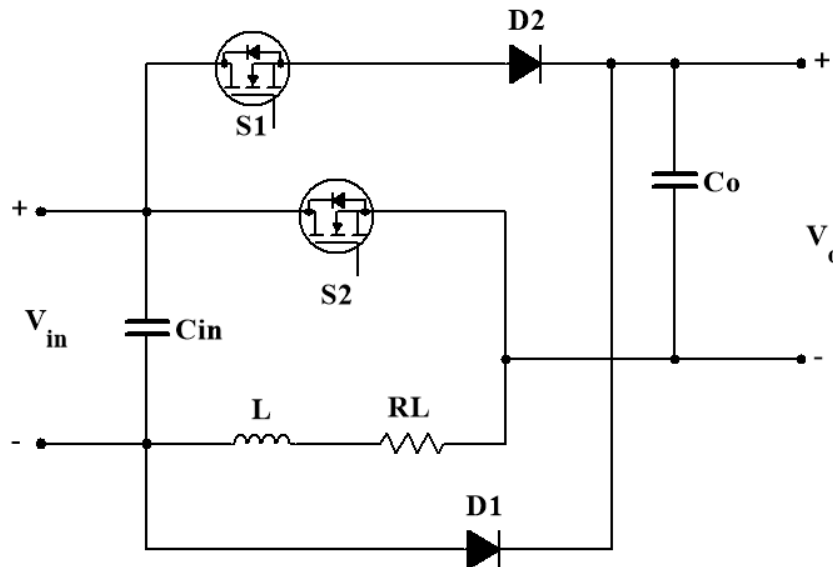


Figure A. 1: unidirectional buck boost circuit.

The buck boost converter works in two modes of operations and each mode has a transfer function. The two modes of operations:

Mode 1: buck -boost converter in grid connected operation.

Mode 2: boost converter in off grid operation.

- **Mode 1: buck -boost converter in grid connected operation:**

This mode has two states of operation:

- State 1: **S₁ off and S₂ on (buck-boost)**

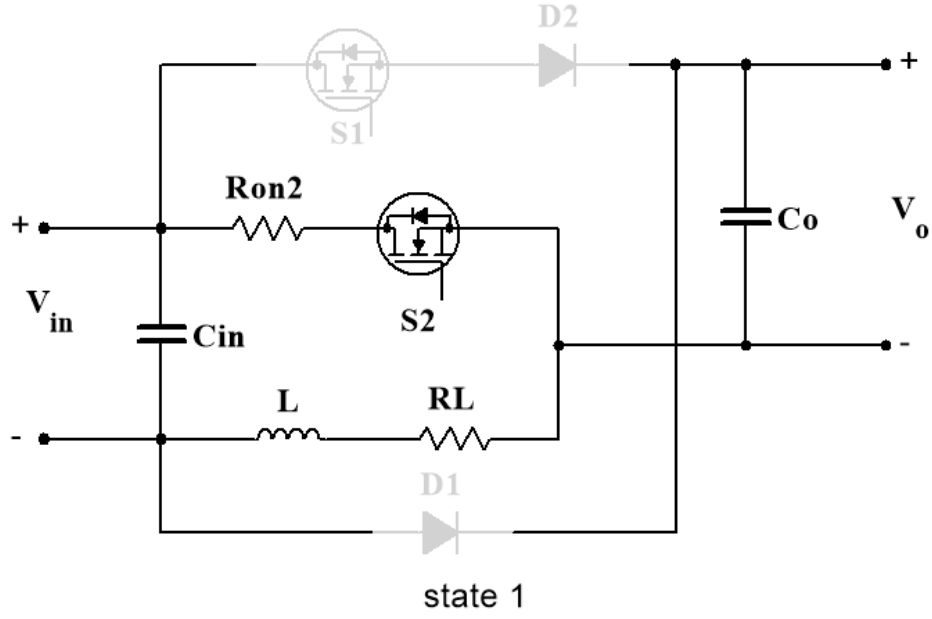


Figure A. 2: 1st state for unidirectional converter in buck boost operation.

$$\frac{di_L}{dt} = \frac{1}{L} [v_{in} - i_L(R_L + R_{on2})] \quad (A11)$$

$$\frac{dv_o}{dt} = \frac{1}{C_o} [-i_o] \quad (A12)$$

$$\frac{dv_{in}}{dt} = \frac{1}{C_{in}} [i_{in} - i_L] \quad (A13)$$

$$A_1 = \begin{bmatrix} \frac{-(R_L + R_{on2})}{L} & 0 & \frac{1}{L} \\ 0 & 0 & 0 \\ \frac{-1}{C_{in}} & 0 & 0 \end{bmatrix}$$

$$B_1 = \begin{bmatrix} 0 & \frac{1}{L} \\ \frac{-1}{C_o} & 0 \\ 0 & 0 \end{bmatrix}$$

$$C_1 = \begin{bmatrix} 0 & \frac{-(R_L + R_{on2})}{L} & 0 \\ 0 & 0 & 0 \\ 1 & -1 & 0 \\ \frac{1}{C_{in}} & \frac{-1}{C_{in}} & 0 \end{bmatrix}$$

$$E_1 = [0]$$

Assume the duty cycle at this state equals D1.

- State 2: **S₁ off and S₂ off (buck-boost)**

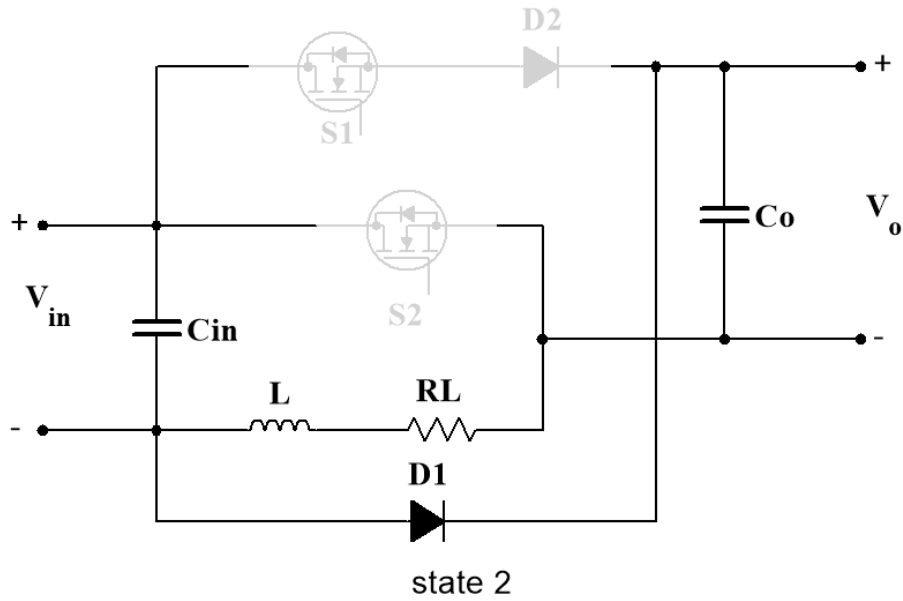


Figure A. 3: 2nd state for unidirectional converter in buck boost operation.

$$\frac{di_L}{dt} = \frac{1}{L} [v_o - i_L(R_L)] \quad (A14)$$

$$\frac{dv_{C_o}}{dt} = \frac{1}{C_o} [i_o - i_L] \quad (A15)$$

$$\frac{dv_{C_{in}}}{dt} = \frac{1}{C_{in}} [-i_{in}] \quad (A16)$$

$$A_2 = \begin{bmatrix} \frac{-(R_L)}{L} & \frac{1}{L} & 0 \\ -1 & 0 & 0 \\ \frac{1}{C_o} & 0 & 0 \\ 0 & 0 & 0 \end{bmatrix}$$

$$B_2 = \begin{bmatrix} 0 & 0 \\ 1 & 0 \\ C_o & 0 \\ 0 & 0 \end{bmatrix}$$

$$C_2 = \begin{bmatrix} 0 & \frac{-(R_L)}{L} & 0 \\ 0 & \frac{-1}{C_o} & 0 \\ \frac{-1}{C_{in}} & 0 & 0 \end{bmatrix}$$

$$E_2 = [0]$$

Assume the duty cycle at this state equals D2.

- **The state space matrices that represent the two states:**

After combining the two states together the state space matrices are:

$$A = \begin{bmatrix} -\frac{(R_L + R_{on2})D_1 + R_L D_2}{L} & \frac{D_2}{L} & \frac{D_1}{L} \\ \frac{-D_2}{C_o} & 0 & 0 \\ \frac{-D_1}{C_{in}} & 0 & 0 \end{bmatrix}$$

$$B = \begin{bmatrix} 0 & \frac{D_1}{L} \\ \frac{D_2 - D_1}{C_o} & 0 \\ 0 & 0 \end{bmatrix}$$

$$C = \begin{bmatrix} 0 & -\frac{(R_L + R_{on2})D_1 + R_L D_2}{L} & \frac{D_2}{L} \\ 0 & \frac{-D_2}{C_o} & 0 \\ \frac{D_1 - D_2}{C_{in}} & \frac{-D_1}{C_{in}} & 0 \end{bmatrix}$$

$$E = [0]$$

The transfer function:

$$\frac{V_o(s)}{V_{in}(s)} = \frac{\frac{s(D_1 - D_2)}{LC_{in}} - \frac{D_1 D_2}{L^2 C_{in}}}{s^2 + \frac{(R_L + R_{on2})D_1 + R_L D_2}{L} s + \frac{D_2^2}{LC_o} + \frac{D_1^2}{LC_{in}}} \quad (A17)$$

- **Mode 2: boost operation**
 - **State 1: S₁ off and S₂ on**

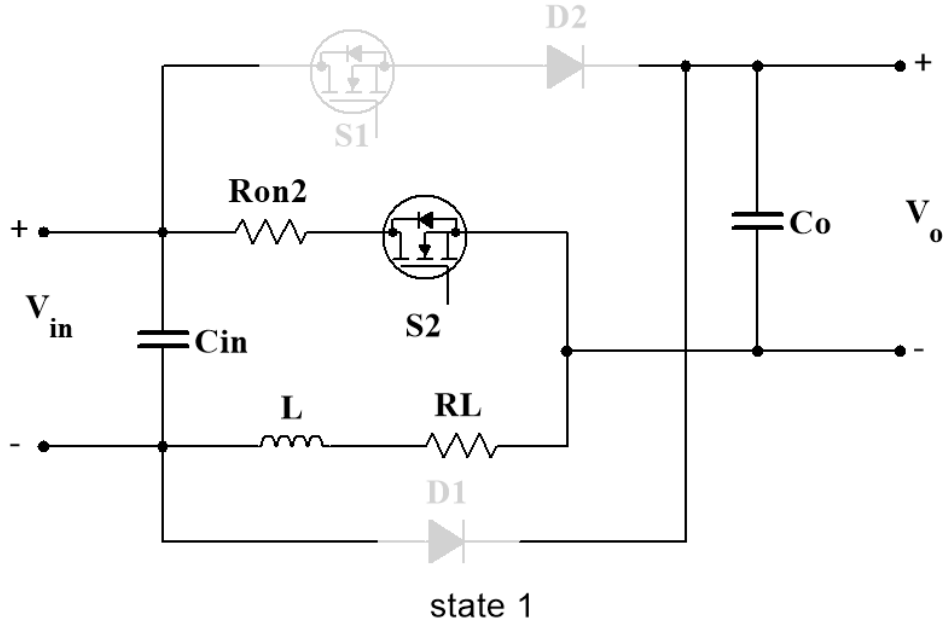


Figure A. 4: 1st state for unidirectional converter in boost operation.

$$\frac{di_L}{dt} = \frac{1}{L} [v_{in} - i_L(R_L + R_{on2})] \quad (A18)$$

$$\frac{dv_o}{dt} = \frac{1}{C_o} [-i_o] \quad (A19)$$

$$\frac{dv_{in}}{dt} = \frac{1}{C_{in}} [i_{in} - i_L] \quad (A20)$$

$$A_1 = \begin{bmatrix} \frac{-(R_L + R_{on2})}{L} & 0 & \frac{1}{L} \\ 0 & 0 & 0 \\ \frac{-1}{C_{in}} & 0 & 0 \end{bmatrix}$$

$$B_1 = \begin{bmatrix} 0 & \frac{1}{L} \\ -\frac{1}{C_o} & 0 \\ 0 & 0 \end{bmatrix}$$

$$C_1 = \begin{bmatrix} 0 & \frac{-(R_L + R_{on2})}{L} & 0 \\ 0 & 0 & 0 \\ \frac{1}{C_{in}} & \frac{-1}{C_{in}} & 0 \end{bmatrix}$$

$$E_1 = [0]$$

Assume the duty cycle at this state equals D1.

- **State 2: S1 on and S2 off**

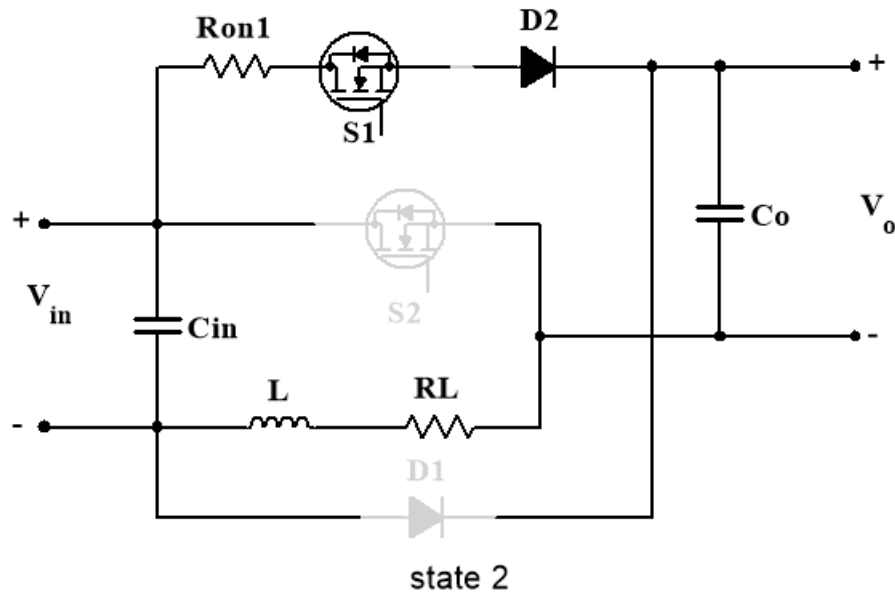


Figure A. 5: 2nd state for unidirectional converter in boost operation.

$$\frac{di_L}{dt} = \frac{1}{L} [v_o - i_L(R_L + R_{on1}) - v_{in}] \quad (A21)$$

$$\frac{dv_{Co}}{dt} = \frac{1}{C_o} [i_L - i_o] \quad (A22)$$

$$\frac{dv_{Cin}}{dt} = \frac{1}{C_{in}} [i_{in} - i_L] \quad (A23)$$

Assume the duty cycle at this state equals D2.

$$A_2 = \begin{bmatrix} \frac{-(R_L + R_{on1})}{L} & \frac{1}{L} & \frac{-1}{L} \\ \frac{1}{C_o} & 0 & 0 \\ \frac{-1}{C_{in}} & 0 & 0 \end{bmatrix}$$

$$B_2 = \begin{bmatrix} 0 & \frac{-1}{L} \\ \frac{-1}{C_o} & 0 \\ 0 & 0 \end{bmatrix}$$

$$C_2 = \begin{bmatrix} 0 & \frac{-(R_L + R_{on1})}{L} & \frac{1}{L} \\ 0 & \frac{1}{C_o} & 0 \\ \frac{1}{C_{in}} & \frac{-1}{C_{in}} & 0 \end{bmatrix}$$

$$E_2 = [0]$$

- **The state space matrices that represent the two states:**

After combining the two states together the state space matrices are:

$$A = \begin{bmatrix} \frac{R_L(D_1 + D_2) + D_2R_{on1} + D_1R_{on2}}{L} & \frac{D_2}{L} & \frac{D_1 - D_2}{L} \\ \frac{D_2}{C_o} & 0 & 0 \\ \frac{-(D_1 + D_2)}{C_{in}} & 0 & 0 \end{bmatrix}$$

$$B = \begin{bmatrix} 0 & \frac{D_1 - D_2}{L} \\ \frac{-(D_1 + D_2)}{C_o} & 0 \\ 0 & 0 \end{bmatrix}$$

$$C = \begin{bmatrix} 0 & -\frac{R_L(D_1 + D_2) + D_2R_{on1} + D_1R_{on2}}{L} & \frac{D_2}{L} \\ 0 & \frac{D_2}{C_o} & 0 \\ \frac{D_1 + D_2}{C_{in}} & \frac{-(D_1 + D_2)}{C_{in}} & 0 \end{bmatrix}$$

$$E = [0]$$

The transfer function:

$$\frac{Vo(s)}{Vin(s)} = \frac{\frac{s(D_1^2 - D_2^2)}{LC_{in}} + \frac{(D_1^2 - D_2^2)D_2}{L^2C_{in}}}{s^2 + \frac{R_L(D_1 + D_2) + D_2R_{on1} + D_1R_{on2}}{L}s - \frac{D_2^2}{LC_o} + \frac{(D_1^2 + D_2^2)}{LC_{in}}} \quad (A24)$$

Appendix B:

- State space representation for bidirectional buck boost converter:

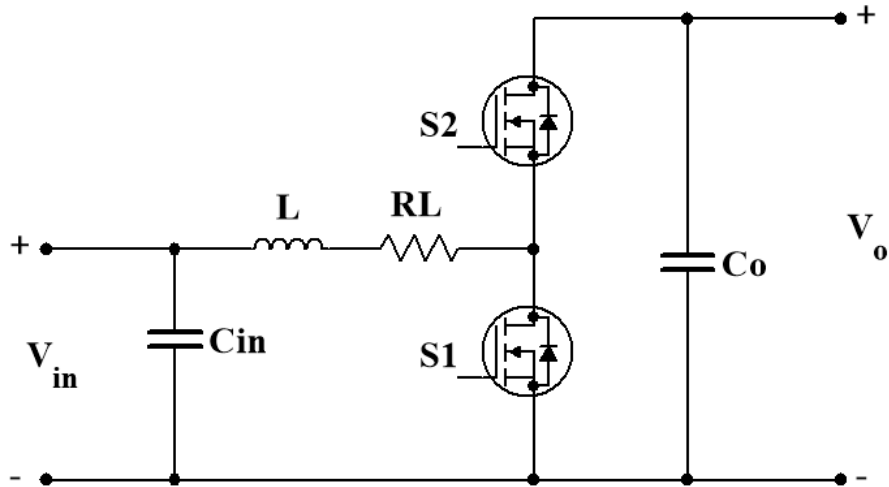


Figure B. 1: Bidirectional buck boost converter circuit.

- **State 1: S₁ on and S₂ off (buck converter)**

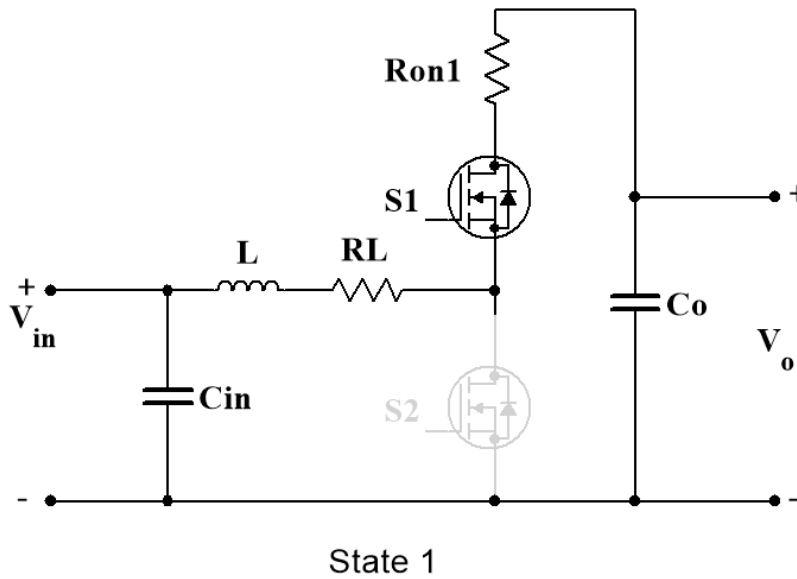


Figure B. 2: 1st state of bidirectional buck boost converter.

$$\frac{di_L}{dt} = \frac{1}{L} [v_o - i_L(R_L + R_{on1}) - v_{in}] \quad (B1)$$

$$\frac{dv_o}{dt} = \frac{1}{C_o} [i_o - i_L] \quad (B2)$$

$$\frac{dv_{in}}{dt} = \frac{1}{C_{in}} [i_L - i_o] \quad (B3)$$

$$A_1 = \begin{bmatrix} \frac{-(R_L + R_{on1})}{L} & \frac{1}{L} & \frac{-1}{L} \\ \frac{-1}{C_o} & 0 & 0 \\ \frac{1}{C_{in}} & 0 & 0 \end{bmatrix}$$

$$B_1 = \begin{bmatrix} 0 & \frac{-1}{L} \\ \frac{1}{C_o} & 0 \\ 0 & 0 \end{bmatrix}$$

$$C_1 = \begin{bmatrix} 0 & \frac{-(R_L + R_{on1})}{L} & \frac{1}{L} \\ 0 & \frac{1}{C_o} & 0 \\ \frac{-1}{C_{in}} & \frac{1}{C_{in}} & 0 \end{bmatrix}$$

$$E_1 = [0]$$

Assume the duty cycle at this state equals D.

- **State 2: S₁ off and S₂ on (boost converter)**

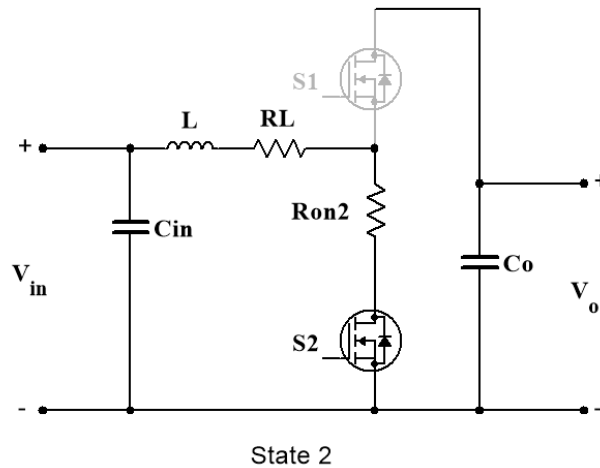


Figure B. 3: 2nd state of bidirectional buck boost converter.

$$\frac{di_L}{dt} = \frac{1}{L} [v_{in} - i_L(R_L + R_{on2})] \quad (B4)$$

$$\frac{dv_{Co}}{dt} = \frac{1}{C_o} [-i_o] \quad (B5)$$

$$\frac{dv_{Cin}}{dt} = \frac{1}{C_{in}} [i_{in} - i_L] \quad (B6)$$

Assume the duty cycle at this state equals 1-D.

$$A_2 = \begin{bmatrix} \frac{-(R_L + R_{on1})}{L} & 0 & \frac{1}{L} \\ 0 & 0 & 0 \\ \frac{-1}{C_{in}} & 0 & 0 \end{bmatrix}$$

$$B_2 = \begin{bmatrix} 0 & \frac{1}{L} \\ \frac{-1}{C_o} & 0 \\ 0 & 0 \end{bmatrix}$$

$$C_2 = \begin{bmatrix} 0 & \frac{-(R_L + R_{on1})}{L} & 0 \\ 0 & 0 & 0 \\ \frac{1}{C_{in}} & \frac{-1}{C_{in}} & 0 \end{bmatrix}$$

$$E_2 = [0]$$

- **The state space matrices that represent the two states:**

After combining the two states together the state space matrices are:

$$A = \begin{bmatrix} \frac{(R_L + R_{on1})D}{L} - \frac{(R_L + R_{on2})(1-D)}{L} & \frac{D}{L} & \frac{-D + (1-D)}{L} \\ \frac{-D}{C_o} & 0 & 0 \\ \frac{D}{C_{in}} - \frac{(1-D)}{C_{in}} & 0 & 0 \end{bmatrix}$$

$$A = \begin{bmatrix} -\frac{(R_L + DR_{on1} + (1-D)R_{on2})}{L} & \frac{D}{L} & \frac{1-2D}{L} \\ \frac{-D}{C_o} & 0 & 0 \\ \frac{2D-1}{C_{in}} & 0 & 0 \end{bmatrix}$$

$$B = \begin{bmatrix} 0 & \frac{1-2D}{L} \\ \frac{2D-1}{C_o} & 0 \\ 0 & 0 \end{bmatrix}$$

$$C = \begin{bmatrix} 0 & \frac{-(R_L + R_{on1})}{L} & 0 \\ 0 & 0 & 0 \\ \frac{1}{C_{in}} & \frac{-1}{C_{in}} & 0 \end{bmatrix}$$

$$E = [0]$$

The transfer function:

$$\frac{V_o(s)}{V_{in}(s)} = \frac{\frac{s(1-2D)^2}{LC_{in}} + \frac{(2D-1)(1-2D)D}{L^2C_{in}}}{s^2 + \frac{R_L + DR_{on1} + (1-D)R_{on2}}{L}s + \frac{D^2}{LC_o} - \frac{4D - 4D^2 - 1}{LC_{in}}} \quad (B7)$$

Appendix C:

- MATLAB code for unidirectional buck boost converter in boost operation:

```
D1=1; % Duty cycle for 1st transistor
D2=0.182; % Duty cycle for 2nd transistor
L=8e-3; % Inductor
Cin=1500e-6; % Input capacitor
Co=800e-6; % Output capacitor
RL=0.1; % Inductor internal resistor
Ron1=0.1; % Conduction resistance for 1st transistor
Ron2=0.1; % Conduction resistance for 2nd transistor
s=sym('s'); % S domain
A =[-(RL*(D1+D2)+D2*Ron1+D1*Ron2)/L D2/L (D1-D2)/L;D2/Co 0 0;-(D1+D2)/Cin 0 0]; % The state
matrix
B= [(D1-D2)/L;0;0]; % The input matrix
C=[(D1+D2)/Cin, -(D1+D2)/Cin,0]; % The output matrix
E=0; % The feedforward matrix
sys=ss(A,B,C,E); % state-space model
[num, den] = tfdata(sys,'v'); % Numerator and Denominator coefficients
Num=vpa(num);
Den=vpa(den);
disp("The numerator:")
disp(Num); % Numerator coefficient display
disp("The denominator:")
disp(Den); % Denominator coefficient display
[zz,pp,kk]=tf2zp(num,den); % Convert transfer function to zero-pole-gain
disp("The poles:")
disp(vpa(pp));
disp("The zeros:")
disp(vpa(zz));
pzmap(pp,zz) % Pole-zero plot of the system
title('Poles & Zeros map for boost converter');
xlabel('Real part')
ylabel('Imaginary part')
[y, t] = step(sys,0.7); % Step response of the system
figure(2);
plot(t, y);
title('Step response for boost converter');
xlabel('Time')
ylabel('Step response')
sys1=minreal(sys); % rank reduction
[num1, den1] = tfdata(sys1,'v');
Num1=vpa(num1);
Den1=vpa(den1);
disp("The new numerator:")
disp(Num1);
disp("The new denominator:")
```



```

[A1,B1,C1,E1] = tf2ss(Num1,Den1);
disp("The new state matrix:")
disp(vpa(A1));
disp("The new input matrix:")
disp(vpa(B1));
disp("The new output matrix:")
disp(vpa(C1));
disp("The new feedforward matrix:")
disp(vpa(E1));
[zz1,pp1,kk1]=tf2zp(num1,den1);
disp("The new poles:")
disp(vpa(pp1));
disp("The new zeros:")
disp(vpa(zz1));
figure(3);
pzmap(pp1,zz1)
title('Poles & Zeros map after reduction');
xlabel('Real part')
ylabel('Imaginary part')
[y1, t1] = step(sys1,0.7);
figure(4);
plot(t1, y1);
title('Step response after reduction');
xlabel('Time')
ylabel('Step response')
[A1,B1,C1,E1] = tf2ss(Num1,Den1);
disp("The new state matrix:")
disp(vpa(A1));
disp("The new input matrix:")
disp(vpa(B1));
disp("The new output matrix:")
disp(vpa(C1));
disp("The new feedforward matrix:")
disp(vpa(E1));

```

- MATLAB code for unidirectional buck boost converter in buck boost operation:

```

D1=0.551;    % Duty cycle for 1st transistor
D2=0.551;    % Duty cycle for 2nd transistor
L=8e-3;      % Inductor value
Cin=1500e-6; % Input capacitor
Co=800e-6;   % Output capacitor
RL=0.1;      % Inductor internal resistor
Ron1=0.1;    % Conduction resistance for 1st transistor
Ron2=0.1;    % Conduction resistance for 2nd transistor
s=sym('s');  % S domain
A=[-((RL+Ron2)*D1+RL*D2)/L D2/L D1/L ; -D2/Co 0 0 ; -D1/Cin 0 0]; % The state matrix
B= [ D1/L;0;0]; % The input matrix
C=[(D1-D2)/Cin ,-D1/Cin,0]; % The output matrix
E=0; % The feedforward matrix
sys=ss(A,B,C,E); % state-space model
[num, den] = tfdata(sys,'v'); % Numerator and Denominator coefficients
Num=vpa(num);
Den=vpa(den);
disp("The numerator:")
disp(Num); % Numerator coefficient display
disp("The denominator:")
disp(Den); % Denominator coefficient display
[zz,pp,kk]=tf2zp(num,den); % Convert transfer function to zero-pole-gain
disp("The poles:")
disp(vpa(pp));
disp("The zeros:")
disp(vpa(zz));
pzmap(pp,zz) % Pole-zero plot of the system
title('Poles & Zeros map for boost converter');
xlabel('Real part')
ylabel('Imaginary part')
[y, t] = step(sys,0.7); % Step response of the system
figure(2);
plot(t, y);
title('Step response for boost converter');
xlabel('Time')
ylabel('Step response')
sys1=minreal(sys); % rank reduction
[num1, den1] = tfdata(sys1,'v');
Num1=vpa(num1);
Den1=vpa(den1);
disp("The new numerator:")
disp(Num1);
disp("The new denominator:")
disp(Den1);

```

```

[A1,B1,C1,E1] = tf2ss(Num1,Den1);
disp("The new state matrix:")
disp(vpa(A1));
disp("The new input matrix:")
disp(vpa(B1));
disp("The new output matrix:")
disp(vpa(C1));
disp("The new feedforward matrix:")
disp(vpa(E1));
[zz1,pp1,kk1]=tf2zp(num1,den1);
disp("The new poles:")
disp(vpa(pp1));
disp("The new zeros:")
disp(vpa(zz1));
figure(3);
pzmap(pp1,zz1)
title('Poles & Zeros map after reduction');
xlabel('Real part')
ylabel('Imaginary part')
[y1, t1] = step(sys1,0.7);
figure(4);
plot(t1, y1);
title('Step response after reduction');
xlabel('Time')
ylabel('Step response')
[A1,B1,C1,E1] = tf2ss(Num1,Den1);
disp("The new state matrix:")
disp(vpa(A1));
disp("The new input matrix:")
disp(vpa(B1));
disp("The new output matrix:")
disp(vpa(C1));
disp("The new feedforward matrix:")
disp(vpa(E1));

```

- MATLAB code for bidirectional buck boost converter:

```

D=0.512;    % Duty cycle
L=8e-3;    % Inductor value
Cin=206e-6; % Input capacitor
Co=500e-6; % Output capacitor
RL=0.1;    % Inductor internal resistor
Ron1=0.1;  % Conduction resistance for 1st transistor
Ron2=0.1;  % Conduction resistance for 2nd transistor
s=sym('s'); % S domain

A =[-(RL+D*Ron1+(1-D)*Ron2)/L D/L (1-2*D)/L ; -D/Co 0 0 ; (2D-1)/Cin 0 0]; % The state matrix
B= [ (1-2*D)/L;0;0]; % The input matrix
C=[1/Cin, -1/Cin,0]; % The output matrix
E=0; % The feedforward matrix
sys=ss(A,B,C,E); % state-space model
[num, den] = tfdata(sys,'v'); % Numerator and Denominator coefficients
Num=vpa(num);
Den=vpa(den);
disp("The numerator:")
disp(Num); % Numerator coefficient display
disp("The denominator:")
disp(Den); % Denominator coefficient display
[zz,pp,kk]=tf2zp(num,den); % Convert transfer function to zero-pole-gain
disp("The poles:")
disp(vpa(pp));
disp("The zeros:")
disp(vpa(zz));
pzmap(pp,zz) % Pole-zero plot of the system
title('Poles & Zeros map for boost converter');
xlabel('Real part')
ylabel('Imaginary part')
[y, t] = step(sys,0.7); % Step response of the system
figure(2);
plot(t, y);
title('Step response for boost converter');
xlabel('Time')
ylabel('Step response')
sys1=minreal(sys); % rank reduction
[num1, den1] = tfdata(sys1,'v');
Num1=vpa(num1);
Den1=vpa(den1);
disp("The new numerator:")
disp(Num1);
disp("The new denominator:")
disp(Den1);

```

```

[A1,B1,C1,E1] = tf2ss(Num1,Den1);
disp("The new state matrix:")
disp(vpa(A1));
disp("The new input matrix:")
disp(vpa(B1));
disp("The new output matrix:")
disp(vpa(C1));
disp("The new feedforward matrix:")
disp(vpa(E1));
[zz1,pp1,kk1]=tf2zp(num1,den1);
disp("The new poles:")
disp(vpa(pp1));
disp("The new zeros:")
disp(vpa(zz1));
figure(3);
pzmap(pp1,zz1)
title('Poles & Zeros map after reduction');
xlabel('Real part')
ylabel('Imaginary part')
[y1, t1] = step(sys1,0.7);
figure(4);
plot(t1, y1);
title('Step response after reduction');
xlabel('Time')
ylabel('Step response')
[A1,B1,C1,E1] = tf2ss(Num1,Den1);
disp("The new state matrix:")
disp(vpa(A1));
disp("The new input matrix:")
disp(vpa(B1));
disp("The new output matrix:")
disp(vpa(C1));
disp("The new feedforward matrix:")
disp(vpa(E1));

```

- The MATLAB code for the Perturbation and observation MPPT algorithm:

```

function Vref = ModPandO(V, I)

Vrefmax=190;
Vrefmin=0;
Vrefinit=165;
deltaVref = 0.1;

persistent Vold Pold Vrefold;

dataType = 'double';

if isempty(Vold)
    Vold=0;
    Pold=0;
    Vrefold=Vrefinit;

end
P= V*I;
dV= V - Vold;
dP= P - Pold;

if dP ~=0
    if dP < 0
        if dV < 0
            Vref = Vrefold + deltaVref;
        else
            Vref = Vrefold - deltaVref;
        end
    else
        if dV < 0
            Vref = Vrefold - deltaVref;
        else
            Vref = Vrefold + deltaVref;
        end
    end

else Vref = Vrefold;
end

if Vref >= Vrefmax | Vref <= Vrefmin
    Vref = Vrefold;
end

Vrefold =Vref;
Vold=V;
Pold=P;

```

The End